

1985

SWARM PARAMETERS IN ELECTRONEGATIVE GASES.

M. SEZAI. DINCER

University of Windsor

Follow this and additional works at: <http://scholar.uwindsor.ca/etd>

Recommended Citation

DINCER, M. SEZAI, "SWARM PARAMETERS IN ELECTRONEGATIVE GASES." (1985). *Electronic Theses and Dissertations*. Paper 3683.

This online database contains the full-text of PhD dissertations and Masters' theses of University of Windsor students from 1954 forward. These documents are made available for personal study and research purposes only, in accordance with the Canadian Copyright Act and the Creative Commons license—CC BY-NC-ND (Attribution, Non-Commercial, No Derivative Works). Under this license, works must always be attributed to the copyright holder (original author), cannot be used for any commercial purposes, and may not be altered. Any other use would require the permission of the copyright holder. Students may inquire about withdrawing their dissertation and/or thesis from this database. For additional inquiries, please contact the repository administrator via email (scholarship@uwindsor.ca) or by telephone at 519-253-3000ext. 3208.

CANADIAN THESES ON MICROFICHE

THÈSES CANADIENNES SUR MICROFICHE



National Library of Canada
Collections Development Branch

Canadian Theses on
Microfiche Service

Ottawa, Canada
K1A 0N4

Bibliothèque nationale du Canada
Direction du développement des collections

Service des thèses canadiennes
sur microfiche

NOTICE

The quality of this microfiche is heavily dependent upon the quality of the original thesis submitted for microfilming. Every effort has been made to ensure the highest quality of reproduction possible.

If pages are missing, contact the university which granted the degree.

Some pages may have indistinct print especially if the original pages were typed with a poor typewriter ribbon or if the university sent us an inferior photocopy.

Previously copyrighted materials (journal articles, published tests, etc.) are not filmed.

Reproduction in full or in part of this film is governed by the Canadian Copyright Act, R.S.C. 1970, c. C-30. Please read the authorization forms which accompany this thesis.

THIS DISSERTATION
HAS BEEN MICROFILMED
EXACTLY AS RECEIVED

AVIS

La qualité de cette microfiche dépend grandement de la qualité de la thèse soumise au microfilmage. Nous avons tout fait pour assurer une qualité supérieure de reproduction.

S'il manque des pages, veuillez communiquer avec l'université qui a conféré le grade.

La qualité d'impression de certaines pages peut laisser à désirer, surtout si les pages originales ont été dactylographiées à l'aide d'un ruban usé ou si l'université nous a fait parvenir une photocopie de qualité inférieure.

Les documents qui font déjà l'objet d'un droit d'auteur (articles de revue, examens publiés, etc.) ne sont pas microfilmés.

La reproduction, même partielle, de ce microfilm est soumise à la Loi canadienne sur le droit d'auteur, SRC 1970, c. C-30. Veuillez prendre connaissance des formules d'autorisation qui accompagnent cette thèse.

LA THÈSE A ÉTÉ
MICROFILMÉE TELLE QUE
NOUS L'AVONS REÇUE

Canada

SWARM PARAMETERS
IN ELECTRONEGATIVE GASES

by
M. Sezai Dincer

A Dissertation
submitted to the Faculty of Graduate Studies
through the Department of Electrical Engineering
in Partial Fulfillment of the requirements for the
Degree of Doctor of Philosophy at
The University of Windsor

Windsor, Ontario, Canada
1985

© M. Sezai Dincer 1985
All Rights Reserved

833229

To my parents

ABSTRACT

Uniform field steady state ionization growth currents are measured in SF_6 , N_2 and SF_6+N_2 mixtures over the E/p range 60-450 $V\text{ cm}^{-1}\text{ Torr}^{-1}$. Analysis of ionization growth currents provided quantitative data on effective ionization, ionization and attachment coefficients.

The variation of effective ionization coefficient in SF_6+N_2 mixtures is found to be nonlinear with the percentage mixture ratio. It is observed that at a given electric field to gas pressure ratio, the effective ionization coefficient decreases with increasing SF_6 component in the mixture. This reduction in the effective ionization coefficient becomes relatively higher as E/p decreases. However, once a certain concentration of SF_6 in the mixture is reached, further addition of SF_6 responds with relatively little effect on the reduction. The same behaviour is observed for spark over voltage measurements. Variation of spark over voltage with SF_6 concentration shows saturation tendency particularly at high pd (cm-torr) levels.

The data for effective ionization, ionization and attachment coefficients is also obtained in $CCl_2F_2+CO_2$ electronegative gas mixtures where it is again observed that the variation of the effective ionization coefficient with respect to mixture percentage ratio is nonlinear at a given E/p in the interval $100 \leq E/p \leq 180\text{ V cm}^{-1}\text{ torr}^{-1}$

A Monte-Carlo simulation technique is used to provide swarm data in SF₆. The swarm parameters evaluated are compared with the experimental values of drift velocity, ratio of radial diffusion coefficient to mobility, ionization and attachment coefficients available in the literature. The electron-molecule collision cross sections adopted in the simulation resulted in good agreement with the experimental values over the E/p range of interest $100 \leq E/p \leq 180 \text{ V cm}^{-1} \text{ Torr}^{-1}$.

The simulation is also extended to EXB uniform fields to observe the effect of perpendicularly applied magnetic fields on the swarm parameters of SF₆.

ACKNOWLEDGEMENTS

I would like to express my deep appreciation and gratitude to my supervisor, Prof. Dr. G. R. Govinda Raju for the opportunity to study under his guidance, for constant encouragement, assistance and helpful suggestions throughout the progress of this work.

I wish to thank Dr. R. Hackam, Professor and Head of Electrical Engineering Department, for his valuable assistance with the experimental system and for letting me use the capacitive manometer during the entire period of this project.

I would like to thank Professor Dr. A. Watson and Professor Dr. W. E. Bayliss of Physics Department for their valuable discussions on part of this work.

I also thank the National Sciences and Engineering Research Council of Canada for providing funds for this project.

Thanks are also due to J. M. Novosad and D. K. Liebsh for their technical assistance.

Last, but not least, I thank Mrs. A. Zeleney for typing this manuscript.

TABLE OF CONTENTS

ABSTRACT	v
ACKNOWLEDGEMENTS	vii
LIST OF FIGURES	xi
LIST OF TABLES	xvi
LIST OF APPENDICES	xvii
NOMENCLATURE	xviii
 CHAPTER	
I. INTRODUCTION	1
1.1 Introduction	1
1.2. Previous Work	2
1.3 Nature of the Present Investigations.	7
 II. EXPERIMENTAL TECHNIQUES AND PROCEDURE	
2.1 Uniform Field Electrodes	9
2.2 Test Chamber and Vacuum System	11
2.2.1 Test Chamber	11
2.2.2 Ion and Sorption Pumps	12
2.2.3 Gas Handling System	13
2.3 High Voltage Supply and Voltage and Current Measurements	14
2.4 Experimental Procedure	14
 III. EXPERIMENTAL STUDIES IN SF ₆ and SF ₆ +N ₂ GAS MIXTURES	
3.1 Introduction	21
3.2 Ionization Growth Curves	24
3.2.1 Behaviour of Ionization Growth in SF ₆	25
3.2.2 Ionization Growth in N ₂	29
3.2.3 Ionization Growth Currents in SF ₂ +N ₂	29
3.3 Analysis of Current Growth Data	37
3.3.1 Effective Ionization Coeffi- cients in SF ₆ and SF ₆ +N ₂	46
3.3.2 Ionization and Attachment Coefficients in SF ₆ and SF ₆ +N ₂	52
3.3.3 Apparent Secondary Ionization Coefficients	57
3.4 Breakdown Voltage Measurements	61

CHAPTER

IV.	IONIZATION GROWTH IN $\text{CCl}_2\text{F}_2 + \text{CO}_2$ BINARY GAS MIXTURES	64
	4.1 Introduction	64
	4.2 The Effective Ionization Coefficients	65
	4.3 Sparking Potentials	71
	4.4 Critical E/p Limits	73
	4.5 Ionization and Attachment Coefficients	76
V.	THEORETICAL CALCULATION OF SWARM PARAMETERS IN SF_6 UNDER UNIFORM FIELDS	79
	5.1 Introduction	79
	5.2 Electron Dynamics in Uniform Electric Fields	85
	5.3 Collision Cross Sections	92
	5.3.1 Momentum Transfer Cross Section	94
	5.3.2 Electronic Excitation Cross Section	95
	5.3.3 Attachment Collision Cross Section	95
	5.3.4 Ionization Collision Cross Section	97
	5.3.5 Vibrational Collision Cross Section	97
	5.4 Deciding on the Nature of Collision	98
	5.5 Computational Method	100
	5.5.1 Introduction	100
	5.5.2 Swarm Parameters	101
	5.6 Results and Discussion	103
	5.6.1 Back Scattering Coefficient	104
	5.6.2 Drift Velocity, Longitudi- nal Diffusion Coefficient and Ratio of Radial Diffu- sion Coefficient to Mobility	104
	5.6.3 Ionization and Electronic Excitation Coefficients	113
	5.6.4 Attachment Coefficient	117
	5.6.5 Energy Distributions and Mean Energy	117
	5.7 Conclusions	125
VI.	BEHAVIOUR OF SWARM PARAMETERS IN EXB UNIFORM FIELDS	126
	6.1 Introduction	126

CHAPTER

6.2	Model and Theory	127
6.3	Results and Discussion	130
6.3.1	Transverse, Perpendicular Drift Velocities and the Magnetic Deflection Angle . . .	130
6.3.2	Energy Distributions and Average Energy	136
6.3.3	Ionization and Attachment Coefficients	136
VII.	CONCLUSIONS AND RECOMMENDATIONS	145
7.1	Conclusions	145
7.2	Recommendations for Further Studies	148
	APPENDICES	152
	REFERENCES	158
	VITA AUCTORIS	167

LIST OF FIGURES

<u>Figure</u>		<u>Page</u>
1.1	AC Breakdown Voltages of SF ₆ Mixtures with 50 mm Diameter Sphere-Sphere gap . . .	4
2.1	Diagram for Electrical Connections	15
2.2	Schematic Diagram of the Experimental Apparatus	16
2.3	General View of the Experimental Setup	17
2.4	Bushing Arrangement	17
3.1	Ionization Growth Represented by Eq. 3.6	26
3.2	Ionization Growth Curves in SF ₆ at p=5 Torr	27
3.3	Ionization Growth in SF ₆ at p=20 Torr	28
3.4	Ionization Growth in SF ₆ at Higher Values of E/p at p=2 Torr	30
3.5	Ionization growth in N ₂ at p=20 Torr	31
3.6	Ionization Growth in N ₂ at p=5 Torr	32
3.7	Ionization Growth in SF ₆ +N ₂ Mixtures with 2.5% SF ₆ at p=20 Torr	33
3.8	Ionization Growth in SF ₆ +N ₂ Mixture with 5% SF ₆ at p=20 Torr	34
3.9	Ionization Growth in SF ₆ +N ₂ Mixture with 10% SF ₆ at p=50 Torr	35
3.10	Ionization Growth Mixture with 20% SF ₆ at p=25 Torr	36
3.11	Ionization Growth Curves in 20% SF ₆ + 80% N ₂ Mixture at p=5 Torr	38
3.12	Ionization Growth Curves in 40% SF ₆ + 60% N ₃ Mixture at p=5 Torr	39
3.13	Ionization Growth Curves in 80% SF ₆ + 20% N ₂ Mixture at p=5 Torr	40

<u>Figure</u>		<u>Page</u>
3.14	A Typical Current-voltage Characteristic in 60% SF ₆ + 40% N ₂ p=5 Torr, d.03 cm.	42
3.15	Effective Ionization Coefficients in SF ₆	47
3.16	Effective Ionization Coefficients in SF ₆ +N ₂ Mixtures	49
3.17	Effective Ionization Coefficient in SF ₆ +N ₂ Mixtures Subjected to Lower E/p Values	50
3.18	Attachment Coefficient in SF ₆	53
3.19	Experimental E/p Limit for 5% SF ₆ at p=100 Torr (E/p) _{limit} =64.5 V cm ⁻¹ Torr	54
3.20	Experimental E/p Limit for 10% SF ₆ at p=50 Torr. (E/p) _{limit} =73.5 V cm ⁻¹ Torr ⁻¹	55
5.21	Experimental E/p Limit for 20% SF ₆ at p=25 Torr. (E/p) _{limit} 82 V cm ⁻¹ Torr ⁻¹	56
3.22	α/p and η/p in SF ₆ +N ₂ Mixtures	58
3.23	Apparent Secondary Ionization Coefficients in SF ₆ +N ₂ Mixtures	59
3.24	Sparkover Voltages in SF ₆ +N ₂ Mixtures	63
4.1	Ionization Growth Curves in CO ₂ at p=4 Torr	66
4.2	Ionization Growth Curves in CCl ₂ F ₂ +CO ₂ with 20% CCl ₂ F ₂ at p=5 Torr	67
4.3	Effective Ionization Coefficients in CO ₂	69
4.4	Effective Ionization Coefficients in CCl ₂ F ₂ +CO ₂ Gas Mixture	70
4.5	Sparking Potentials as a Function of pd in CCl ₂ F ₂ +CO ₂ Mixtures	72
4.6	Experimental E/p Limits in CCl ₂ F ₂ +CO ₂ Mixtures	74

<u>Figure</u>	<u>Page</u>
4.7 Breakdown Voltages in $\text{CCl}_2\text{F}_2 + \text{CO}_2$ Mixtures at $p=760$ Torr	75
4.8 Variation of Ionization and Attachment Coefficients in 20% CO_2 + 80% CCl_2F_2	77
4.9 Variation of α/p and n/p in $\text{CCl}_2\text{F}_2 +$ CO_2 Mixtures with 40% and 60% CO_2	77
5.1 The Link Between Microphysical and Macroscopic Properties	80
5.2 Percentage Difference in Mean Free Flight Times at the Beginning and End of a time Step	89
5.3 Percentage Difference in Mean Free Flight Times at the Beginning and End of a Time Step for Electron Energies over 3 eV	90
5.4 Electron-molecule Collision Cross Sections in SF_6	93
5.5 Deciding on the Nature of Collision	99
5.6 Back Scattering Coefficient at 0.1 eV Emission Energy	105
5.7 Variation of Average Distance Along the Field Direction with Respect to Time at $E/p=100 \text{ V cm}^{-1}\text{Torr}^{-1}$	106
5.8 Variation of Average Distance Along the Field Direction with Respect to Time at $E/p=120 \text{ V cm}^{-1}\text{Torr}^{-1}$	107
5.9 Variation of Average Distance Along the Field Direction with Respect to Time at $E/p=150 \text{ V cm}^{-1}\text{Torr}^{-1}$	108
5.10 Variation of Average Distance Along the Field Direction with Respect to Time at $180 \text{ V cm}^{-1}\text{Torr}^{-1}$	109
5.11 Drift Velocities in SF_6	111
5.12 Longitudinal Diffusion Coefficient	112

<u>Figure</u>		<u>Page</u>
5.13.	D_{\perp}/μ in SF_6	114
5.14	Ionization Coefficient in SF_6	115
5.15	Electronic Excitation Coefficient	116
5.16	Attachment Coefficient	118
5.17	Energy Distribution Sampled per Mean Free Flight Time at 100 E/p V $cm^{-1}Torr^{-1}$	119
5.18	Energy Distribution Sampled per Mean Flight Time at E/p=120 V $cm^{-1}Torr^{-1}$	120
5.19	Energy Distribution Sampled per Mean Flight Time at E/p=150 V $cm^{-1}Torr^{-1}$	121
5.20	Energy Distribution Sampled per Mean Free Flight Time at E/p=180 V $cm^{-1}Torr^{-1}$	122
5.21	Mean Energy in SF_6	123
6.1	A Basic Flowchart for the Simulation	129
6.2	Average Drift Distances Along the Electric Field Direction with Respect to Time at 180 V $cm^{-1}Torr^{-1}$ for Various Magnetic Fields.	132
6.3	Average Drift Distances with Respect to Time Along the Electric Field Direction for Various Applied Electric and Magnetic Fields	133
6.4	Variation of Transverse Drift Velocity with Respect to Increasing Magnetic Fields at Constant Applied Electric Fields	134
6.5	Energy Distributions in EXB Fields at E/p=180 V $cm^{-1}Torr^{-1}$	137
6.6	Energy Distributions in EXB Fields at E/p=240 V $cm^{-1}Torr^{-1}$	138
6.7	Energy Distributions in EXB Fields at E/p=300 V $cm^{-1}Torr^{-1}$	139

<u>Figure</u>		<u>Page</u>
6.8	Variation of Average Energy With Increasing Magnetic Fields at Constant Electric Fields	140
6.9	Ionization Coefficients in EXB Fields . . .	141
6.10	Attachment Coefficients in EXB Fields . . .	142
A.1	A Point Uniformly Distributed on Unit Sphere	155
A.2	Routine to Find Direction Cosines	155

LIST OF TABLES

<u>Table</u>		<u>Page</u>
1.1	Dew Points in SF ₆ +N ₆ Mixtures	6
3.1	Experimental Range of E/p	45
3.2	Accuracy of Experimental Measurements	46
3.3	(α-n)/p in SF ₆ Mixtures at Lower E/p	51
3.4	(α-n)/p in SF ₆ +N ₂ Mixtures	52
4.1	α-n/p in CCl ₂ F ₂ +CO ₂ Mixtures	71
4.2	E/p Limit and α/p for Various CO ₂ Concentrations	73
4.3	Breakdown Field Strength of CCl ₂ F ₂ + CO ₂ Mixtures at p=760 Torr	76
6.1	Ratio of Perpendicular Drift Velocity to Transfers Drift Velocity and the Magnetic Deflection Angle	135
6.2	Critical B/p Limits in SF ₆	143

LIST OF APPENDICES

<u>Appendix</u>	<u>Page</u>
I. Distribution of Free Time Between Collisions	152
II. Isotropic Scattering	154
III. Deciding on the Nature of Collision . .	157

NOMENCLATURE

B	magnetic field flux density, T
D_I	radial diffusion coefficient, cm^2s^{-1}
D_L	longitudinal diffusion coefficient, cm^2s^{-1}
d	electrode gap, cm
E	electric field, V/cm
e	electron charge, C
I	ionization current, A
I_O	externally maintained photoelectric current, A
L	mean free path, cm
M	molecular mass, gm
m	electron mass, gm
N	molecular number density, dimensionless
n	number of electrons, dimensionless
n_C	average number of collisions in time t, dimensionless
n_O	number of initial electrons, dimensionless
n_+	number of positive ions, dimensionless
n_-	number of negative ions, dimensionless
n^*	number of excited states, dimensionless
$P(t)$	<u>probability distribution function, dimensionless</u>
p	pressure, Torr
Q_M	momentum transfer cross section, cm^2
Q_T	total collision cross section, cm^2
Q_V	vibrational excitation cross section, cm^2
Q_{at}	attachment collision cross section, cm^2

Q_{ex}	electronic excitation cross section, cm^2
Q_{ion}	ionization collision cross section, cm^2
R	random number, dimensionless
R	radial position of an electron, cm^2
V_0	initial electron velocity, $cm\ s^{-1}$
V_p	perpendicular velocity, $cm\ s^{-1}$
V_s	sparkover voltage, V
V_z	transverse velocity, $cm\ s^{-1}$
V_{ll}	transverse drift velocity, $cm\ s^{-1}$
v	electron velocity, $cm\ s^{-1}$
W	drift velocity, $cm\ s^{-1}$
\bar{z}	average drift distance, cm
$\langle z \rangle$	average value of z, cm
α	ionization coefficient, cm^{-1}
$\bar{\alpha}$	effective ionization coefficient, cm^{-1}
α_{ex}	excitation coefficient, cm^{-1}
e	electron energy, eV
η	attachment coefficient, cm^{-1}
γ'	apparent secondary ionization coefficient dimensionless
λ	back scattering coefficient, dimensionless
μ	mobility, $V^{-1}\ cm^2\ s^{-1}$
μ_m	absorption coefficient, cm^{-1}
ν	collision frequency, s^{-1}
ϕ	azimuthal angle, radian

τ

mean free time, s

θ

polar angle, radian

ϕ_M

magnetic deflection angle, radian

CHAPTER I

i. INTRODUCTION

1.1 Introduction

Power transmission systems are called upon to deliver thousands of megawatts and the demands on them will increase in the future.

Since economical considerations do not permit an arbitrary increase of current carrying capacity, for efficient transmission of high powers, it pays to increase the voltage level rather than the current. The power transmitted is then limited by the limitations on the voltage level. Hence, the insulation medium used and the space between conductors and enclosures play a major role on the transmission capacity.

In a gas under an applied electric field, electrons gain energy and as the voltage is increased, their energy distribution shifts to higher energy range. When a sufficient fraction of the electron population can cause ionization, gaseous dielectric loses its dielectric property and breakdown occurs. An effective way to prevent breakdown initiation is to remove the electrons from the

medium by attachment to gas molecules forming negative ions.

Of the many negative ion forming gases SF_6 (Sulphur-hexafluoride) has found a wide range of applications due to its superior insulating properties and chemical stability. However, operating voltages in practical SF_6 systems are only 10-50% of the ideal breakdown voltage as a result of particle contamination and surface effects. In addition, SF_6 is an expensive gas compared to common gases. Since a single gas cannot meet all the requirements of a power apparatus, there is an increasing interest in the possible applications of mixtures of SF_6 and other common gases.

To use a cheaper gas component that is less sensitive to surface roughness or particle contamination while maintaining the required dielectric strength is the major objective to be accomplished. It is also necessary that the new gas mixture should be nonflammable, non-toxic and have adequate temperature range, among other requirements.

1.2 Previous Work

As an important additive to SF_6 , N_2 which is non-toxic, non-flammable and less expensive is found to be very promising for applications in high voltage systems.

One of the earliest investigations in SF_6+N_2 gas mixtures is that of Howard [1], where he has examined

the dielectric strength of the mixture under quasi-uniform fields with AC voltages using 50 mm diameter sphere electrodes up to 5 mm gap distance and a total pressure of 4 bar. Although this investigation clearly indicated the dielectric behaviour of the mixture (Fig. 1.1), at that time there was a lack of interest in the area of gas mixtures.

Uniform and quasi-uniform field breakdown voltage measurements for SF_6+N_2 mixtures have been reported in the literature by Cookson [2], Wieland [3], Baumgartner [4], Ermel [5], Pace et al. [6], and Wootton et al. [7].

These investigations have shown that addition of SF_6 into N_2 increases the breakdown strength appreciably until a certain SF_6 percentage in the mixture is reached. As the percentage of SF_6 is increased further, the mixture exhibits a saturation of breakdown voltage. However, under identical conditions 50% SF_6 + 50% N_2 mixture shows a relative dielectric strength of 88% of pure SF_6 [7] with a reduction of 35% in gas cost.

A reduction of 35% in gas cost alone, may translate into a savings of \$50,000/km of compressed gas insulated transmission lines (CGIT) at 800 KV or \$8,000 for a transformer using 2654 ft³ of gas [8].

Theoretical calculations based on the streamer model show that SF_6+N_2 mixtures are less sensitive to surface

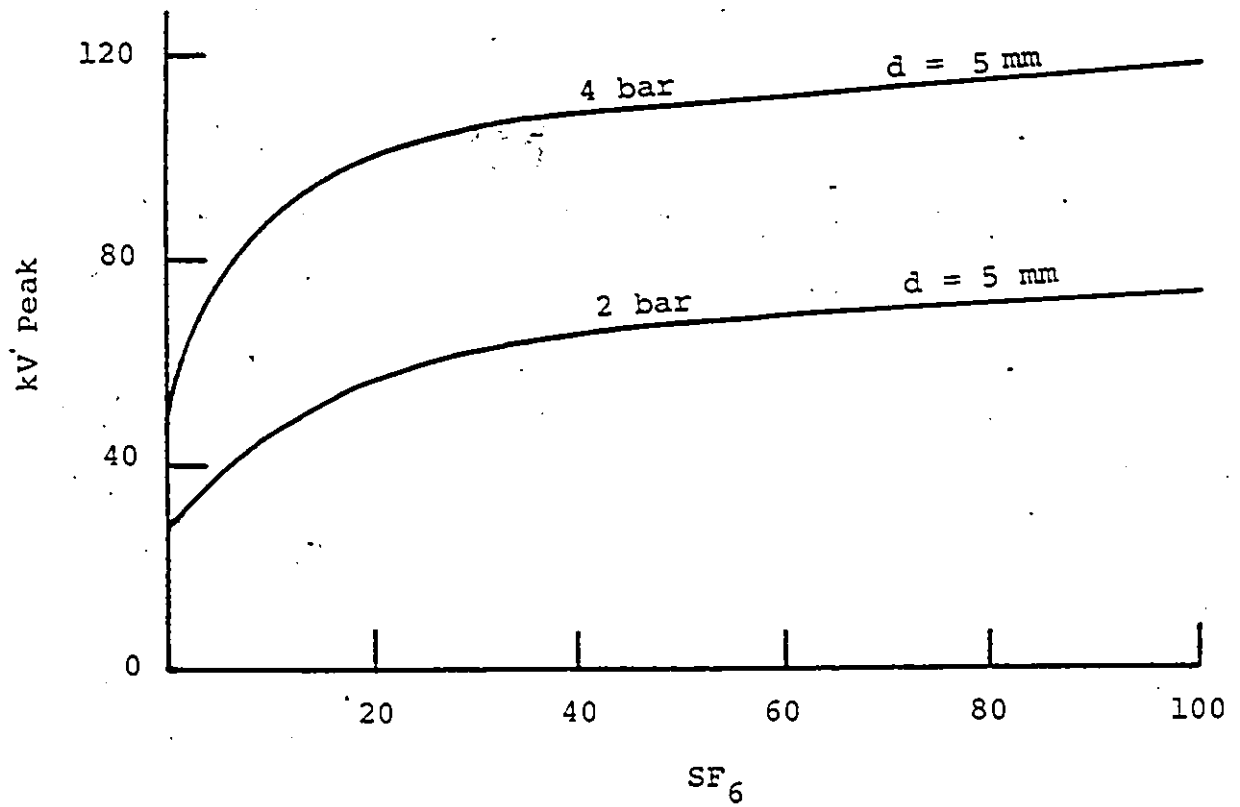


Fig. 1.1. AC breakdown voltages of SF₆/N₂ mixtures with 50 mm diameter sphere-sphere gap [1].

roughness effects on breakdown voltages [9, 10]. There is also experimental evidence to support this behaviour [11].

In a practical gas insulated system, contamination by metallic particles may lower the dielectric strength of pure SF_6 by a factor of 2-10. SF_6+N_2 mixtures have been found to be less susceptible to particle contamination [12, 13,] than pure SF_6 .

SF_6 is widely used in circuit breakers due to its insulation and arc interruption properties. However, there is a possibility of enhancing these properties using N_2 together with SF_6 [14, 15] with respect to the rate of rise of recovery voltage (RRRV) for a synchronous interrupter, SF_6+N_2 mixtures having 50% SF_6 additive showed -1.4 times better performance compared to pure SF_6 at pressures of 1300 to 1900 kPa [14].

Garzon et al. [15] investigated the influence of gas mixture ratio and pressure on the RRRV for SF_6+N_2 mixtures. They observed that the peak in RRRV versus SF_6 percentage moves towards lower SF_6 concentrations at higher pressures.

Furthermore, addition of N_2 into SF_6 extends the operation temperature range. Miners et al. [16] experimentally verified the reduction in dew point that can be achieved in SF_6 by using N_2 . The results are shown in Table 1.1.

Table 1.1
Dew Points in SF₆+N₂ Mixtures

Composition (Vol. %) SF ₆ +N ₂	Loading Pressure at 25°C		
	1 atm	3 atm	5 atm
20/80	-92.1	-77.1	-68.9
40/60	-82.4	-66.9	-57.3
60/40	-76.7	-59.6	-50.5
80/20			
100/00	-68.7*	-50.1	-37.7

* represents sublimation point.

This characteristic of the mixture makes it very suitable for applications in northern climates provided that the other requirements are met.

Due to the promising dielectric behaviour of this binary mixture, investigations into the swarm parameters are of technological interest since the intrinsic properties of the gas dielectric itself are responsible for the effects on breakdown. Quantitative swarm data must be available for discharge modeling or to design a gas insulated apparatus.

However, in most of the previous research concerning SF₆ and SF₆+N₂ gas mixtures, emphasis has been on the measurements of breakdown voltage or its prediction using empirical or semi-empirical expressions [3,5,17,18]. The investigations of Govinda Raju and Hackam, who have used a rigorous approach are an exception [19]. These models may not always be useful and even they can elude a high voltage design engineer [20].

1.3 Nature of the Present Investigations

In order to provide swarm data towards the understanding of performance of SF_6 and its mixtures with N_2 , as a high voltage insulant, experimental and theoretical investigations are undertaken by the author.

1. Very little is known about effective ionization, attachment and ionization coefficients in SF_6+N_2 mixtures [21,22].

In the present work effective ionization coefficients as well as attachment and ionization coefficients are measured in SF_6 and SF_6+N_2 mixtures [23].

These parameters are also measured at lower values of E/p , where E is the applied field in $V\text{ cm}^{-1}$ and p , the gas sample pressure in Torr, for the first time together with limiting values of E/p where $\alpha=n$ [24].

2. Using electron-molecule collision cross sections, a Monte Carlo simulation is used for the first time to provide swarm parameters in SF_6 . The results are then compared with the experimental values [25,26]. The practical applicability of this theoretical approach is to explore the possibility of modelling an electrical discharge in newer dielectrics. A successful theoretical approach may reduce the need to obtain all data on electrical discharges experimentally.

3. The experimental data on effective ionization, ionization and attachment coefficients of $\text{CCl}_2\text{F}_2+\text{CO}_2$ binary gas mixtures is lacking in the literature. These data are provided in this study [27].

4. The response of SF_6 under uniform EXB fields, which may find future applications in high voltage apparatus, is studied using a Monte Carlo simulation technique [28].

The thesis is divided into seven chapters. The first chapter is introductory and the second chapter describes the experimental system designed and used for the experimental investigations. The third and fourth chapters are confined to the experimental part of the present work. Chapter V describes a simulation model for SF_6 swarm parameters. The results obtained are also discussed and compared in that chapter with the available data in the literature.

In Chapter VI, behaviour of swarm parameters for SF_6 in EXB uniform fields is considered. Chapter VII deals with the conclusions and also recommendations are given in this chapter for future investigations.

References and appendices pertaining to the chapters are provided at the end of the dissertation.

CHAPTER II

EXPERIMENTAL TECHNIQUES AND PROCEDURE

This chapter gives information on the experimental system and electrode arrangements designed for the present investigation.

In the steady state measurements, provided that the parameter $E/p=V/pd$ is kept constant by adjusting the applied voltage V and varying the gap distance d where p is the sample pressure, analysis of the ionization and attachment coefficients depends on the current growth curves obtained. The methods used for evaluating the coefficients and the errors involved in these studies are described in Chapter three.

2.1 Uniform Field Electrodes

In uniform field studies of ionization phenomena, the electrode profiles used should meet the main requirement that there should be a uniform electric field in the inter-electrode gap.

The electrode profile consists of a flat region which provides a uniform field and this region is guarded by a curved edge whose purpose is to give a surface over which the electric field is lower than that in the central

region. Electrode profiles which have been in general use are Bruce [29], and Rogowski [30] profiles and they have an empirical basis for the curved parts.

There is experimental evidence that in strongly attaching gases breakdown may occur between the edges of Bruce or 120° Rogowski profiled electrodes [31]. Computer analysis of Harrison [31] has shown that, on the curved part of Bruce profile, the electric field is 10% higher than the flat region and also 120° Rogowski profile has the same behaviour. Although 90° Rogowski profile does not suffer from this effect, its diameter to gap distance ratio which is approximately equal to 10 is a disadvantage.

Harrison has designed a profile solving Laplace's equation on digital computer using finite difference. This profile is a compromise between Bruce and 90° Rogowski profiles and has the added advantage that the field at the curved section is lower than that in the flat region [31].

Hence, the brass electrodes used in this study are machined according to the Harrison profile with an overall radius of 3.36 cm for a gap setting of 1.2 cm. Although in Ref. 31, it was found that the test chamber radius could be reduced to the point where breakdown would occur between the edge of the electrode and the chamber wall without there being any change in the field values along the axis, the distance between the edge of the electrodes

to the test chamber wall, for the worst case, is kept 2.3 times the gap distance.

The anode contains 100 holes each of 0.5 mm diameter and evenly distributed in a central circle of 2 cm diameter. To avoid field distortion [32], the distance between the hole centres is kept greater than twice the hole diameter and gap distances smaller than 3 mm are not used during the experiments.

2.2 Test Chamber and Vacuum System

2.2.1 Test Chamber

The discharge chamber is in the shape of a four-way cross having a volume of approximately 5.6 liters and is made of stainless steel (304 Huntington) with an inner tube diameter of 12.7 cm and a length of 27 cm.

The electrodes are positioned in the centre of the four-way cross with their common axis vertical. The anode is mounted rigidly on an insulating hollow tube machined from ceramics which extends to the top flange of the pyrex glass bushing without discontinuity. The electrical connection is provided by means of an inner stainless steel hollow tube concentric with the ceramic tube. A sapphire window with a light transmission range from 0.25 to 5.5 microns is utilized on the top flange of the glass bushing. This arrangement provides a clear path for the ultra-

violet light to be admitted to the chamber and to fall on the cathode.

The cathode, mounted on a ceramic disc with three adjustable pillars for leveling purposes, has a continuous smooth movement to provide a variation in the gap length up to 1.3 cm. The gap length is measured by a micrometer having an accuracy of 0.01 mm.

At one port of the four-way ionization chamber a classical hot cathode Bayard-Alpert ion gauge is used and, at the other port, a viewport is provided to observe the discharge gap.

2.2.2 Ion and Sorption Pumps

In the system a VacIon 82/s diode pump is used which operates by ionizing gas in a magnetically confined cold cathode discharge. The mechanisms which combine to pump virtually all gases are: trapping of electrons in orbits by a magnetic field, ionization of gas molecules by collision with electrons, sputtering of titanium, diffusion of hydrogen and helium into titanium and dissociation of complex molecules into simple ones for easy pumping.

The pressure at the pump inlet flange over the range 10^{-4} to 10^{-8} torr can be read directly from the VacIon pump control unit.


This ion pump is backed by a sorption pump that operates with liquid nitrogen and synthetic zeolite mole-

cular sieve. The roughing pressure is measured at the inlet by a Huntington TCT-1518 gauge tube and TGC-200 controller in the range of 0.1 to 1000 microns.

2.2.3 Gas Handling System

The gas handling system consists of a capacitance manometer (Model 03 Granville-Phillips), an oil manometer and a rotary pump. The capacitance manometer is a sensitive differential pressure measuring instrument. It permits the accurate comparison of the pressure in a clean vacuum system with a reference pressure without exposing the clean system to oil, mercury, or other manometer fluids.

The capacitance manometer consists of a sensing head, a balancing unit and an indicator. The sensing head has two chambers separated by a thin metal diaphragm. One chamber is directly connected to the clean high vacuum system and the other chamber is connected to the reference pressure side. The diaphragm remains in its equilibrium region as long as the pressures in both chambers are equal. If the pressure in one chamber exceeds that in the other, the diaphragm will be displaced in the direction of the lower pressure. As the diaphragm moves relative to a fixed probe, the capacitance between the diaphragm and probe changes. This change in capacitance unbalances a capacitance bridge in the balance unit result-



ing in an electrical signal which is displayed on the indicator meter. This system will measure differential pressures with a minimum detectable pressure differential of less than 5×10^{-3} Torr.

The reference pressure is provided by an oil manometer, the silicone oil having a specific gravity $0.89/\text{cm}^3$ and a rotary pump on the low vacuum side. The oil manometer is capable of measuring pressures within $\pm 3 \times 10^{-3}$ Torr.

2.3 High Voltage Supply and Voltage and Current

Measurements

Figure 2.1 shows a diagram for electrical connections. Brandenburg Model 2507R and 2807R regulated high voltage supplies are used as a DC voltage source. The line stability against $\pm 10\%$ mains change is 10 ppm. The voltage applied to the ionization chamber is measured within 0.2% for a 0-1000 volts with a Sabtronix Model 12010A digital multimeter. Above 1 KV, Brandenburg Model 139D digital high voltage meter is used with an accuracy of 0.25% .

The ionization currents are measured within $\pm 2\%$ using a type 610C Keithley electrometer from 10^{-12} to 10^{-6} A.

2.4 Experimental Procedure

A schematic diagram of the experimental apparatus is shown in Fig. 2.2 Figures 2.3 and 2.4 show the actual

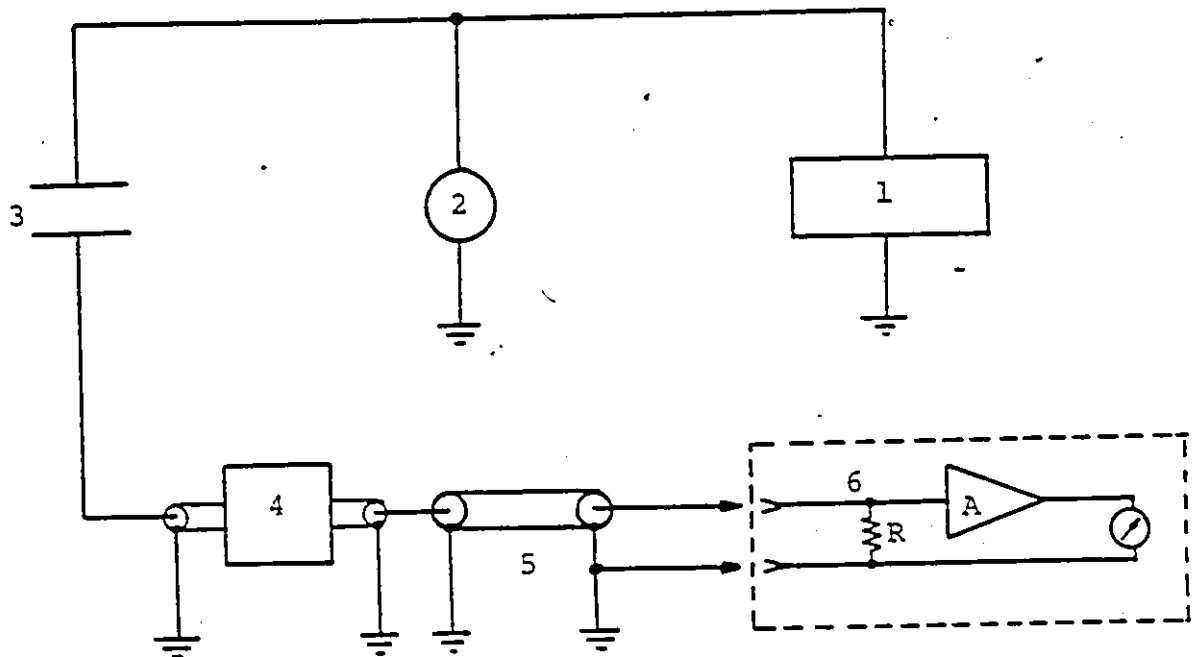


Fig. 2.1. Diagram for electrical connections:
 1) regulated H.V. supply, 2) digital H.V. meter,
 3) test gap, 4) protective device, 5) Teflon
 insulated UHF type connector, 6) electrometer.

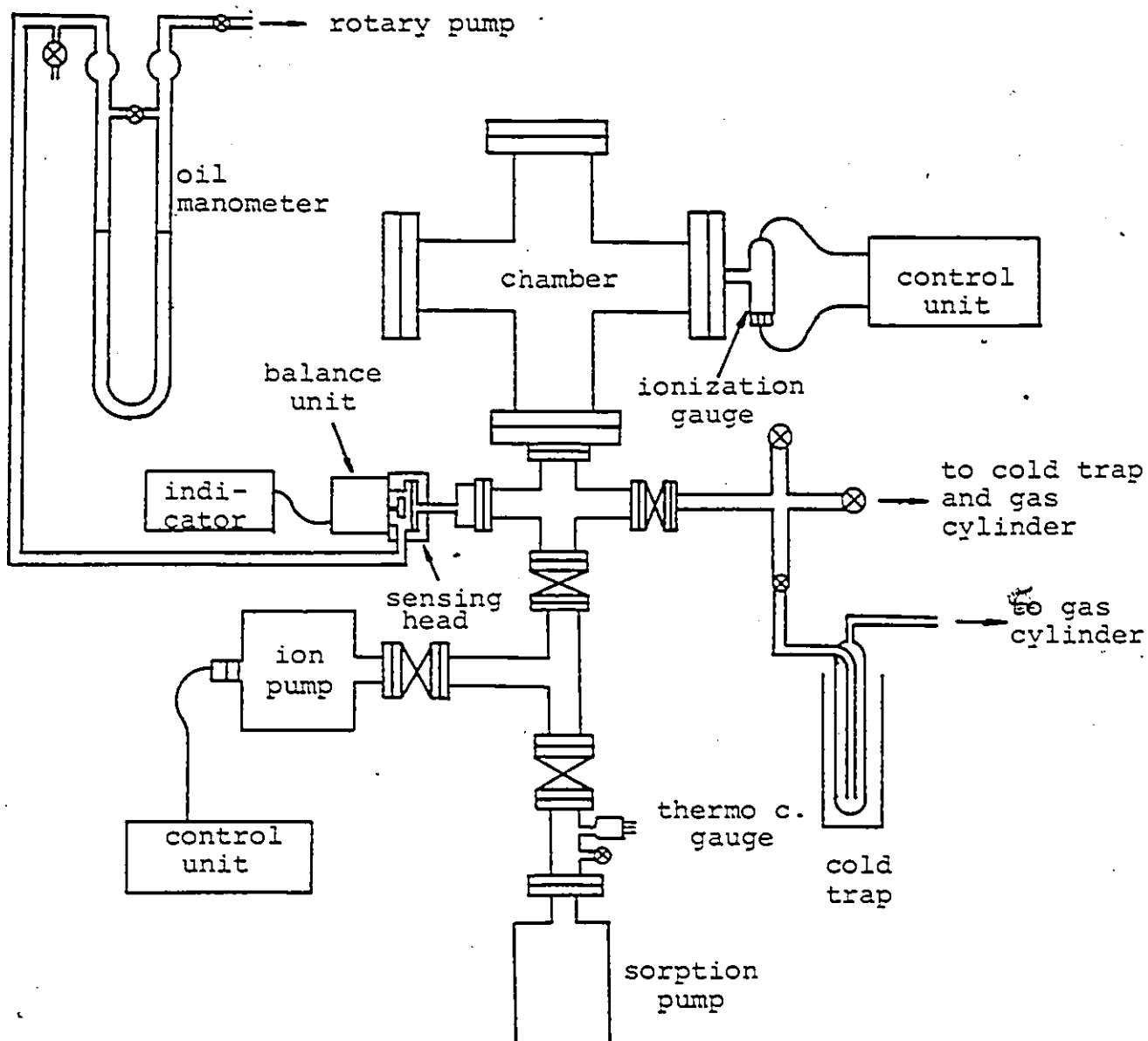


Fig. 2.2. Schematic diagram of the experimental apparatus.

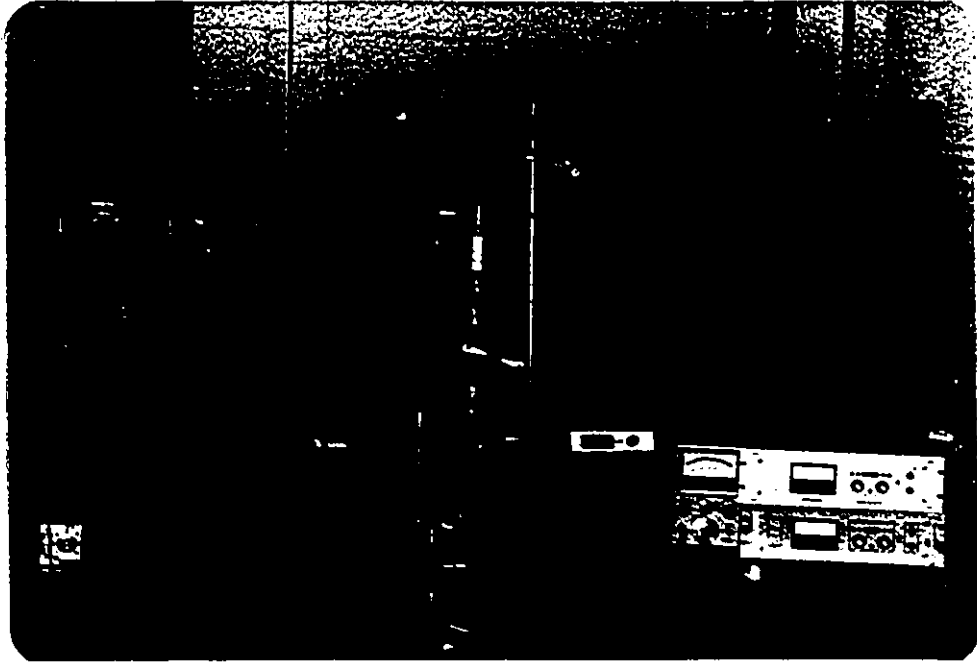


Fig. 2.3. General view of the experimental setup.



Fig. 2.4. Bushing arrangement.

experimental setup. It is a clean high vacuum system constructed from stainless steel and the entire system is bakeable. Copper gaskets are used for compression seals and metal sealed bakeable right angle valves provide isolation for the ionization chamber and sorption and ion pump connections.

Starting from atmospheric pressure the baking process, up to elevated temperatures of 180°C with continuous sorption pumping, requires approximately nine hours to obtain a vacuum of the order of 10^{-5} torr. Occasionally the sorption pump will become saturated and begin to desorb. Then it is necessary to isolate it from the system and remove the liquid nitrogen. The sorption pump desorbs the occluded gas when it is heated by a hot-air blower. Desorbed gases can be removed by pumping with the rotary pump or the sorption pump can be opened to atmosphere. A safety valve is provided against over pressure build-up when the pump is isolated and withdrawn from the liquid nitrogen.

After a base pressure of 10^{-5} torr is obtained, the sorption pump is shut off and the ion pump is operated. An overnight ion pumping results in a vacuum pressure of 10^{-8} torr which is measured at the test chamber by the ionization gauge and a Model 271 Granville-Phillips ionization gauge controller.

In the steady state ionization growth experiment, one of the main sources of error is the instability of the photoelectric current from the cathode surface. The cathode emission stability mainly depends on the photoelectric sensitivity of the surface and the variation in the intensity of the irradiation. In order to obtain a stable cathode surface, the surface is conditioned by running a glow discharge in a few torr of N_2 at 10-20 mA for a period of one hour.

After evacuating the chamber by repeating the pumping procedure, it is observed that, in vacuum (10^{-8} torr), the cathode emission is stable within $\pm 2\%$ for a period of 3 hours, provided that the mercury discharge ultraviolet lamp is warmed up initially for one hour.

The ultraviolet lamp used is a Cenco Mercury Arc light source with a wavelength range from 250 to 280 nanometers. The peak wavelength is at 254 nanometers. The lamp is enclosed in a well ventilated housing with a slot of 4 cm by 2 cm. It is mounted on a base and a stand tube support is used. The intensity of radiation is 250 microwatts per square centimeter at a 50 cm distance from the slot. However, the intensity of the vacuum photoelectric current is found to vary slightly with the electrode gap separation. This fluctuation is avoided by placing the ultraviolet lamp at the focal length of a

sapphire lens located between the lamp and the cathode.

The gas samples are introduced into the system through cold traps (for SF_6 samples maintained at -30°C , for CCl_2F_2 at -25°C and for CO_2 at -60°C) using the gas handling system. In the case of gas mixtures, the gas sample with lower partial pressure is first admitted into the test chamber. The reference pressure on the oil manometer is set to the required sample pressures and the sample introduction is stopped when the pressures on both sides of the diaphragm are equal. Thus, the indicator is used as a null meter.

The stated purity claimed by supplier of the gases used is as follows:

SF_6 - 99.8%, N_2 - 99.9%, CCl_2F_2 - 99.0% (at liquid state) and CO_2 - 99.5%. To remove the condensable impurities, N_2 gas is passed through a cold trap which is immersed into liquid nitrogen. For SF_6 , CCl_2F_2 and CO_2 gas samples, the traps are exposed to liquid nitrogen vapour and when the required trap temperature is reached the gas sample is introduced into the test chamber.

CHAPTER III

EXPERIMENTAL STUDIES IN SF₆, N₂ AND SF₆+N₂

GAS MIXTURES

3.1 INTRODUCTION

The spatial growth of pre-breakdown ionization in a uniform electric field E is dependent on the processes of primary and secondary ionization and in the case of electronegative gases the growth is also affected by processes of attachment.

In SF₆, mass spectrometric measurements indicate that SF₆⁻ and SF₅⁻ are the predominant negative ions exceeding the other possible negative ions (F⁻, F₂⁻, SF₂⁻, SF₃⁻) at least by a factor of 100 [32].

Although quantitative agreement among the different experiments is not perfect [32], there is agreement about the qualitative behaviour. At low E/p where E is the applied electric field and p is the gas pressure, SF₆⁻ is the clearly dominant ion. Above 80 V cm⁻¹ Torr⁻¹ SF₅⁻ becomes dominant. The mass spectrometer analysis indicates the importance of the following reactions [34]:



involving $(SF_6^-)^*$ as an intermediate excited state.

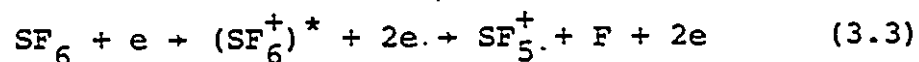
The molecular attachment process, yielding the negative ion of the parent molecule, can only proceed via an excited state, since it is a resonance process and the molecule has a real electron affinity. The excited state, which can be purely vibrational, may either be deactivated collisionally or pass radiatively to the ground state. Another possibility for polyatomic molecules is that the negative ion exists for periods of the order of microseconds, detaching spontaneously after this time.

Reaction 3.2 is the result of dissociative attachment process that can occur before $(SF_6^-)^*$ stabilizes. It is also possible that an autodetachment process may take over before dissociative attachment can proceed. Various authors have determined negative ion life times for SF_6 and found values of the order of tens of microseconds.

The electron detachment process is not yet well understood and quantified for SF_6 [35]. However, the effective detachment coefficient is about one hundred times less than the attachment coefficient up to approximately $150 \text{ V cm}^{-1} \text{ Torr}^{-1}$ [34]. Hence it can be neglected in calculations of current growth analysis.

SF_5^+ is the most dominant ion in the positive ion spectrum of SF_6 . The following reaction requires the

lowest electron energy of 15.8 eV to ionize SF₆ molecule upon impact [36].



Ionization of N₂ results in the formation of the N₂⁺ ion through the reaction



The ground state of N₂⁺ has an appearance potential of 15.6 eV. Other positive ions that can be present in the discharge depending on the experimental conditions are N⁺, N₃⁺ and N₄⁺. The N₂ molecule has also a number of metastable and active states.

For electronegative gases, (or gas mixtures) neglecting detachment processes, the growth of ionization current is [37]:

$$I = I_0 \frac{\left[\frac{\alpha}{\alpha - \eta} \exp[(\alpha - \eta)d] - \frac{\eta}{\alpha - \eta} \right]}{1 - \gamma' [\exp[(\alpha - \eta)d] - 1]} \quad (3.5)$$

where, I is the current at an electrode separation d, and I₀ is the initial externally maintained photoelectric current from the cathodes α, η and γ' are respectively the ionization, attachment and apparent secondary ionization coefficients.

Equation 3.5 is analytically similar to the well known Townsend equation if the parameter η is set to zero.

Provided that only those current measurements are considered in which contributions due to secondary processes are negligible, that is the measurements are restricted to the region where values of the product pd are well below the value at breakdown, Equation 3.5 can be reduced to

$$I = I_0 \left[\frac{\alpha}{\alpha - \eta} \exp[(\alpha - \eta)d] - \frac{\eta}{\alpha - \eta} \right] \quad (3.6)$$

It has also been shown that at the limiting value of the parameter E/p where, $\alpha/p = \eta/p$ [38], the current growth equation can be modified as [39]

$$I = I_0 (1 + \alpha d) \quad (3.7)$$

that is, a plot of I versus d is a straight line and yields I_0 under the experimental conditions where $\alpha/p = \eta/p$, with an accuracy depending on the determination of the (E/p) limit and the accuracy of the current measurements.

3.2 IONIZATION GROWTH CURVES

Measurements of the spatial growth of ionization currents are conveniently expressed as graphs of $\log I$ vs d , and the shape of such curves gives information concerning the mechanism by which ionization develops. In a uniform electric field, when the growth is due to the action of both primary and secondary ionization processes modified by attachment, equation 3.5 gives the form of the growth.

The ideal growth of ionization represented by Equation 3.5 is given in Fig. 3.1.

When the coefficient n is small compared to the effective ionization coefficient, $\bar{\alpha} = \alpha - n$, the form of growth is nearly linear as indicated by region 2-3 of the growth curve. If secondary ionization processes are negligible and the term $\frac{n}{\bar{\alpha}}$ is significant then there is a downward departure from linearity as shown by section 1-2 of the curve. At large values of gap distance d , the current increases more rapidly with gap distance and up-curving can be observed as region 3-4 indicating the significance of secondary ionization processes.

3.2.1 Behaviour of Ionization Growth in SF₆

Figure 3.2 shows typical ionization growth curves at various constant values of the parameter E/p and such data are obtained over the range of $100 \leq E/p \leq 190 \text{ V cm}^{-1} \text{ Torr}^{-1}$ at sample pressures of 5 Torr.

In Fig. 3.3, ionization growth curves are given in SF₆ at 20 Torr for several constant E/p values.

All these curves are obtained from current measurements in the pd region where secondary ionization processes are negligible. It can be seen from these figures that the general behaviour of ionization growth in SF₆ is nonlinear. However, as the parameter E/p increases, the deviation from linearity tends to

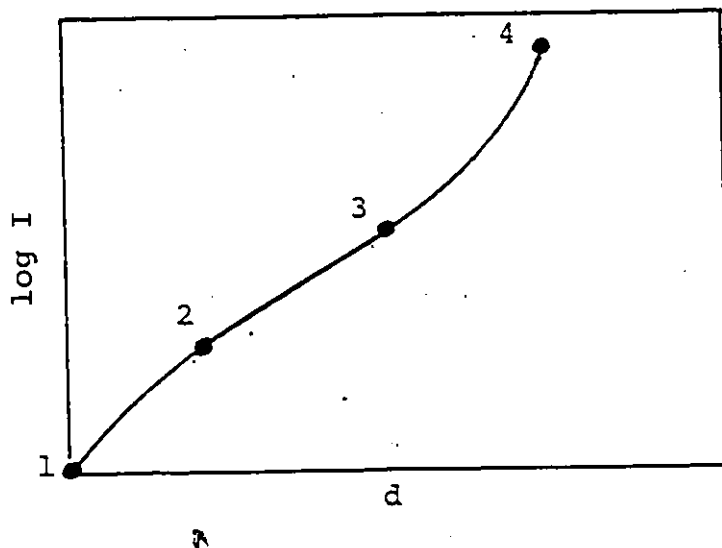


Fig. 3.1. Ionization growth as given by Equation 3.5.

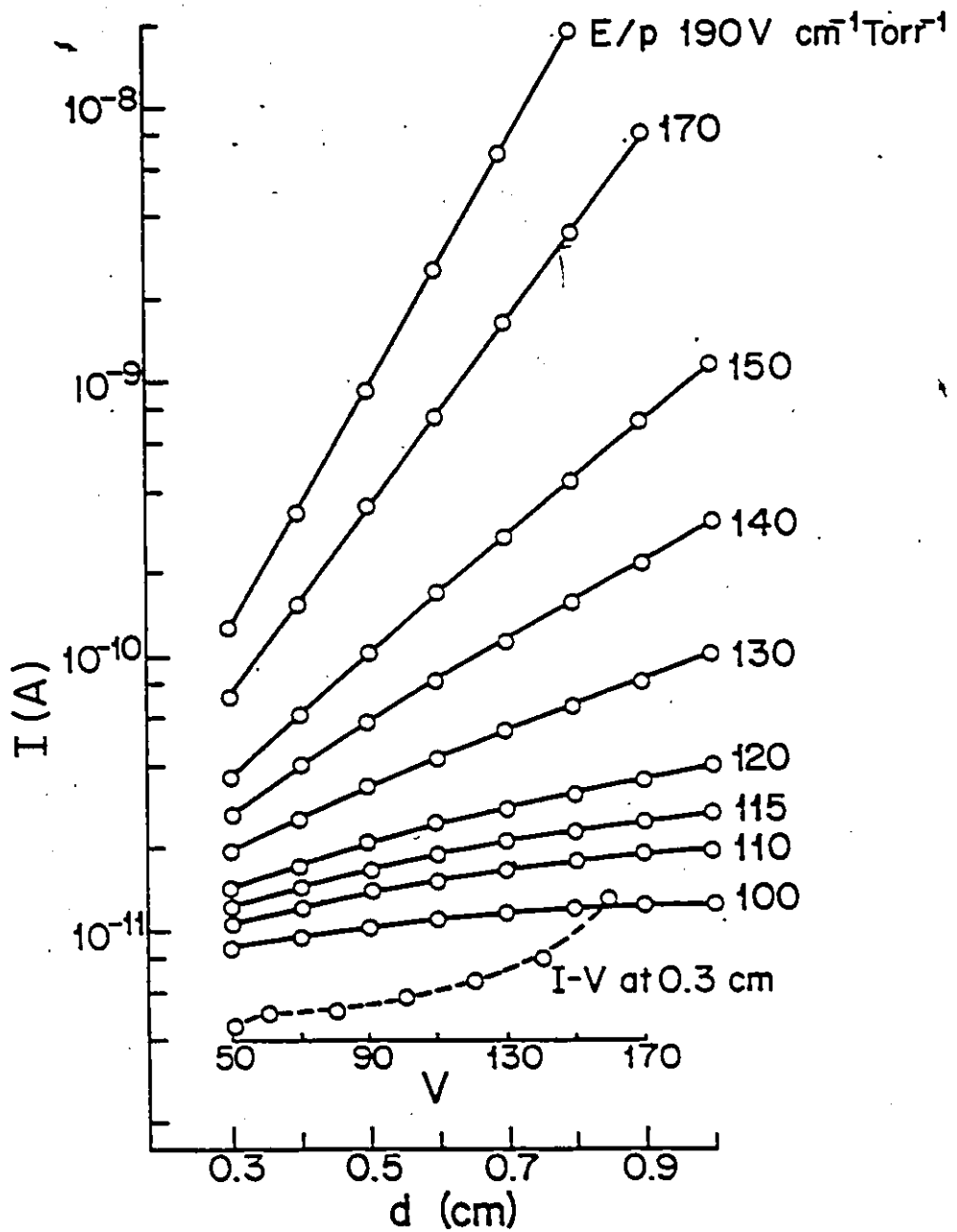


Fig. 3.2. Ionization growth curves in SF₆ at $p=5$ Torr.

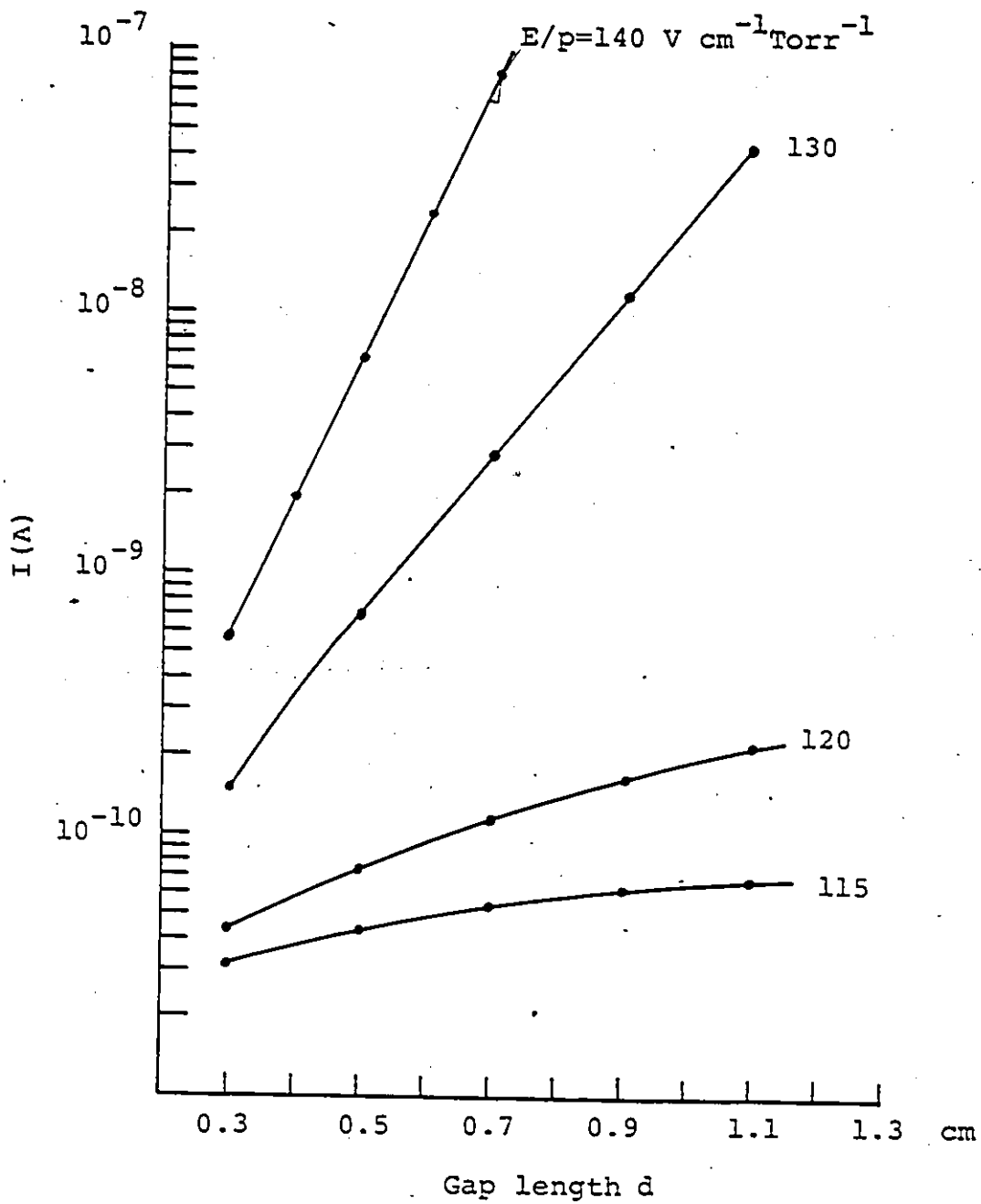


Fig. 3.3. Ionization growth in SF_6 at $p=20$ Torr.

decrease and at high E/p $\log I-d$ curve shows almost linear behaviour as in the case of non-attaching gas.

Such behaviour can be seen from Figure 3.4 where $\log I-d$ growth curves are given in SF_6 at 2 Torr sample pressure for higher values of E/p . On the other hand, at lower E/p , the current amplification becomes so small that the currents saturate with increasing gap distance.

3.2.2 Ionization Growth in N_2

Ionization growth curves in N_2 follow the well known Townsend equation. Figure 3.5 shows typical ionization growth plots at a sample pressure of 20 Torr for N_2 . In this figure, a current-voltage characteristic curve is also given at a fixed gap distance of 0.5 cm.

In Fig. 3.6 growth curves are given in N_2 at 5 Torr sample pressure. Upcurving in the ionization growth plots indicates the significance of the secondary ionization processes.

3.2.3 Ionization Growth Currents in $SF_6 + N_2$

In this section, typical ionization growth curves are given at constant pressure reduced electric fields for $SF_6 + N_2$ mixtures.

The family of curves in Figs. 3.7, 3.8, 3.9 and 3.10 obtained from ionization current measurements are in the

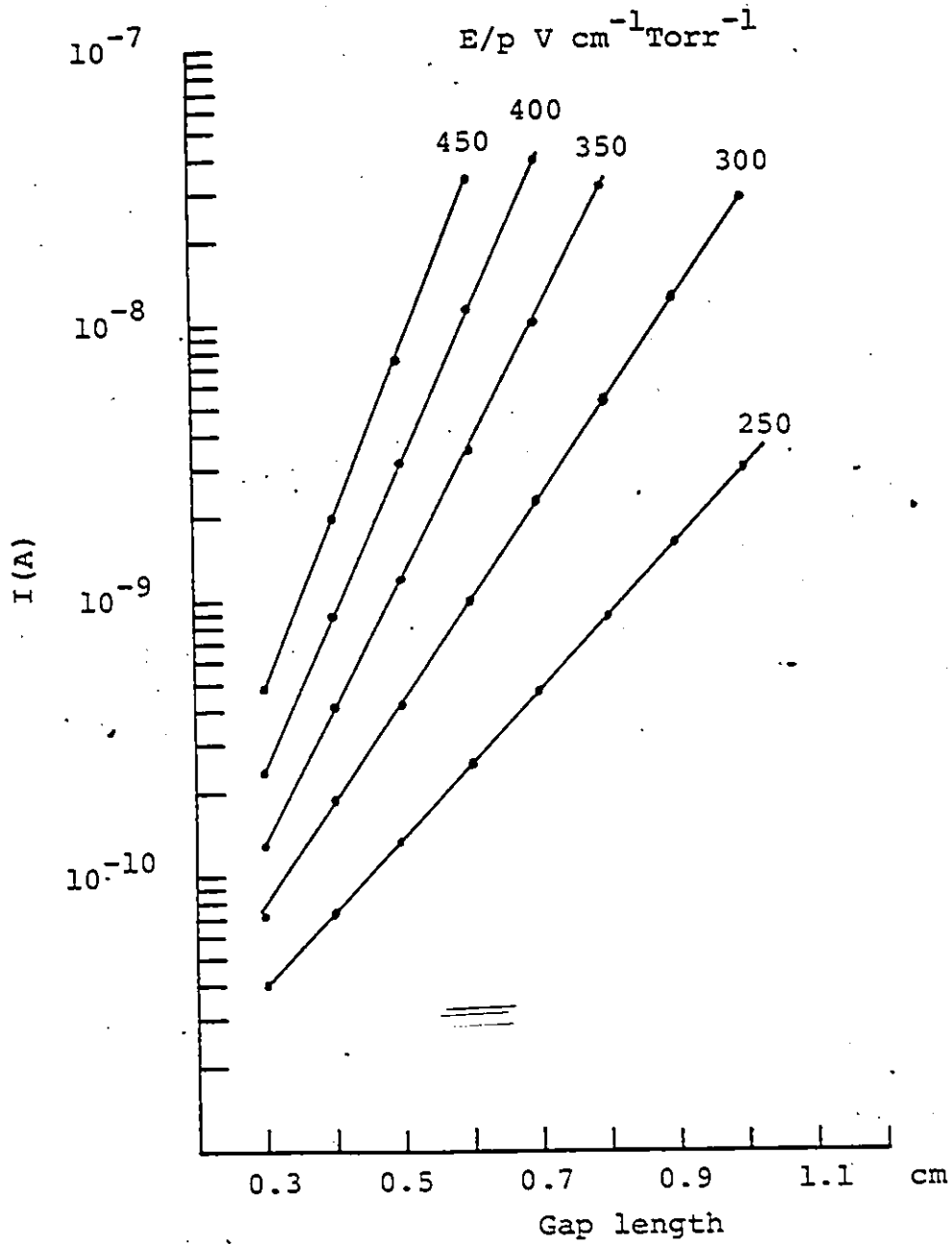


Fig. 3.4. Ionization growth in SF_6 at higher values of E/p at $p=2$ Torr.

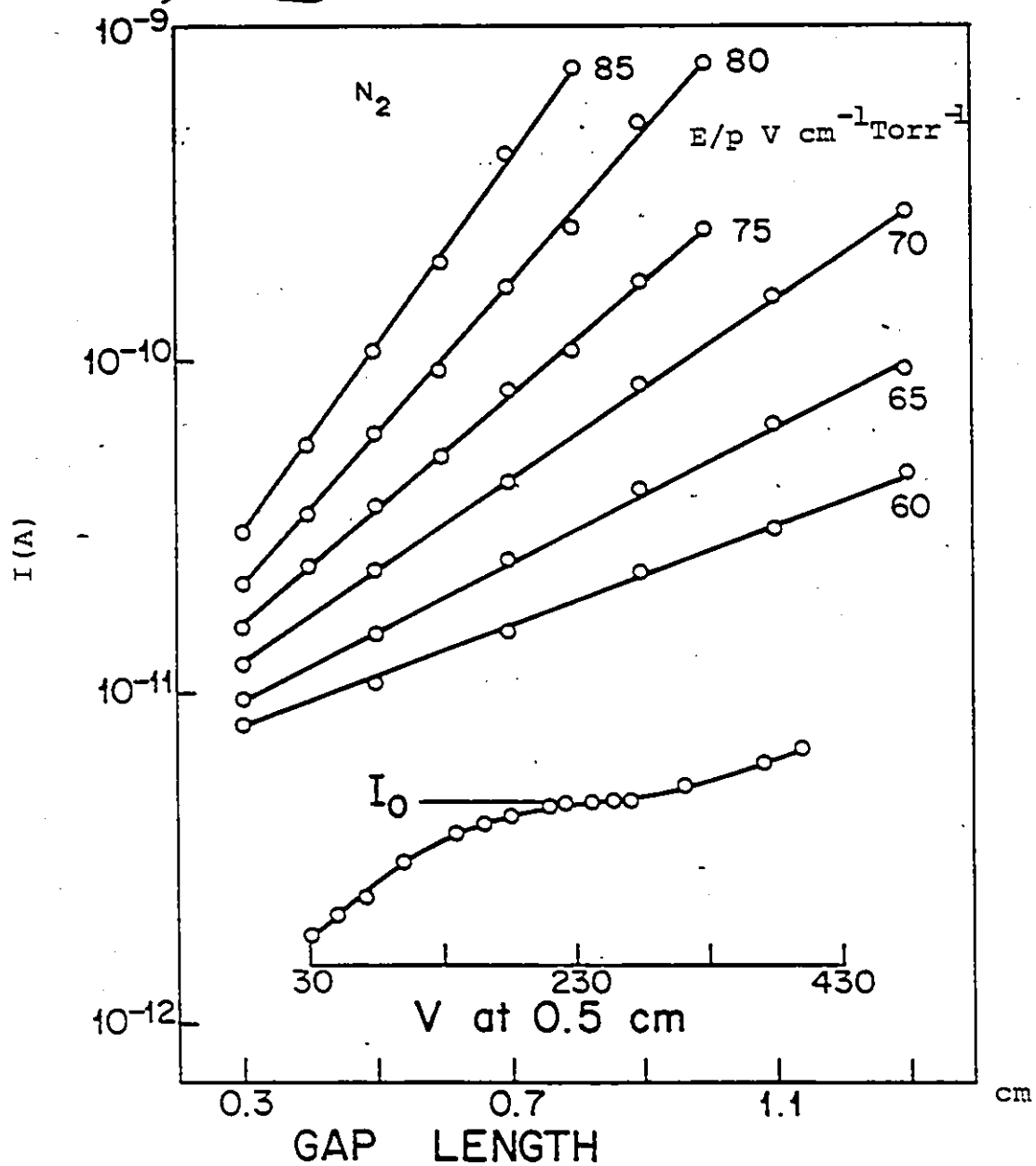


Fig. 3.5. Ionization growth in N_2 at $p=20$ Torr.

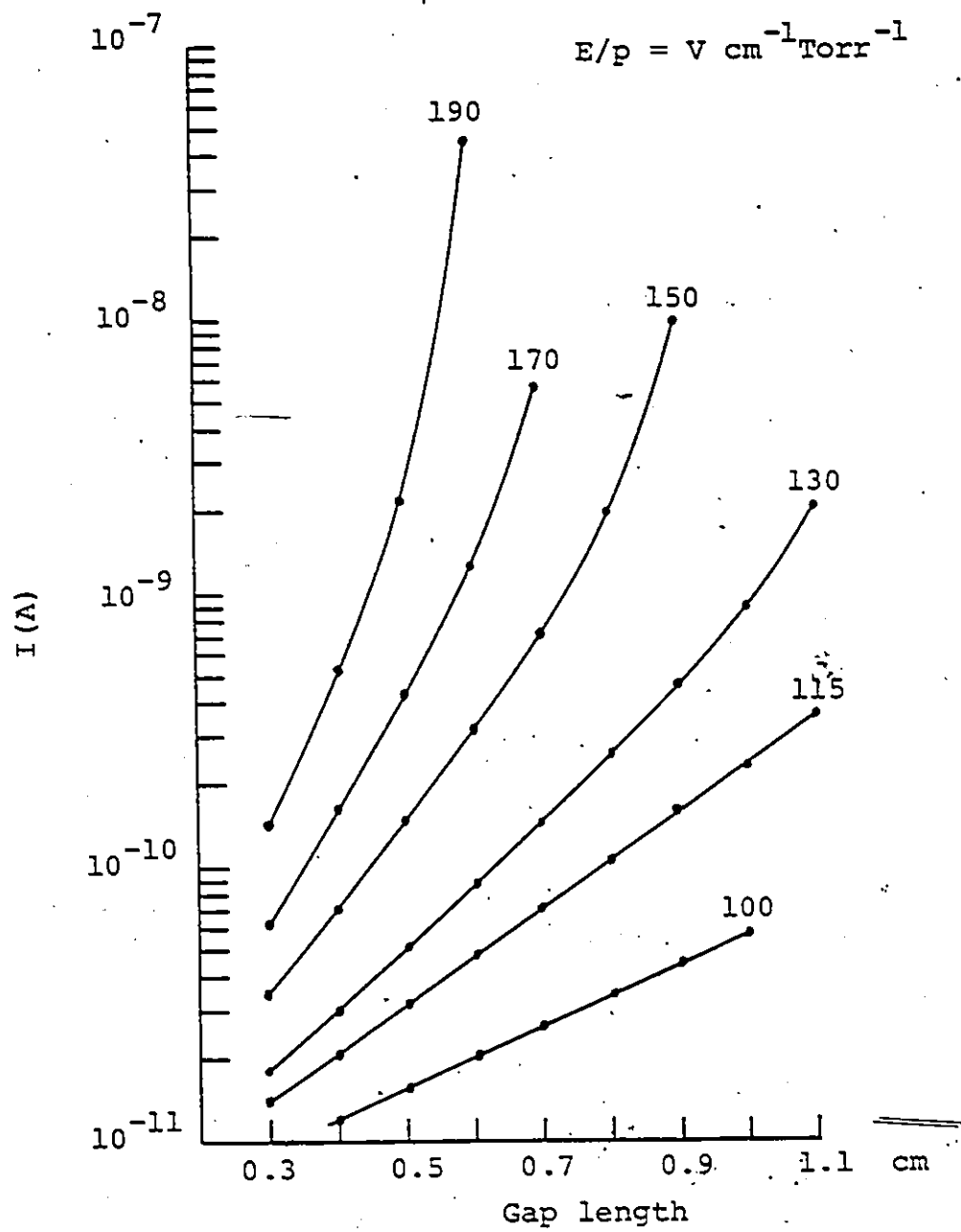


Fig. 3.6. Ionization growth in N_2 at $p=5$ Torr.

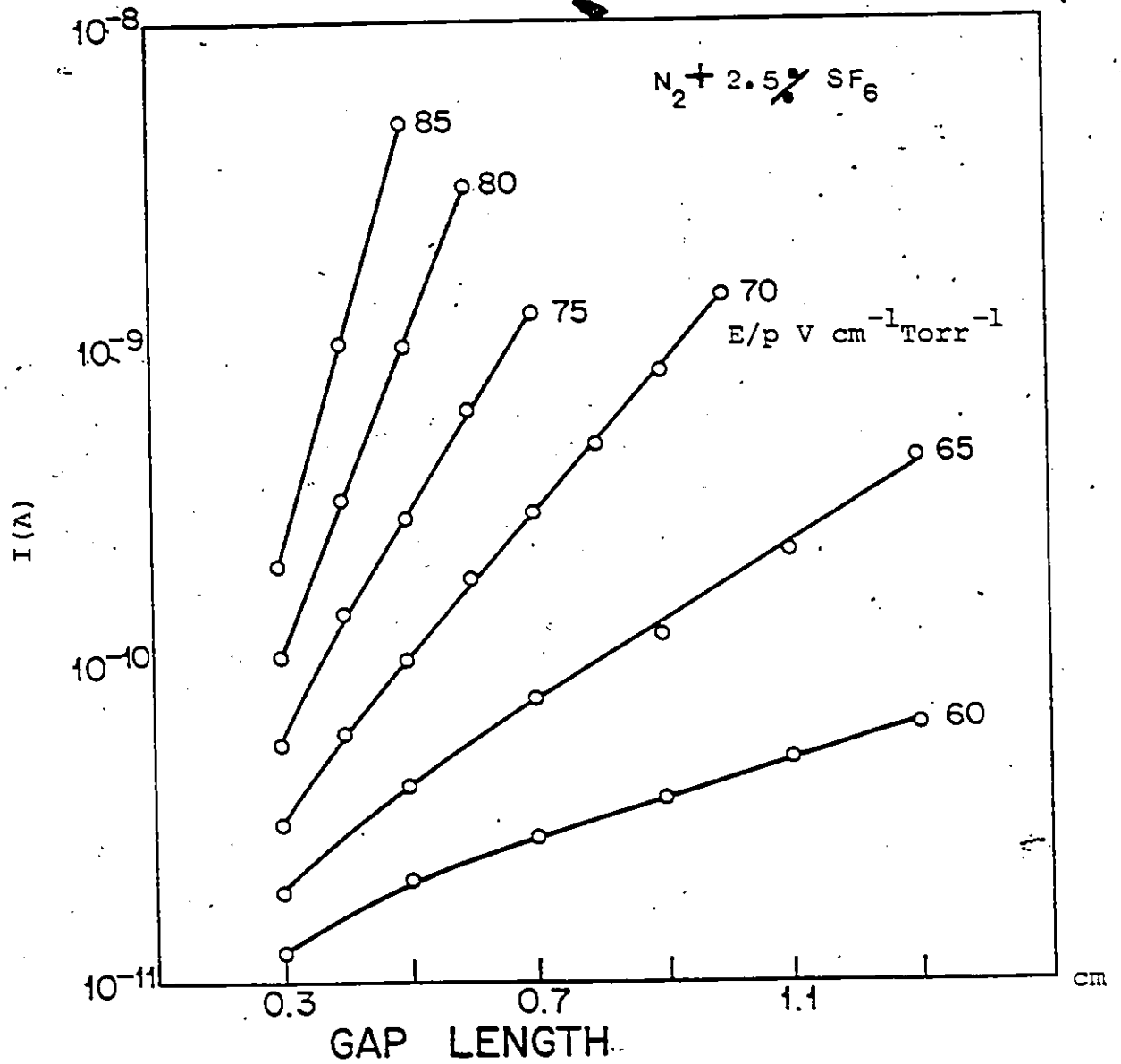


Fig. 3.7. Ionization growth in $SF_6 + N_2$ mixture with 2.5% SF_6 at $p=20$ Torr.

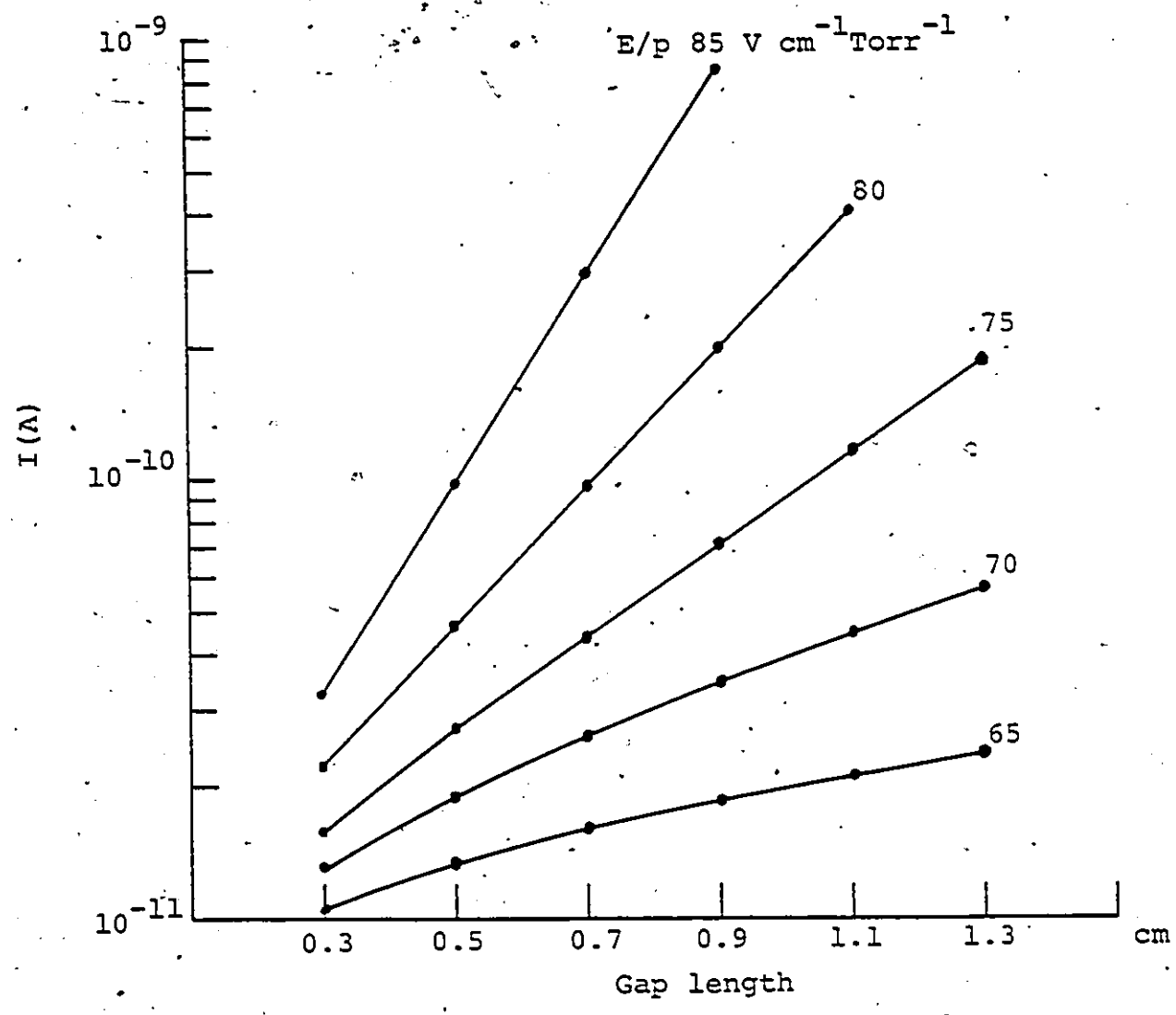


Fig. 3.8. Ionization growth in $\text{SF}_6 + \text{N}_2$ mixture with 5% SF_6 at $p=20$ Torr.

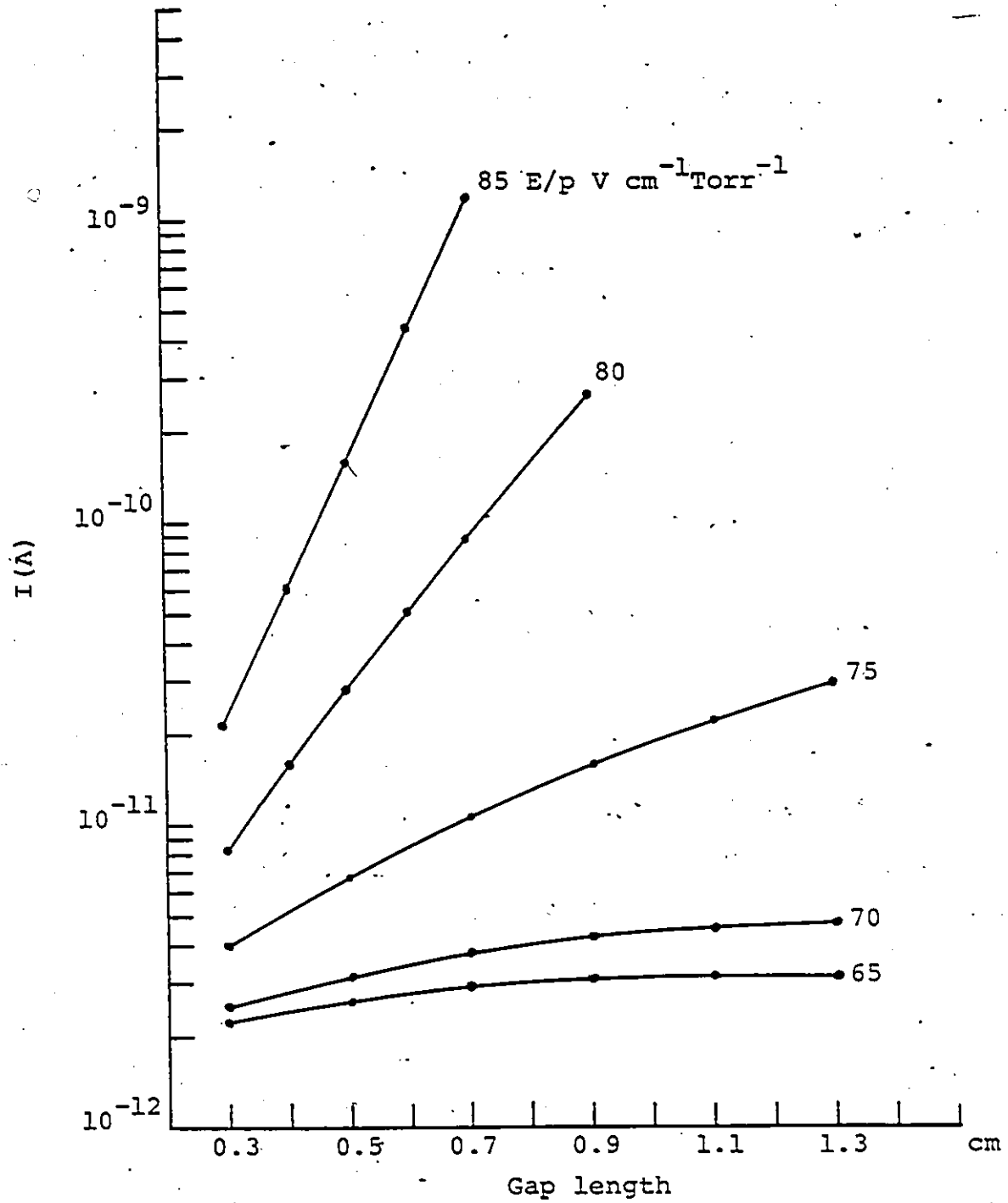


Fig. 3.9. Ionization growth in $\text{SF}_6 + \text{N}_2$ mixture with 10% SF_6 at $p=50$ Torr.

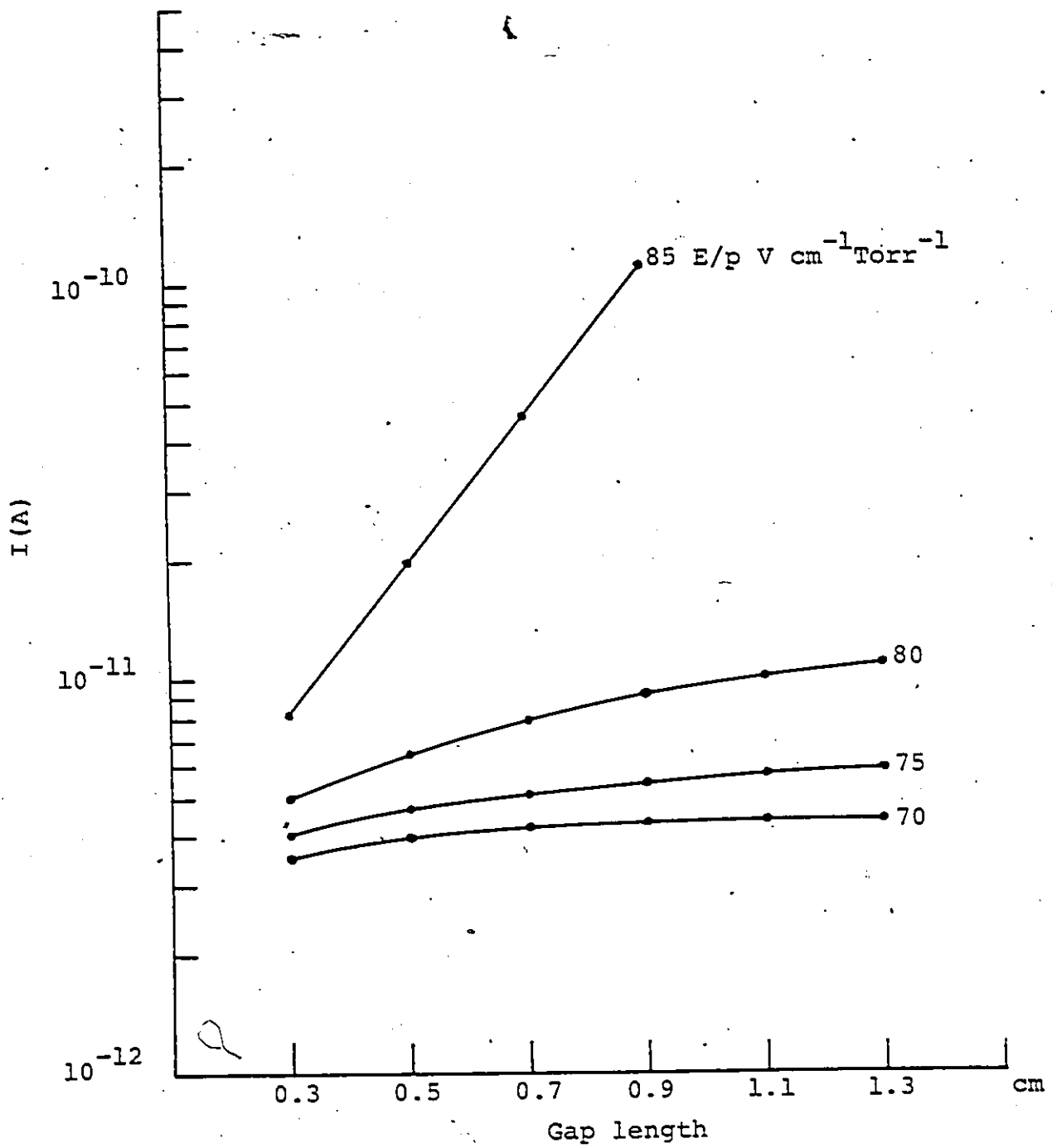


Fig. 3.10. Ionization growth mixture with 20% SF_6 at $p=25$ Torr.

low E/p range of the present investigation. Figures. 3.11 to 3.13 correspond to higher E/p range. Each number on the curves represents the constant pressure reduced electric field E/p $V\text{ cm}^{-1}\text{ Torr}^{-1}$ at which current measurements are carried out by varying the gap distance, d , and adjusting the applied gap voltage.

The general behaviour of ionization growth curves in SF_6+N_2 mixtures is similar as in the case of pure SF_6 , that is $\log I$ vs d plots are nonlinear, and deviation from linearity increases at a constant E/p as SF_6 percentage in the mixture increases. The curvature in the growth curves becomes insignificant at high reduced electric fields. However, the general tendency is that the slope of the growth curve of a constant E/p decreases with increasing SF_6 component in the mixture. The upcurving that can be observed in some of the curves is due to the secondary ionization processes.

3.3 ANALYSIS OF CURRENT GROWTH DATA

Since the ionization and attachment coefficients are not measured directly but determined from experimental ionization growth curves it is necessary to define the method of analysis used.

In N_2 , where secondary ionization processes are negligible, $\log I$ - d plots are linear. Hence, least

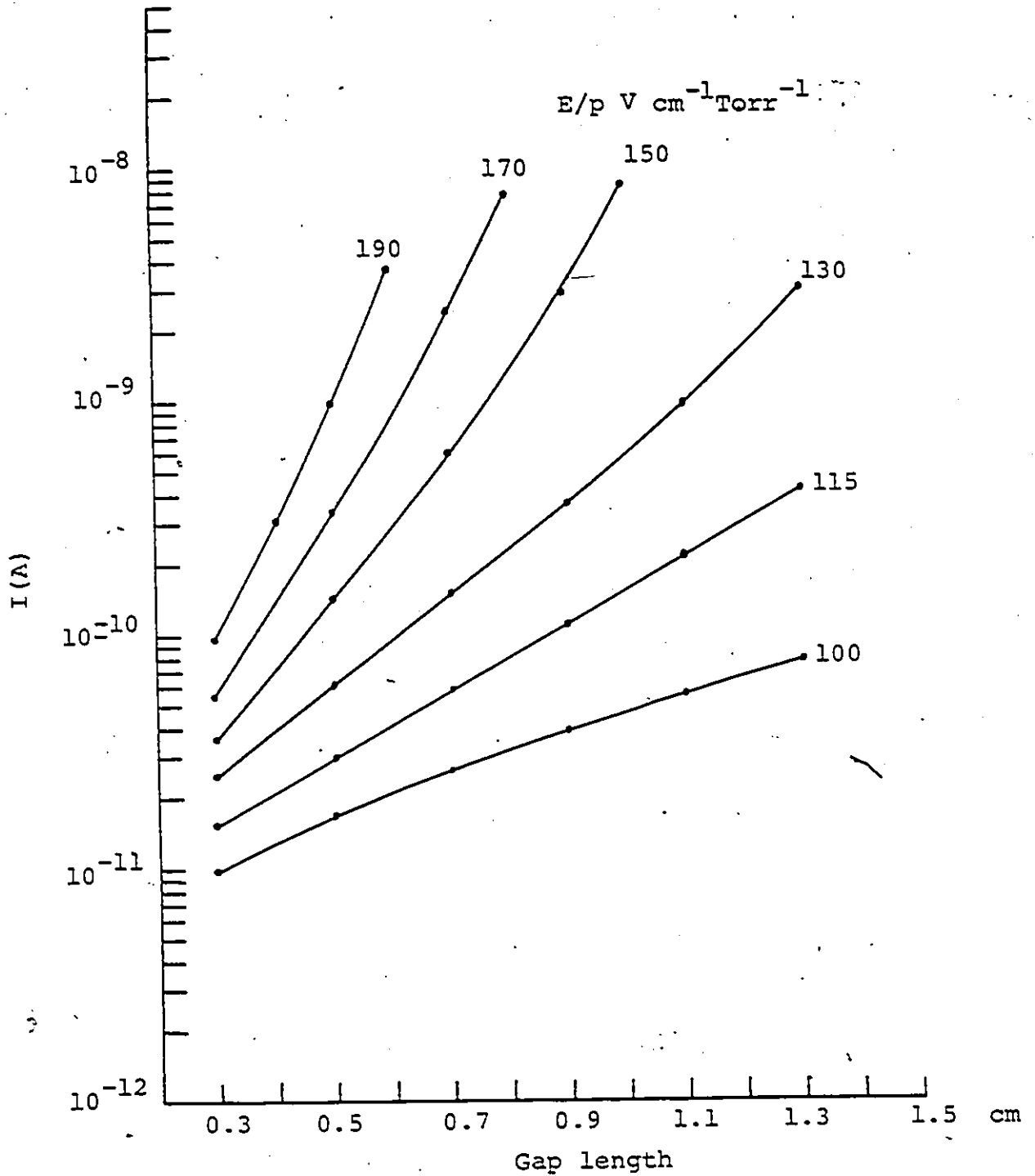


Fig. 3.11. Ionization growth curves in 20% SF_6 + 80% N_2 mixture at $p=5$ Torr.

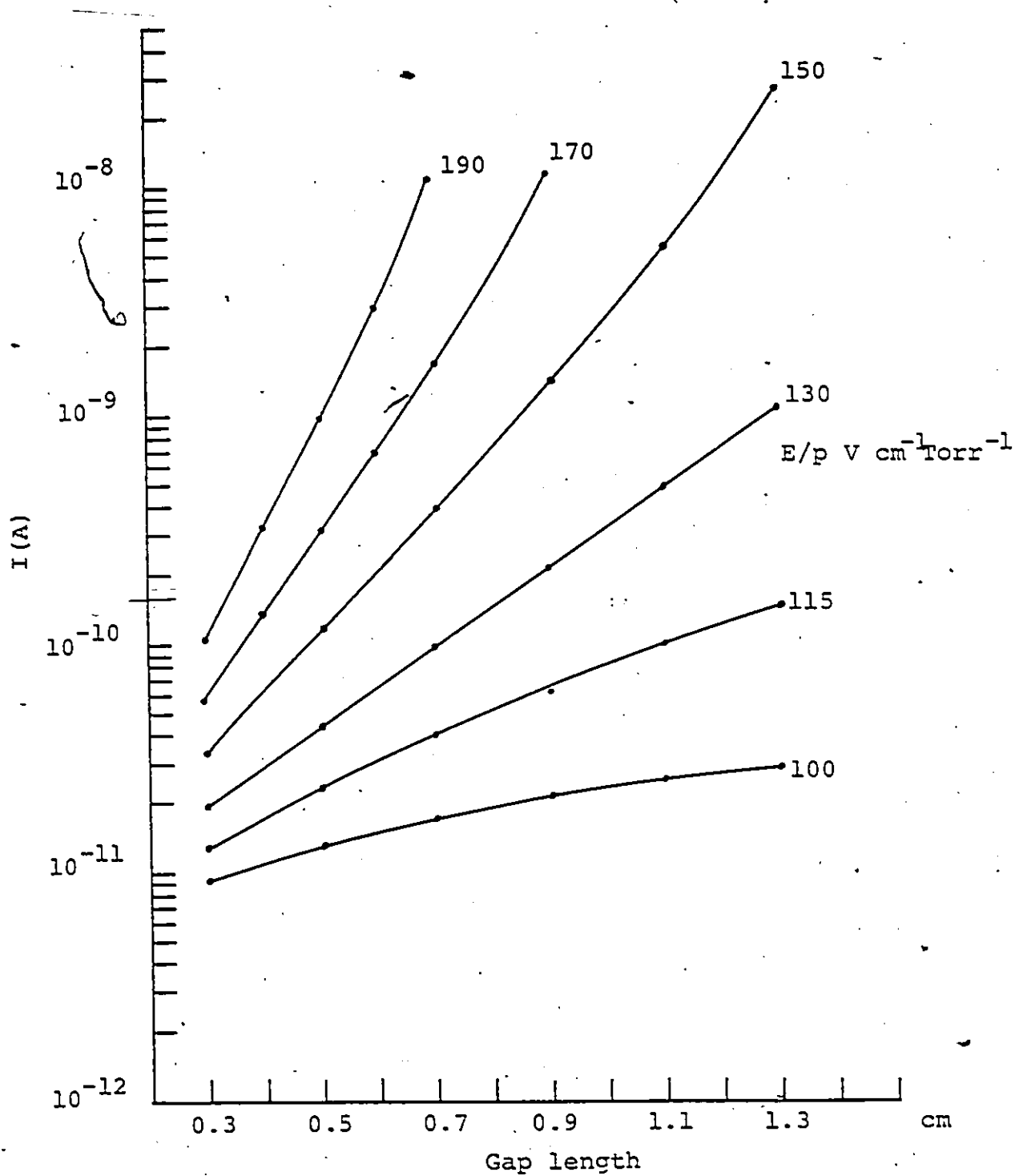


Fig. 3.12. Ionization growth curves in 40% SF_6 + 60% N_2 mixture at $p=5$ Torr.

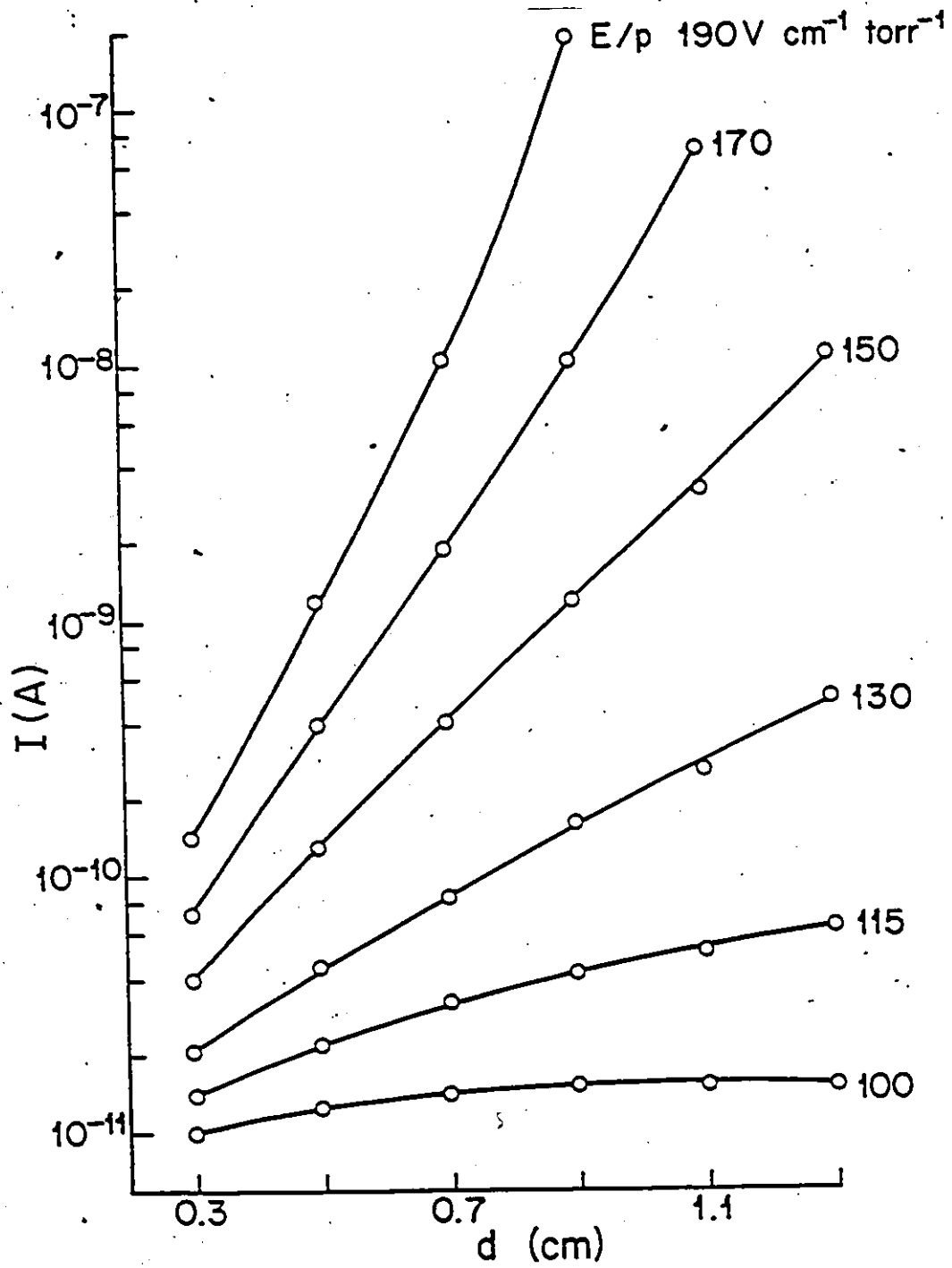


Fig. 3.13. Ionization growth curves in 80% SF_6 + 20% N_2 mixture at $p=5$ Torr.

square analysis yields the first ionization coefficient α from the slope of least square lines and the intercepts give the initial photoelectric current. Such analysis carried out for growth curves in Fig. 3.5 results in a mean value of the photoelectric current, $I_0 = 4.74 \times 10^{-12} \text{ A}$ with $\pm 2\%$ variation. The value obtained from current-voltage saturation curve is $4.65 \times 10^{-12} \text{ A}$ under the same experimental conditions. This confirms that the experimental set-up and procedure is free of systematic errors.

However, it is not always possible to observe current saturation from current-voltage curves obtained at a fixed gap distance. Figure 3.14 shows a typical current-voltage characteristic in 60% SF_6 + 40% N_2 gas mixture at 5 Torr with fixed electrode spacing $d = 0.3 \text{ cm}$. Saturation is not evident.

As mentioned in Section 3.2, evaluation of the coefficients from current growth curves depends on the relative magnitude of these coefficients. Hence, Equation 3.5 should be reduced to the appropriate form for curve fitting.

For those values of E/p at which $\log I-d$ plots indicate sufficient downward curvature Equation 3.6 is employed as

$$I = A \exp(Bd) - C$$

where $A = I_0 [\alpha / (\alpha - n)]$, $B = \alpha - n$ and $C = I_0 [n / (\alpha - n)]$.

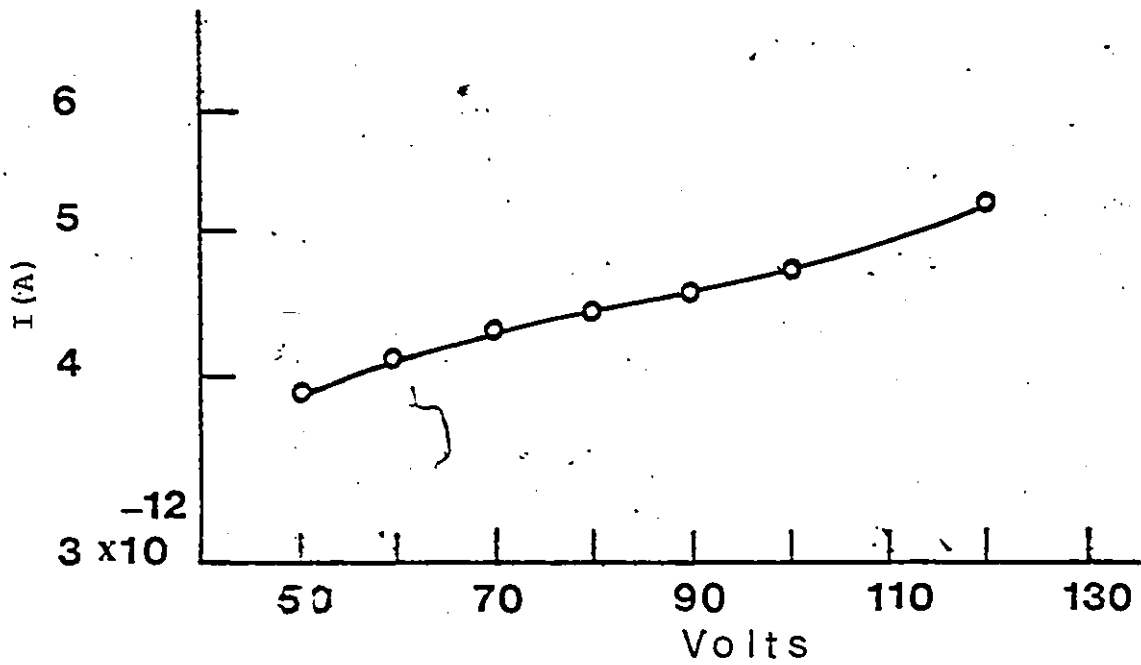


Fig. 3.14. A typical current-voltage characteristic in 60% SF_6 + 40% N_2 $p=5$ Torr, $d=0.3$ cm.

Equation 3.7 is a nonlinear equation with three unknowns A, B and C related by $A-C = I_0$ and $A/C = \alpha/\eta$.

In growth curves where secondary ionization is effective the growth can be represented by

$$I = \frac{A \exp(Bd)}{1-D[\exp(Bd)-1]} \quad (3.8)$$

For log I-d plots where the growth is almost linear, Equation 3.8 can be reduced to $I = A \exp[Bd]$. If only N_2 is under investigation then $A = I_0$ and $B = \alpha$ where D represents secondary ionization coefficient.

A nonlinear least squares program using modified Gauss-Newton iterative method [40, 41] which regresses the residuals on the partial derivatives of the model with respect to the parameters is used to evaluate the coefficients. This program performs a grid search to determine starting values for the parameters before the iteration cycle. Maximum and minimum limits of starting values are found from initial calculations of the slopes of different regions in growth curves. For a growth curve possible models are tried out carrying out initial runs and checking the residual sum of squares and parameter correlation matrices. Then the appropriate equation is chosen.

Another method employed is Modified Gosseries technique [42, 43]. Evaluation of this method has shown

that it is very suitable for the growth curves that can be modelled with Equation 3.6. However, if secondary ionization processes are not negligible, slopes of modified Gosseries least square lines result in an artificially high effective ionization coefficient, α_{-n} , because Eq. 3.6 does not account for the secondary ionization coefficients.

Since the coefficients are calculated from curve fittings it is very difficult to assess the errors on the coefficients. The basis of the estimate is the accuracy of repetition of independent calculations from ionization growth curves. A summary of the growth curves recorded is given in Table 3.1.

Table 3.2 shows the accuracy of experimental measurements.

Table 3.1
Experimental Range of E/p

Gas	E/p (V cm ⁻¹ Torr ⁻¹)	Sample Pressure (torr)	No. of different exp. curve family	$\bar{\alpha}/p$ percentage deviation from mean	
SF ₆	100-115	5	8	4.0	
	120-190	5	7	2.0	
	115-140	20	4	2.5	
	250-450	2	3	2.0	
N ₂	115-190	4	3	1.5	
	115-190	5	2	2.0	
	60-85	20	3	1.5	
SF ₆ +N ₂	60-85	40	3	2.0	
	60-85	20, 100	4, 3	1.5, 2.00	
	65-85	50	4	1.5	
	70-85	25	5	2.5	
	115-190	5	4	1.5	
	115-190	5	4	1.6	
	115-190	5	6	2.0	
	115-190	5	6	2.0	
	SF ₆ %: 2.5				
	5.0				
10.0					
20.0					
20.0					
40.0					
60.0					
80.0					

Table 3.2
Accuracy of Experimental Measurements

	Range	Accuracy %	
Growth current (A)	10^{-12} - 10^{-7}	±2	
Gas pressures (Torr)	2-100	±1.5-±3.3x10 ⁻²	
Electrode separation (cm)	0.3-1.3	±0.05	
		<u>(min)</u>	<u>(max)</u>
Electric field to gas pressure ratio (V cm ⁻¹ Torr ⁻¹)	60-450	±0.3	±2

3.3.1 Effective Ionization Coefficients in

SF₆ and SF₆+N₂

Figure 3.15 shows the effective ionization coefficients, $(\alpha-\eta)/p$ cm⁻¹ Torr⁻¹, in SF₆ obtained in the present study. The effective ionization coefficients are in agreement with those of Bhalla and Craggs [44] and Boyd and Chrichton [45]. In the interval $100 \leq E/p \leq 190$ V cm⁻¹ torr⁻¹, the variation of $(\alpha-\eta)/p$ as a function of E/p is apparently linear. For E/p above 200 V cm⁻¹ Torr⁻¹, the increase in $(\alpha-\eta)/p$ with E/p is not linear. This behavior is also present in the results of Maller and Naidu [46], who used a pressure variation steady state measurement technique. The values of $(\alpha-\eta)/p$ evaluated from pulse techniques in the high E/p range are in contradiction with Maller and Naidu's and present results to the extent that, the pulse technique yields values of $(\alpha-\eta)/p$ which increase linearly

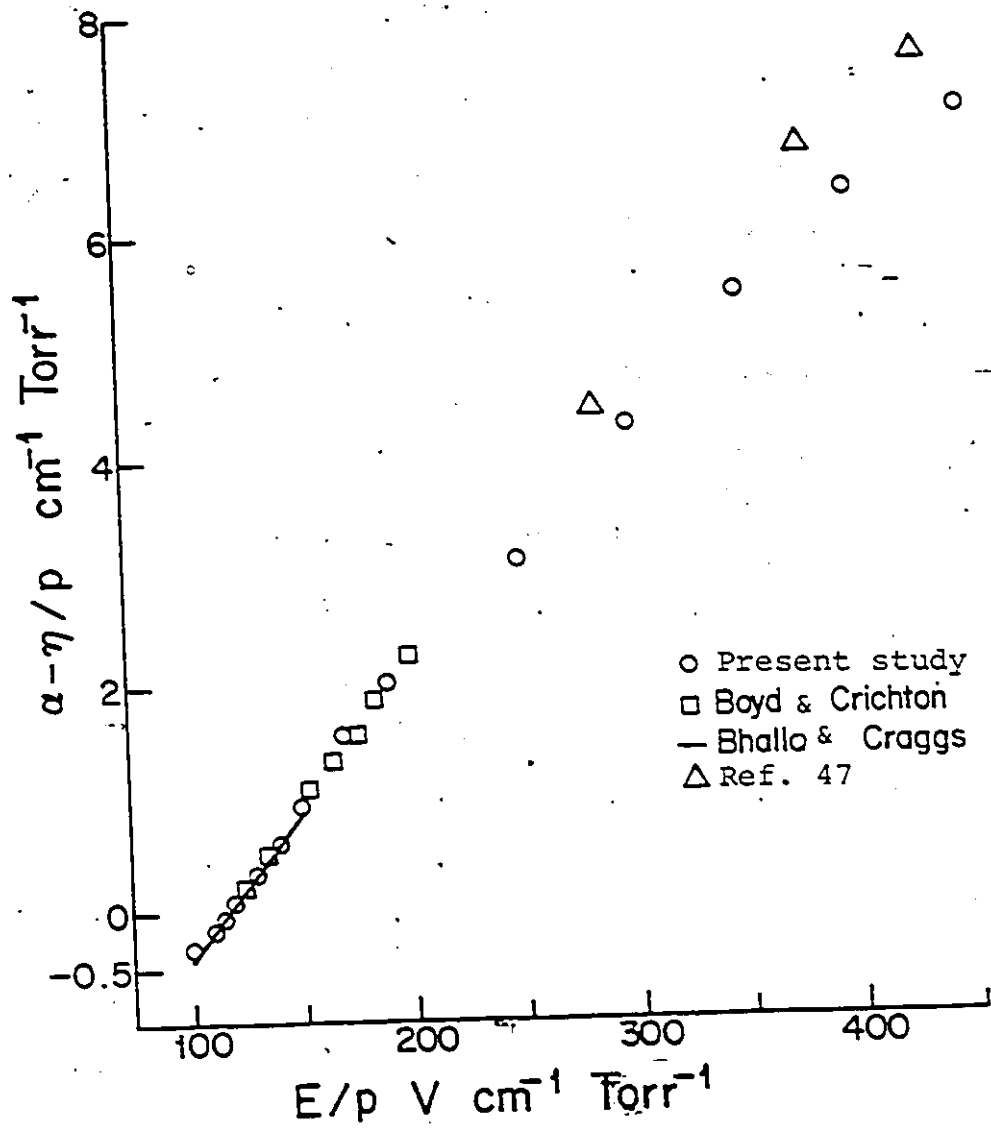


Fig. 3.15. Effective ionization coefficients in SF₆.

with E/p [47, 48]. It is not easy to explain this discrepancy at high E/p values. However, the divergence from linearity is observed in many gasses.

In Fig. 3.16 the effective ionization coefficients in SF_6+N_2 mixtures are given as a function of SF_6 partial pressure in the mixture for the interval $100 \leq E/p \leq 190$ $V\text{ cm}^{-1}\text{Torr}^{-1}$. The change in the values of $(\alpha-n)/p$ compared with those in SF_6 depends on both the percentage of N_2 in the mixture and E/p . At a given E/p the term $(\alpha-n)/p$ decreases with a decreasing nitrogen component in the mixture.

The reduction in the effective ionization coefficient becomes relatively higher as E/p decreases. This can be attributed to the magnitude of the attachment collision cross section of the mixture in the lower energy range. All of the E/p curves in Fig. 3.16 show a decreasing tendency with the increasing concentration of SF_6 in the mixture.

It also appears that once a certain concentration of SF_6 in the mixture is reached, most of the low energy electrons in the electron population gets attached and further addition of SF_6 responds with relatively little effect on the reduction of the effective ionization coefficient.

Figure 3.17 gives the effective ionization coefficient

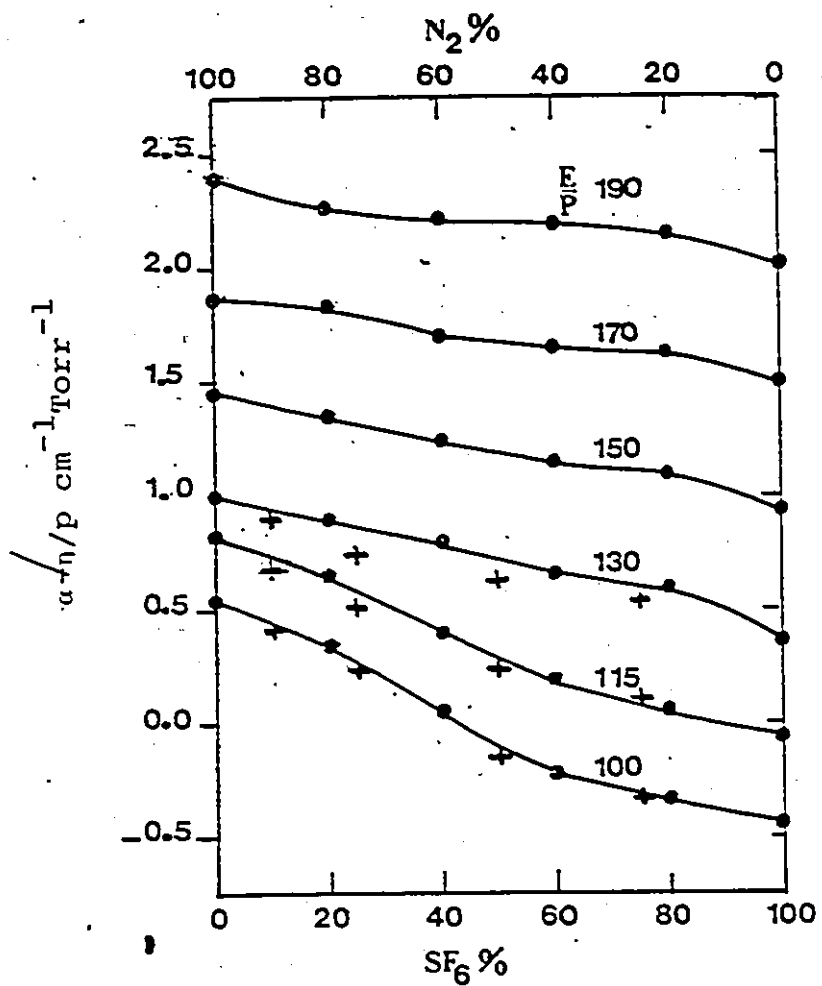


Fig. 3.16. Effective ionization coefficients in $\text{SF}_6 + \text{N}_2$ mixtures.

- present study
- + ref. 22

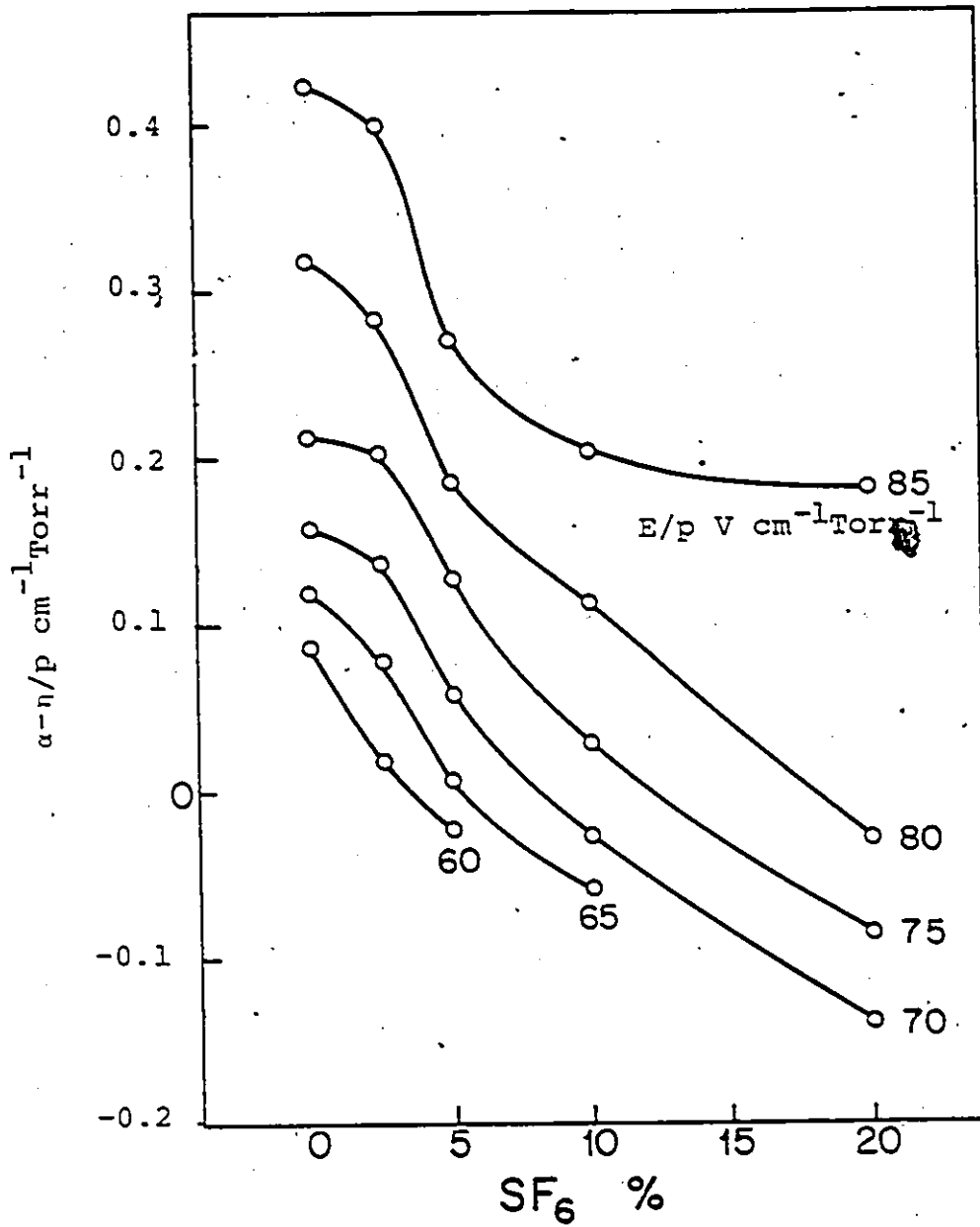


Fig. 3.17. Effective ionization coefficient in SF_6+N_2 mixtures subjected to lower E/p values.

ent in $\text{SF}_6 + \text{N}_2$ mixtures for the E/p region of $60 \leq E/p \leq 85$ $\text{V cm}^{-1} \text{Torr}^{-1}$ for lower partial pressure of SF_6 in the mixture. It can be seen that a small increase in SF_6 concentration in the mixture causes significant reduction in this coefficient. Itoh et al. [22], from their experimental values, suggested that $(\alpha - \eta)/p$ may be approximated by a linear function of the fractional SF_6 partial pressure. The present results show that the representation of $(\alpha - \eta)/p$ by a linear function of SF_6 partial pressure may result in error even at high E/p values. The theoretical study of Itoh et al. [49] also confirms that as E/p decreases the representation by a linear function becomes more difficult.

In view of the industrial importance of this gas mixture, the effective ionization coefficients are also presented in Tables 3.3 and 3.4. It should be noted that

Table 3.3
 $(\alpha - \eta)/p$ in SF_6 Mixtures at lower E/p*

E/p	SF_6 %	2.5	5	10	20
60	0.0857	0.018	-0.0245		
65	0.116	0.0776	0.0043	-0.0593	
70	0.158	0.133	0.0573	-0.0279	-0.138
75	0.210	0.199	0.1246	0.0278	-0.0879
80	0.315	0.280	0.1828	0.1126	-0.0304
85	0.420	0.394	0.267	0.200	0.177

* E/p in $\text{V cm}^{-1} \text{Torr}^{-1}$ $\alpha - \eta/p$ in $\text{cm}^{-1} \text{Torr}^{-1}$

Table 3.4
 $(\alpha-n)/p$ in SF_6+N_2 Mixtures

E/p $V\text{ cm}^{-1}\text{Torr}^{-1}$	$SF_6\%$	20	40	60	80	100
100	0.540	0.346	0.041	-0.242	-0.352	-0.427
115	0.820	0.660	0.406	0.174	0.082	-0.056
130	1.000	0.900	0.796	0.667	0.620	0.352
150	1.460	1.355	1.260	1.140	1.100	0.950
170	1.864	1.836	1.700	1.660	1.640	1.530
190	2.400	2.260	2.230	2.200	2.145	2.028

* $\alpha-n/p$ in $\text{cm}^{-1}\text{Torr}^{-1}$

"mixing time" dependence of the $(\alpha-n)/p$ values is not observed in the present investigation for a maximum mixing period of 4 hours.

3.3.2 Ionization and Attachment Coefficients in SF_6 and SF_6+N_2

The attachment coefficient n/p in SF_6 is shown in Fig. 3.18 together with the previous results. The attachment coefficient decreases with increasing E/p . The ionization coefficients α/p in N_2 are given in Tables 3.3 and 3.4 and they are in agreement with the results of previous workers in the literature [50,51,52,53].

In Figs. 3.19, 3.20 and 3.21 ionization current growths are shown for E/p values in the vicinity of E/p limits where $\alpha/p=n/p$. Least-square analysis of experimental data in these particular experiments resulted in E/p limit values of $64.5\text{ V cm}^{-1}\text{Torr}^{-1}$ ($E/N=1.958\times 10^{-15}\text{ V cm}^2$), $73.5\text{ V cm}^{-1}\text{Torr}^{-1}$ ($2.23\times 10^{-15}\text{ V cm}^2$) and

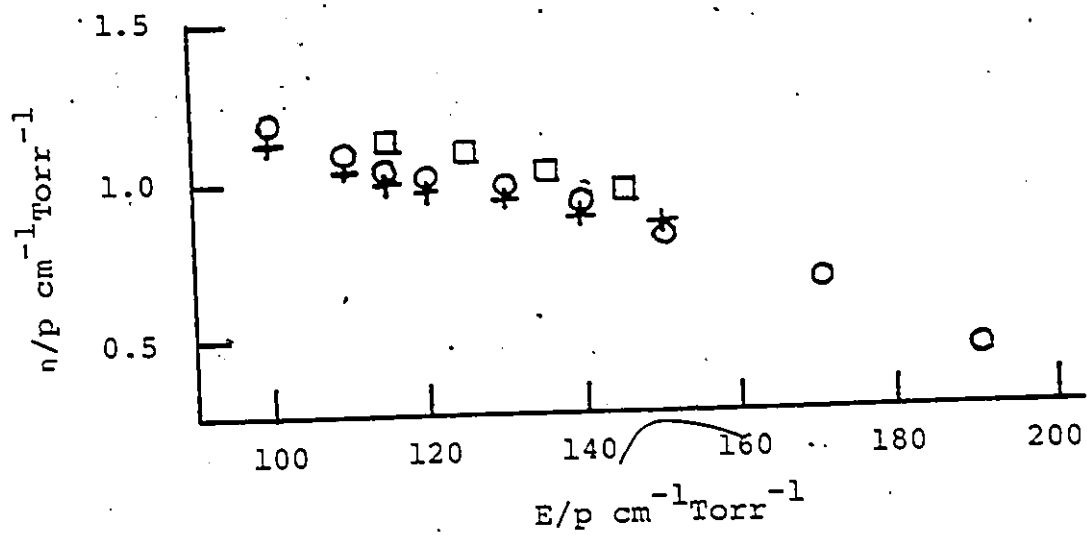


Fig. 3.18. Attachment coefficient in SF_6 .
 o - present study; + - ref. 44;
 \square - ref. 45.

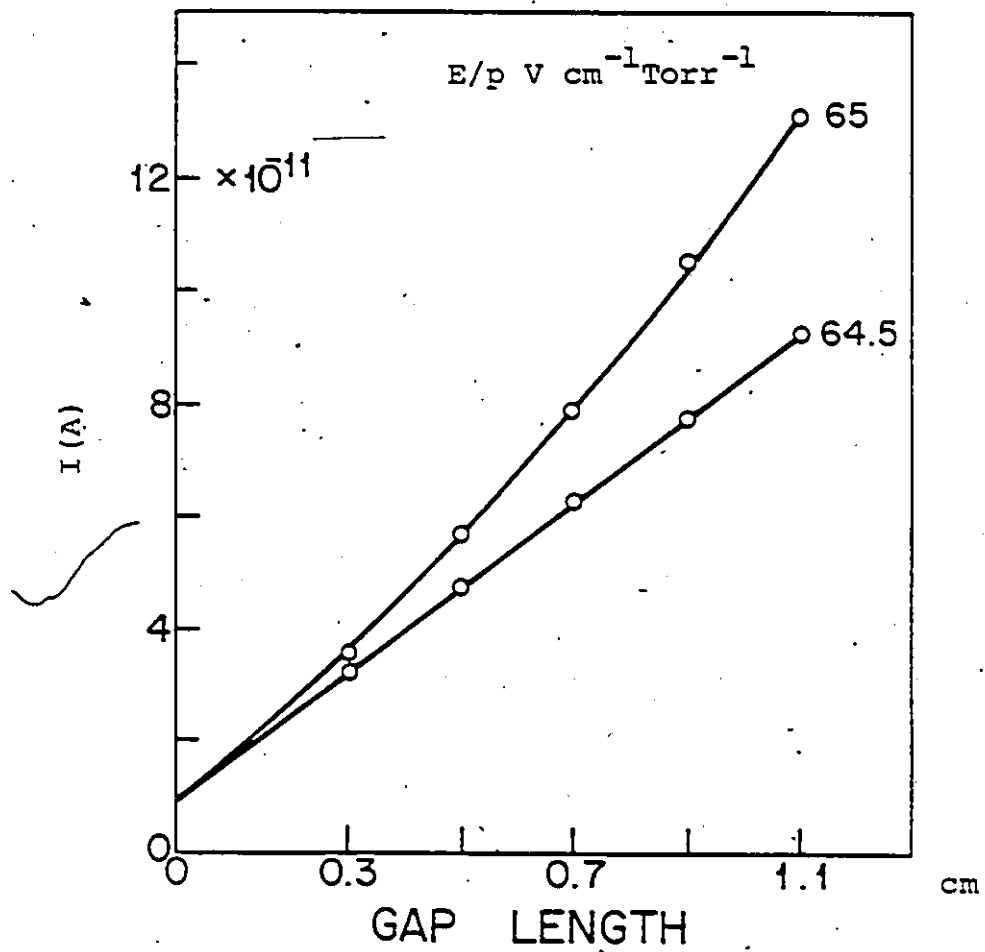


Fig. 3.19. Experimental E/p limit for
 5% SF_6 at $p=100$ Torr
 $(E/p)_{\text{limit}} = 64.5 \text{ V cm}^{-1} \text{ Torr}$

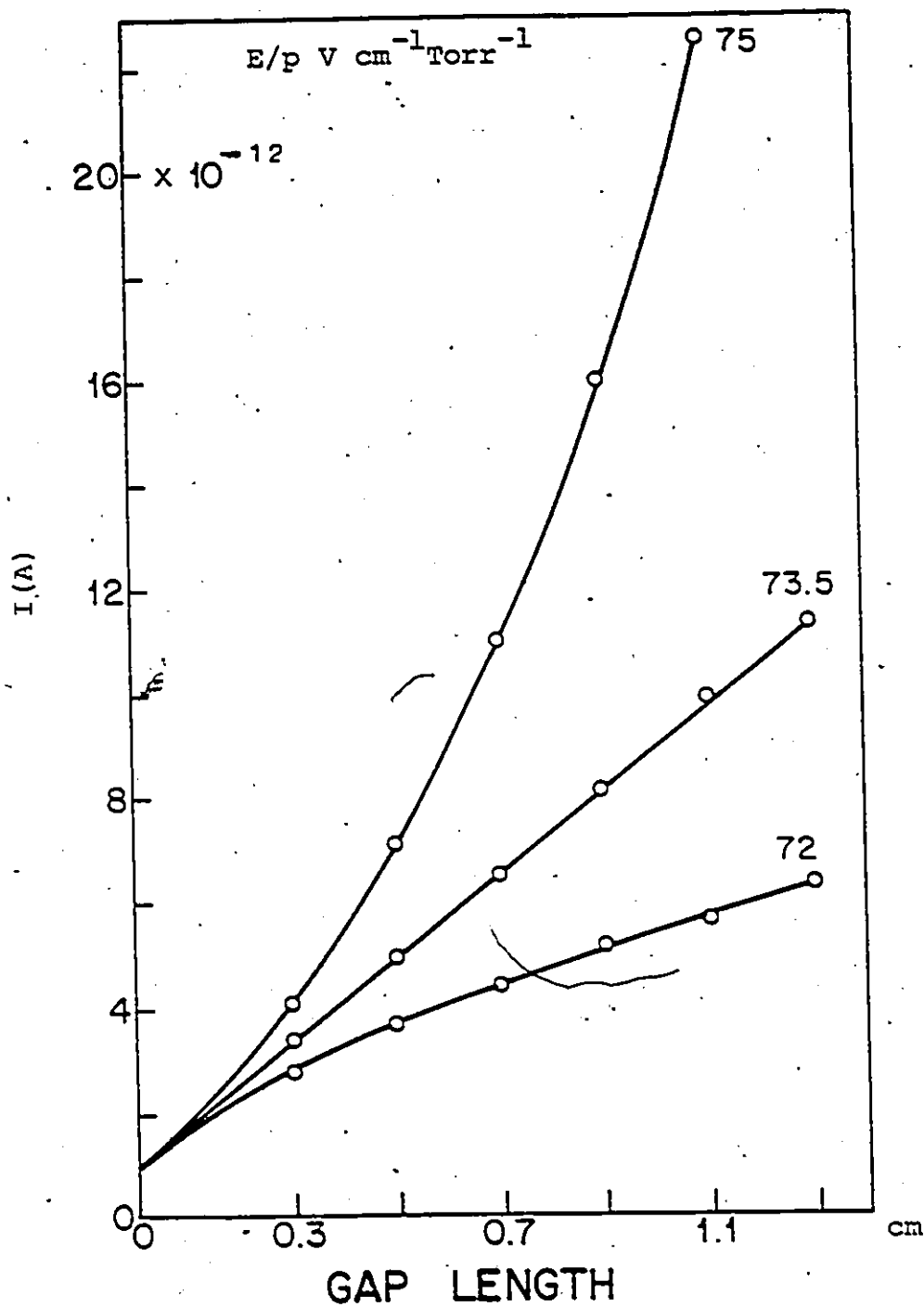


Fig. 3.20. Experimental E/p limit for 10% SF_6 at $p=50$ Torr. $(E/p)_{\text{limit}} = 73.5 \text{ V cm}^{-1} \text{ Torr}^{-1}$.

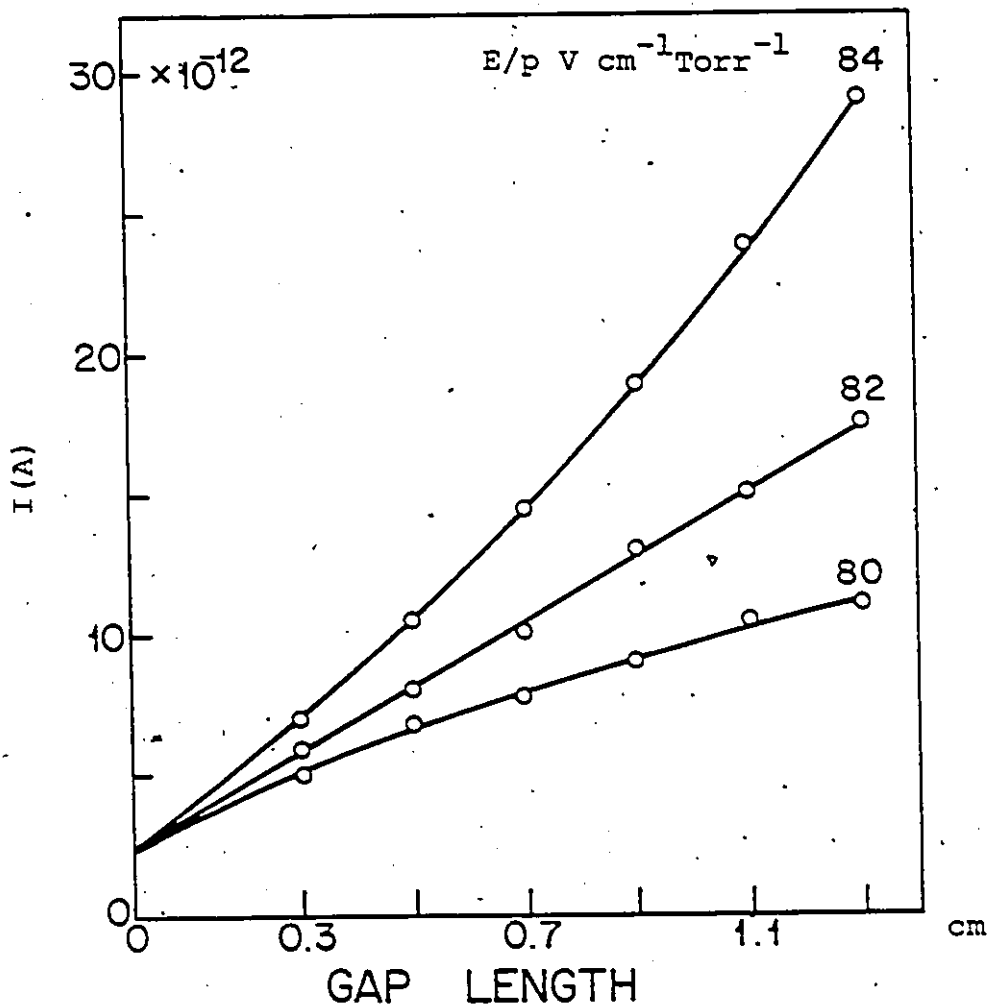


Fig. 3.21. Experimental E/p limit for 20% SF_6 at $p=25$ Torr. (E/p) limit = $82 \text{ V cm}^{-1} \text{Torr}^{-1}$.

82 V cm⁻¹Torr⁻¹ (2.489x10⁻¹⁵ V cm²), respectively for 5, 10 and 20% of SF₆ concentration in the mixture. Estimated values of E/p limit for 5% and 10% SF₆ concentration given by Itoh et al. [22] are respectively 70 and 74.4 V cm⁻¹Torr⁻¹ where they have assumed a linear relationship between (α-n)/p and E/p. The results of Ermel [5] for the same percentage SF₆ in SF₆+N₂ mixtures from sparkover measurements are 65.8, 79.2, and 88.6 V cm⁻¹Torr⁻¹, respectively.

In Fig. 3.22 variations of α/p and n/p with respect to E/p are shown for specific values of SF₆ concentration in the mixture. It can be observed from this figure that, as E/p increases the ionization coefficient of the mixture increases while there is a reduction in the attachment coefficient. A comparison between 5 and 10% SF₆ component in the mixture shows a slightly increased ionization coefficient at the higher percentage of SF₆ in the mixture. The reason might be due to a possible change in the electron energy distribution with a change in the percentage ratio of the component gasses in the mixture.

3.3.3 Apparent Secondary Ionization Coefficients

The variation of the apparent secondary ionization coefficients with concentration of SF₆ in the mixture is given in Fig. 3.23. It is interesting to observe the steep fall in the coefficients with the addition of SF₆.

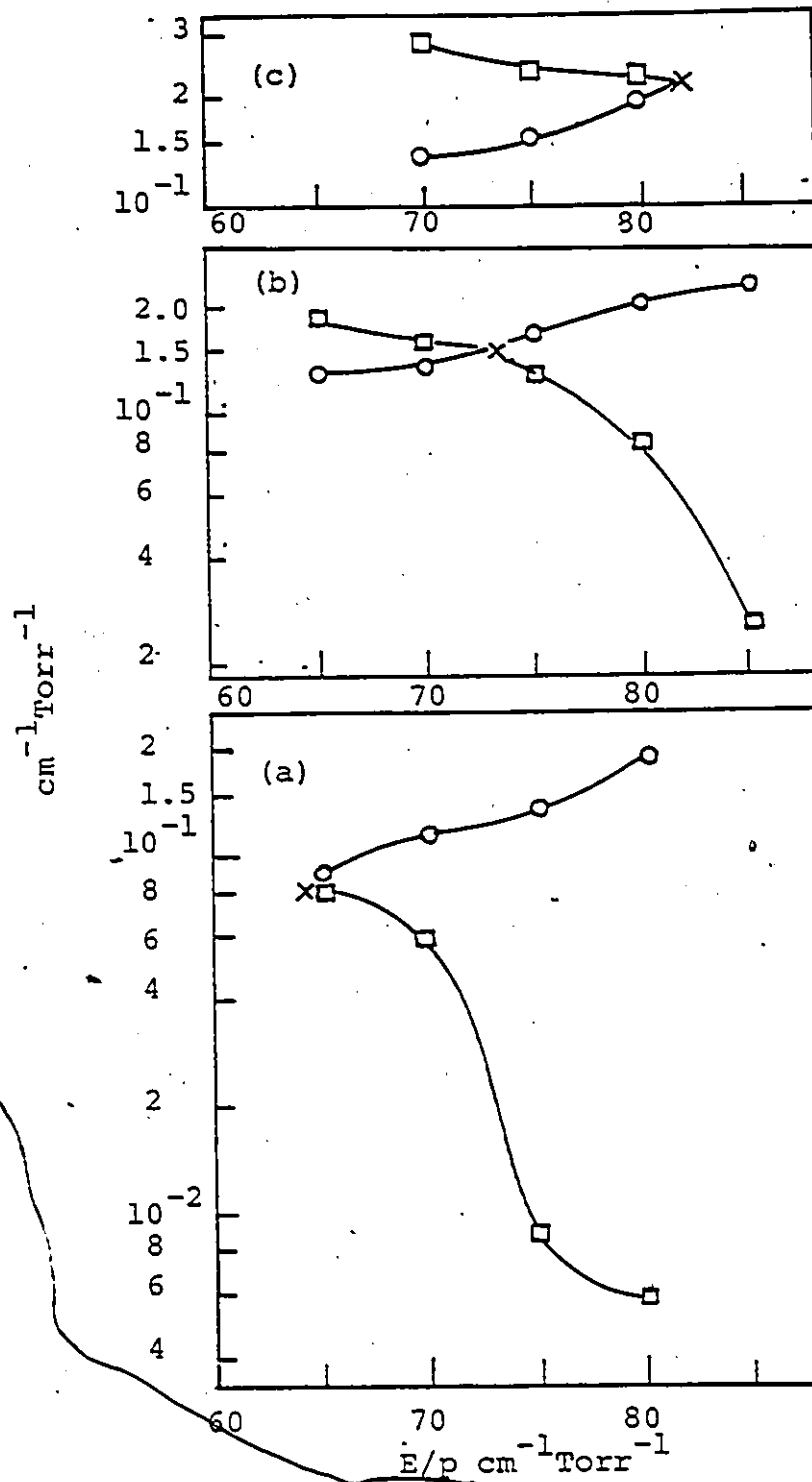


Fig. 3.22. α/p and n/p in $\text{SF}_6 + \text{N}_2$ mixtures.
 (a) 5% SF_6 ; (b) 10% SF_6 ; (c)
 20% SF_6 ; \circ - α/p ; \square - n/p ; x-indi-
 cates E/p limit.

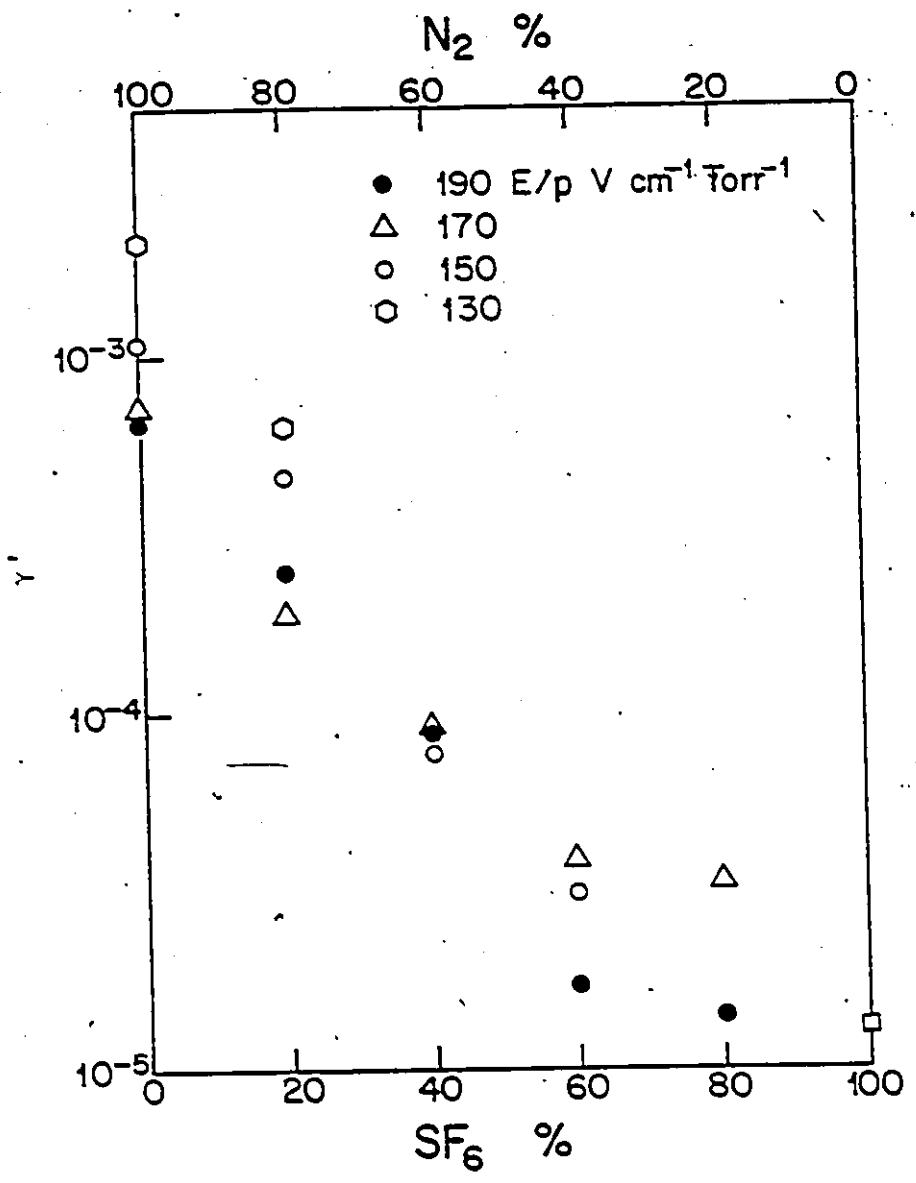


Fig. 3.23. Apparent secondary ionization coefficients in SF₆+N₂ mixtures.

into the mixture.

Although a comprehensive analysis is not carried out for γ' , care is taken to collect data under the same cathode surface conditions. That is, the cathode surface is conditioned by running a glow discharge and all the experiments are conducted at the same vacuum photo-electric current. At the end of each experiment this current is checked to ensure that the surface condition remains the same. The results shown in Fig. 3.23 are obtained from current growth measurements using curve fitting. At each point three different experiments are conducted. The deviation from mean for γ' is within $\pm 20\%$.

In N_2 , this coefficient tends to decrease with increasing E/p in the range of the present investigation. Legler has shown that for N_2 , the photon secondary coefficient γ_p decreases with increasing E/p and the decay has a similar behaviour with respect to the decay for the ratio of α/α_{ex} where α is the ionization and α_{ex} is the excitation coefficient [54].

Hence, it may be reasonable to explain the fall in the apparent secondary ionization coefficient with the addition of SF_6 into the mixture by considering that γ' is mainly governed by photon impact on the cathode surface. With the addition of SF_6 into the mixture the absorption coefficient of the mixture may increase, result-

ing in the decreased photon impact on the cathode.

On the basis that γ' of the mixture is mainly governed by photon impact on the cathode surface a simple relation is

$$\gamma' = \gamma_N e^{-\mu_m d}$$

where γ_N is the secondary coefficient in N_2 and μ_m the absorption coefficient of the mixture. For a gap setting of $d=1$ cm, without claiming high accuracy the absorption coefficients may be calculated from the results shown in the figure. For example, with 20% SF_6 the absorption coefficient, $\mu_{m/p}$, obtained in this study is $0.97 \text{ cm}^{-1} \text{ Torr}^{-1}$ compared with the measured value of $0.91 \text{ cm}^{-1} \text{ Torr}^{-1}$ given by Blair et al [55] for a wavelength of 1084 \AA . It is interesting to note that this wavelength corresponds to the transition of predominant excited state, $C^3\Pi_u$ of N_2 .

3.4 BREAKDOWN VOLTAGE MEASUREMENTS

Sparkover voltages for low values of pd Torr-cm at various concentrations are important in engineering applications, for example, in the calculation of discharge inception voltages in voids and triple junctions in equipments which use SF_6+N_2 mixtures.

Sparkover voltage measurements are carried out with SF_6 , N_2 , and SF_6+N_2 mixtures in the pd range of $3.5 \leq pd \leq 25$ Torr-cm with p varying in the interval, $5 \leq p \leq 40$

Torr at various concentrations. To establish clearly the variation of V_s with p and d at the same product pd , the first experiments are conducted at constant d by varying the pressure p . Alternatively, for constant p , d is varied and V_s is determined. The data so obtained showed that V_s depended both on p and d at the same value of pd . The maximum variation of $\pm 1.5\%$ is observed in V_s at $pd=3.5$ Torr-cm which decreased to within $\pm 0.5\%$ for higher pd values. Hence, under the experimental conditions it is observed that Paschen's Law holds well in pd range of V_s measurements. Figure 3.24 shows the variation of sparkover voltages with SF_6 concentration in the mixture. As expected the breakdown withstand level of the mixture increases with the addition of SF_6 into the mixture. However, once certain concentrations of SF_6 is reached further addition of SF_6 responds with relatively little effect on the withstand level which is consistent with the relatively less reduction observed in effective ionization coefficients.

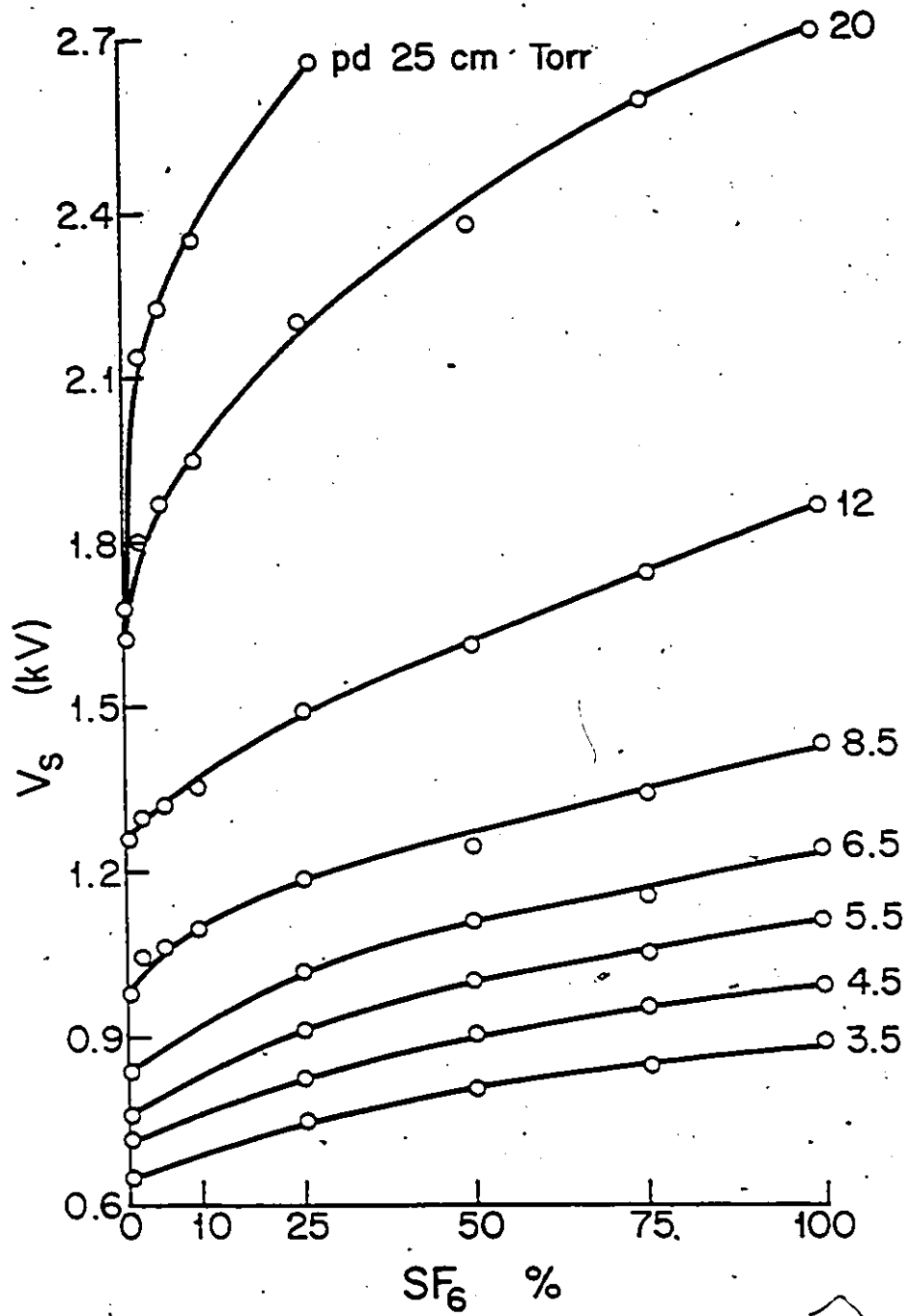


Fig. 3.24. Sparkover voltages in SF₆+N₂ mixtures.

CHAPTER IV

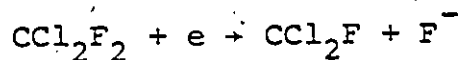
IONIZATION GROWTH IN

CCl₂F₂ + CO₂ BINARY GAS MIXTURES

4.1 INTRODUCTION

For engineering purposes, the sparking potentials of N₂ and CO₂ may be increased by mixing these inexpensive gasses with a strongly attaching gas. To the author's knowledge the information on the basic aspects of ionization growth in CCl₂F₂ + CO₂ electronegative gas mixtures appears to be lacking in the literature. This chapter provides data on the ionization growth of CCl₂F₂ + CO₂ binary gas mixtures.

Attachment in CCl₂F₂ (difluoro-dichloromethane) has been recognized before [56], and shown to be largely the result of dissociation, that is,



The experimental techniques and current growth analysis are the same as described in Chapters II and III. The spatial growth of ionization currents is studied in the

range of $100 \leq E/p \leq 180 \leq V \text{ cm}^{-1} \text{ Torr}^{-1}$. Also, the critical E/p limits at which $\alpha/p = \eta/p$ are determined by obtaining the best linear variation of ionization growth with respect to increasing gap settings. After reaching the maximum gap setting, the values of d are decreased to the identical values previously used and currents are remeasured at the identical corresponding values of E/p .

The experimental parameters p and d are chosen in such a way that secondary cathode processes have negligible contribution on the ionization growth curves. For these measurements the gas sample pressures used are 4 and 5 Torr. Each experiment is repeated with three different fresh samples. The current growth data is reproducible within $\pm 3\%$ over the range of experimental parameters.

4.2 THE EFFECTIVE IONIZATION COEFFICIENTS

The effective ionization coefficients measured in CO_2 and CCl_2F_2 are in good agreement with the previous values available in literature [57,58,59,60].

Figure 4.1 shows typical ionization growth curves in CO_2 . In Fig. 4.2 such curves are shown in $\text{CCl}_2\text{F}_2 + \text{CO}_2$ with 20% CCl_2F_2 . As in the case of pure CO_2 , separation of α/p and η/p with 20% CCl_2F_2 is not possible due to the fact that the $\log I-d$ plots are straight

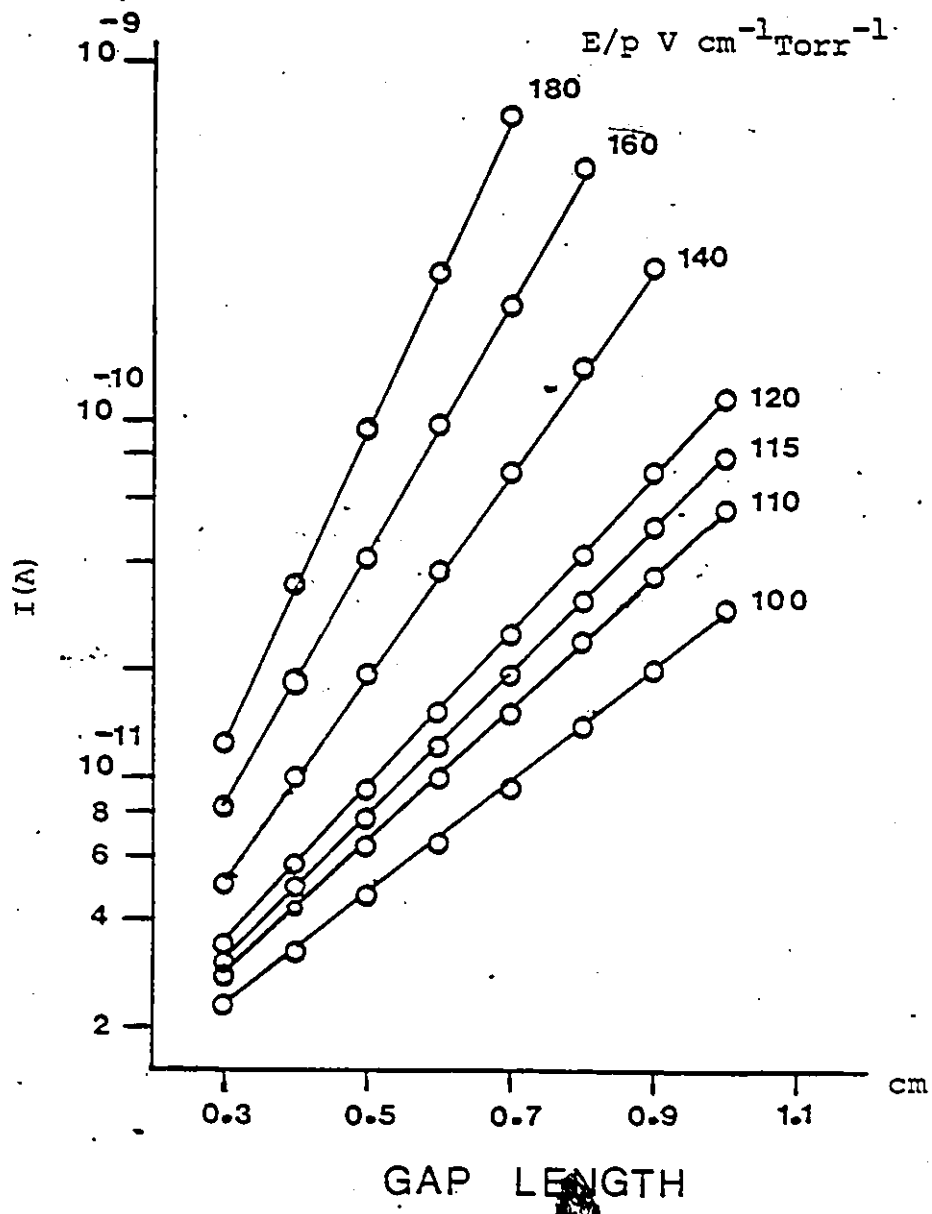


Fig. 4.1. Ionization growth curves in CO_2 at $p=4$ Torr.

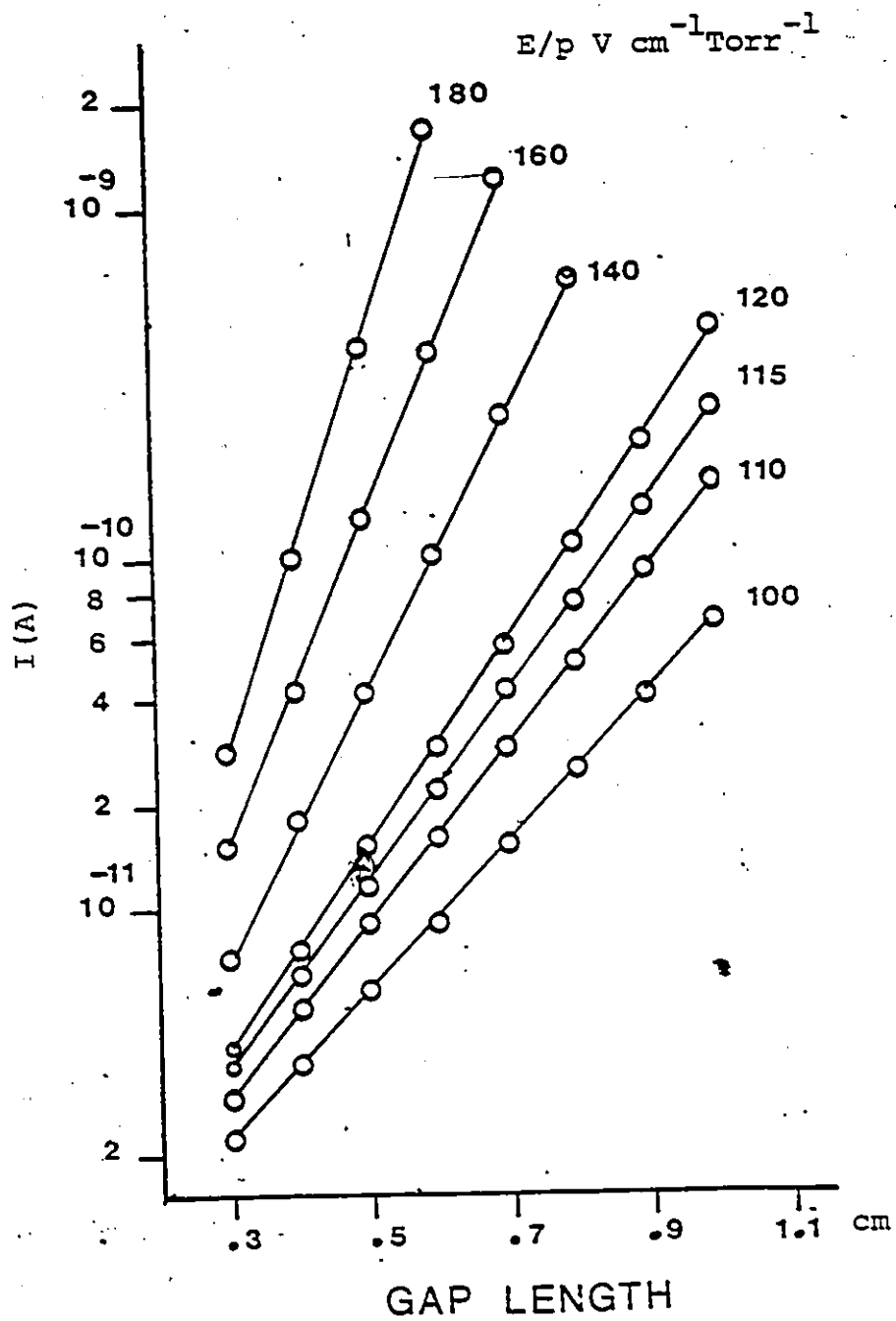


Fig. 4.2. Ionization growth curves in $\text{CCl}_2\text{F}_2 + \text{CO}_2$ with 20% CCl_2F_2 at $p = 5$ Torr.

lines and hence $(\alpha-\eta)/p$ only could be evaluated. The effective ionization coefficient in CO_2 is shown in Fig. 4.3.

In Fig. 4.4 the effective ionization coefficients in $\text{CCl}_2\text{F}_2 + \text{CO}_2$ gas mixtures are given for various reduced electric fields. As can be seen from these figures particularly at high E/p values and low concentration of CCl_2F_2 (<30%), the effective ionization coefficient of the mixture increases with the addition of CCl_2F_2 in the mixture. This behaviour is significant at $180 \text{ v cm}^{-1} \text{ Torr}^{-1}$ with 20% CCl_2F_2 in the mixture. Similar behaviour is observed in $\text{CCl}_2\text{F}_2 + \text{N}_2$ mixtures [61].

It is possible that at high reduced electric fields, with certain percentage of CCl_2F_2 additive, the mean energy of the swarm increases resulting in an increased ionization rate which is greater than that of either component of the mixture. However, there are no data on the swarm parameters of this binary mixture in the literature. At lower reduced electric fields, if the CCl_2F_2 additive of the mixture is increased beyond 20%, the electronegative component of the mixture is sufficiently effective to control the electron growth in the swarm giving the observed reduction of $(\alpha-\eta)/p$. These coefficients are presented in Table 4.1.

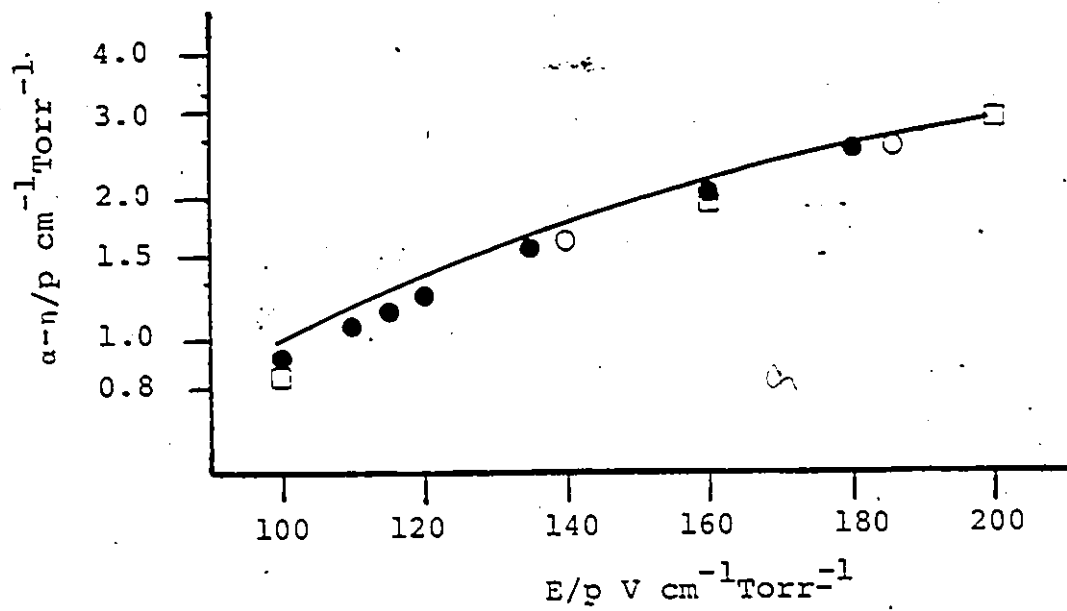


Fig. 4.3 Effective ionization coefficients in CO_2 . ● present study, □ ref. 57, ○ ref. 58, — ref. 59.

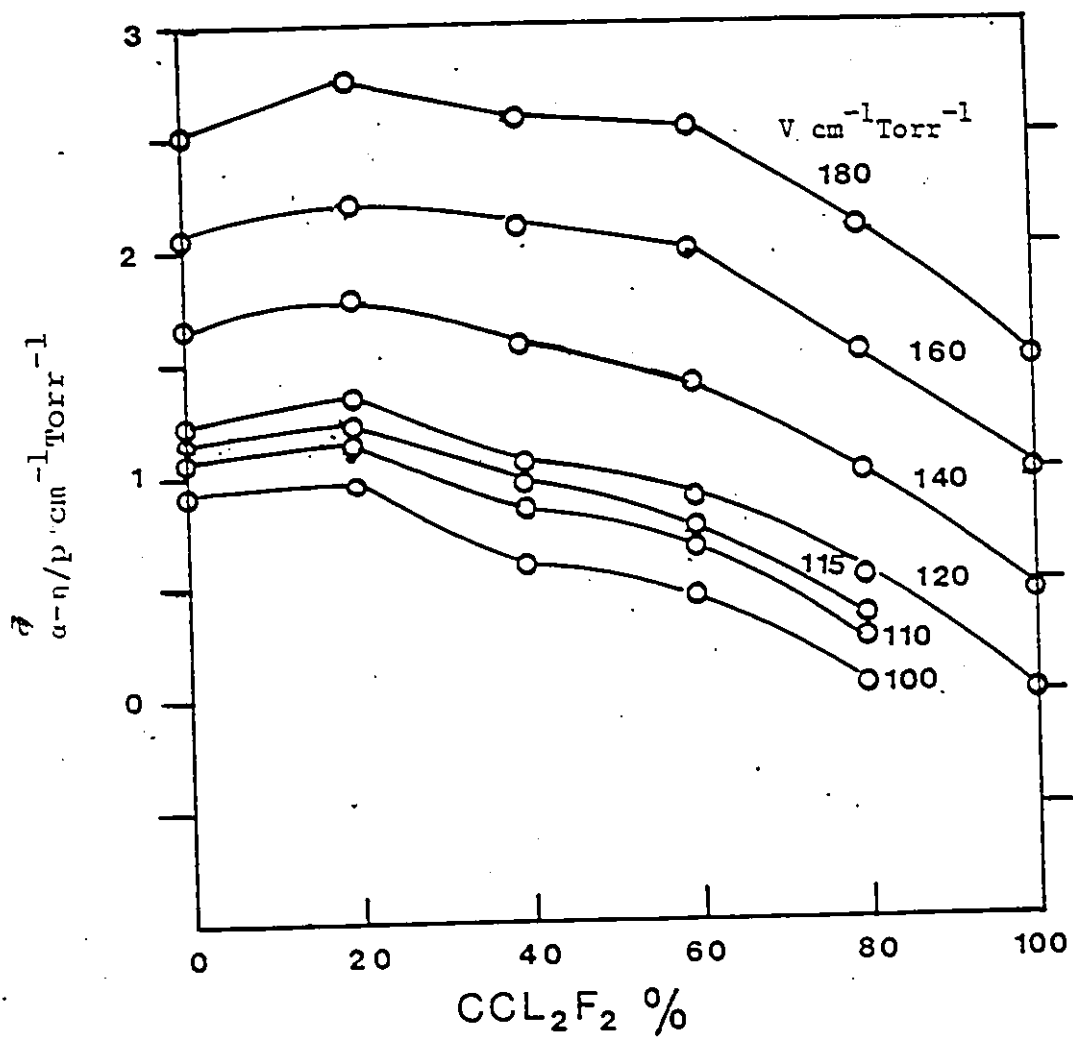


Fig. 4.4. Effective ionization coefficients in $\text{CCL}_2\text{F}_2 + \text{CO}_2$ gas mixtures.

Table 4.1
 α -n/p in $\text{CCl}_2\text{F}_2 + \text{CO}_2$ Mixtures*

E/p	$\text{CCl}_2\text{F}_2\%$					
	0	20	40	60	80	100
100	0.909	0.965	0.589	0.455	0.0398	
110	1.077	1.146	0.849	0.672	0.249	-0.26**
115	1.159	1.215	0.952	0.774	0.359	
120	1.248	1.341	1.067	0.889	0.524	0
						-0.02**
140	1.657	1.782	1.575	1.419	0.998	0.451
						0.47**
160	2.062	2.210	2.095	2.009	1.528	0.952
						1.00**
180	2.526	2.750	2.576	2.589	2.082	1.486
						1.55**

* α -n/p in $\text{cm}^{-1}\text{Torr}^{-1}$, E/p in $\text{V cm}^{-1}\text{Torr}^{-1}$.

**Ref. 60.

4.3 SPARKING POTENTIALS

The sparking potential, V_s , in the mixture is shown in Fig. 4.5. It is observed that at higher pd values, the sparking potential of the mixture increases effectively with the addition of CCl_2F_2 into the mixture. However, as the product pd decreases, this effect starts to decrease. The 20% CCl_2F_2 curve overlaps with that of pure CO_2 in the vicinity of 10 Torr-cm pd. Over the range of pd studied, the sparking potentials are found to be a function of pd only. The maximum deviation from the mean value is observed in the vicinity of 10 Torr-cm pd as $\pm 2\%$. Gas sample pressures used are also shown in Fig. 4.5.

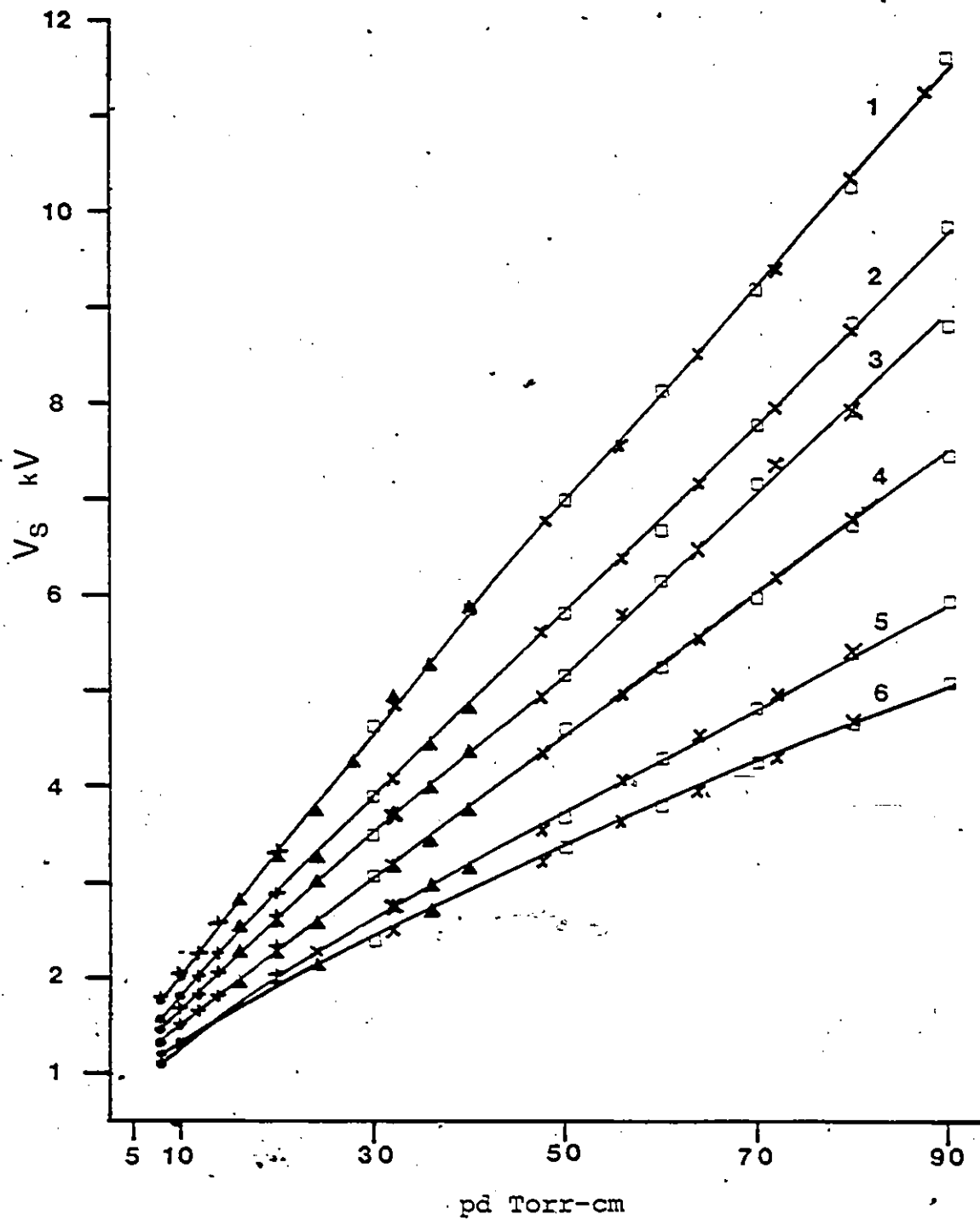


Fig. 4.5. Sparking potentials as a function of pd in $\text{CCl}_2\text{F}_2 + \text{CO}_2$ mixtures. Curves 1 - 100% CCl_2F_2 , 2 - 80%, 3 - 60%, 4 - 40%, 5 - 20%, 6 - 0%. ● 10 Torr, + 20, ▼ 40, x 80, □ 100 Torr.

4.4 CRITICAL E/p LIMITS

The critical limiting reduced electric fields are given in Fig. 4.6 with respect to CO₂ percentage in the mixture. The limiting value of E/p for CCl₂F₂ is found to be 120 V cm⁻¹Torr⁻¹ in the present study which is in good agreement with the previous results [60,62,63].

The limiting E/p of the mixture decreases with the addition of CO₂ into the mixture. At 60% CO₂ concentration this value is determined as 70 V cm⁻¹Torr⁻¹. Table 4.2 gives the limiting E/p values for various CO₂ concentrations in the mixture together with α/p values.

Table 4.2

E/p Limit and α/p for Various CO₂ Concentrations

CO ₂ %	0	10	20	40	60
E/p	120	103	96	81	70
α/p = n/p	0.863	1.206	0.869	0.815	0.792
*E/p in V cm ⁻¹ Torr ⁻¹ α/p in cm ⁻¹ Torr ⁻¹					

For uniform field gaps having large pd products, a prediction of critical E/p limit for an electronegative gas or gas mixture is essentially equivalent to a prediction of the dielectric strength [18]. Hence, at p=760 Torr and d=0.3 cm, breakdown voltages are also measured in CCl₂F₂+ CO₂ mixtures. The results are given in Fig. 4.7. Table 4.3 compares the breakdown field strengths

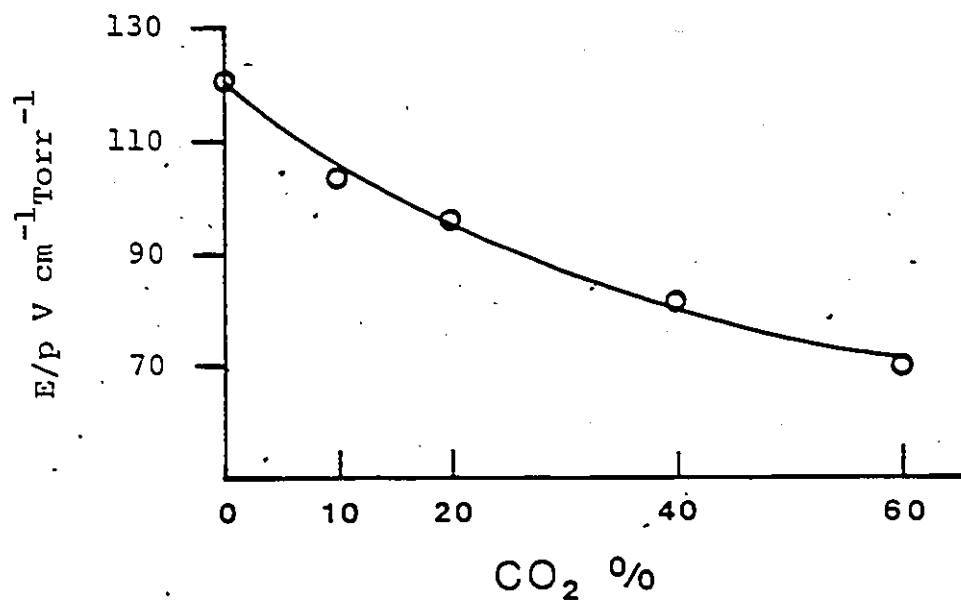


Fig. 4.6. Experimental E/p limits in CCl₂F₂ + CO₂ mixtures.

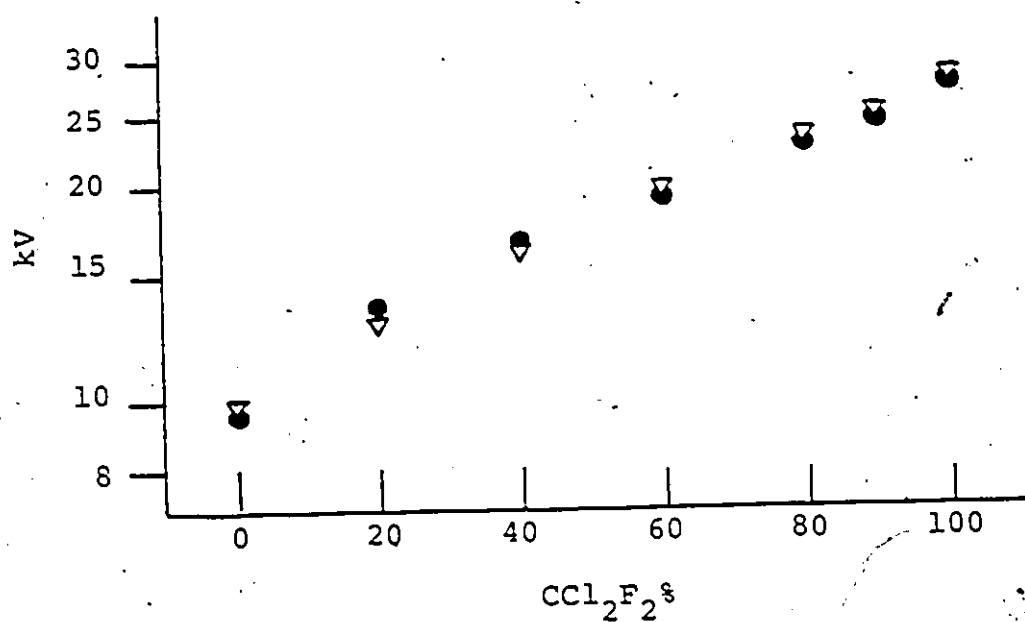


Fig. 4.7 Breakdown voltages in $\text{CCl}_2\text{F}_2 + \text{CO}_2$ mixtures at $p=760$ Torr.
● present study ($d=0.3$ cm).
▽ ref. 64.

obtained from Fig. 4.7 with the values in Table 4.2 which are converted to atmospheric pressure.

Table 4.3

Breakdown Field Strength of $\text{CCl}_2\text{F}_2 + \text{CO}_2$
Mixtures at $p = 760$ Torr

$\text{CO}_2\%$	0	10	20	40	60
E^* (kVcm^{-1})	91.2	78.28	72.96	61.56	53.20
E (kVcm^{-1})	93.48	83.96	77.46	63.96	56.12

*Results from current growth measurements.

4.5 IONIZATION AND ATTACHMENT COEFFICIENTS

The variation of α/p and n/p for 20% CO_2 concentration in the mixture is shown in Fig. 4.8. Figure 4.9 shows these coefficients with 40% and 60% CO_2 in the mixture.

It can be observed from these figures that, as E/p increases, the ionization coefficient of the mixture increases while there is a reduction in the attachment coefficient. Only for the 20% CO_2 mixture if E/p is greater than $100 \text{ V cm}^{-1}\text{Torr}^{-1}$, there is a slight increase in the attachment coefficient. Since CCl_2F_2 additive of the mixture is 80%, this behaviour is expected. At this particular value the attachment rate of CCl_2F_2 is the highest level. The reported value of n/p in pure CCl_2F_2 at $E/p=100 \text{ V cm}^{-1}\text{Torr}^{-1}$ is $1.41 \text{ cm}^{-1}\text{Torr}^{-1}$ [65].

As the CO_2 additive of the mixture increases, re-

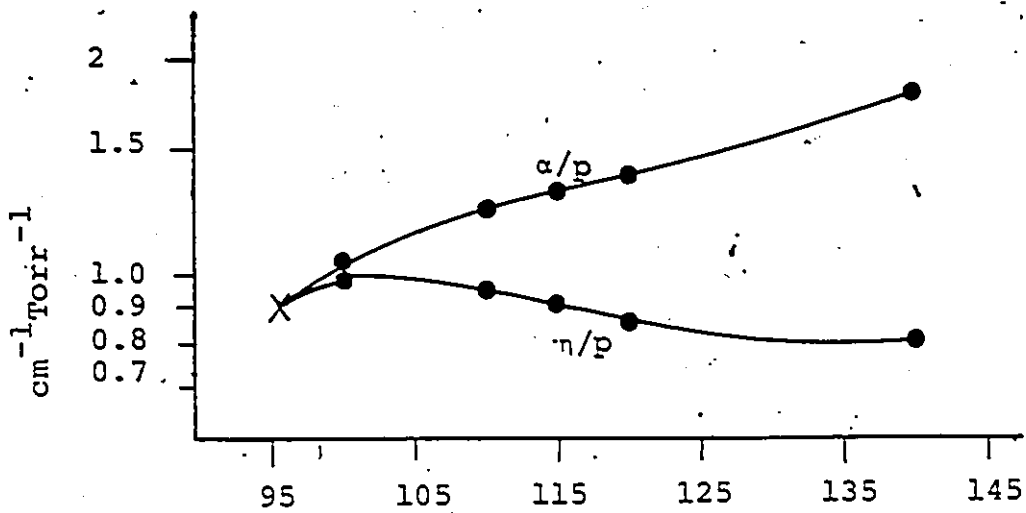


Fig. 4.8. Variation of ionization and attachment coefficients in 20% CO_2 + 80% CCl_2F_2 .

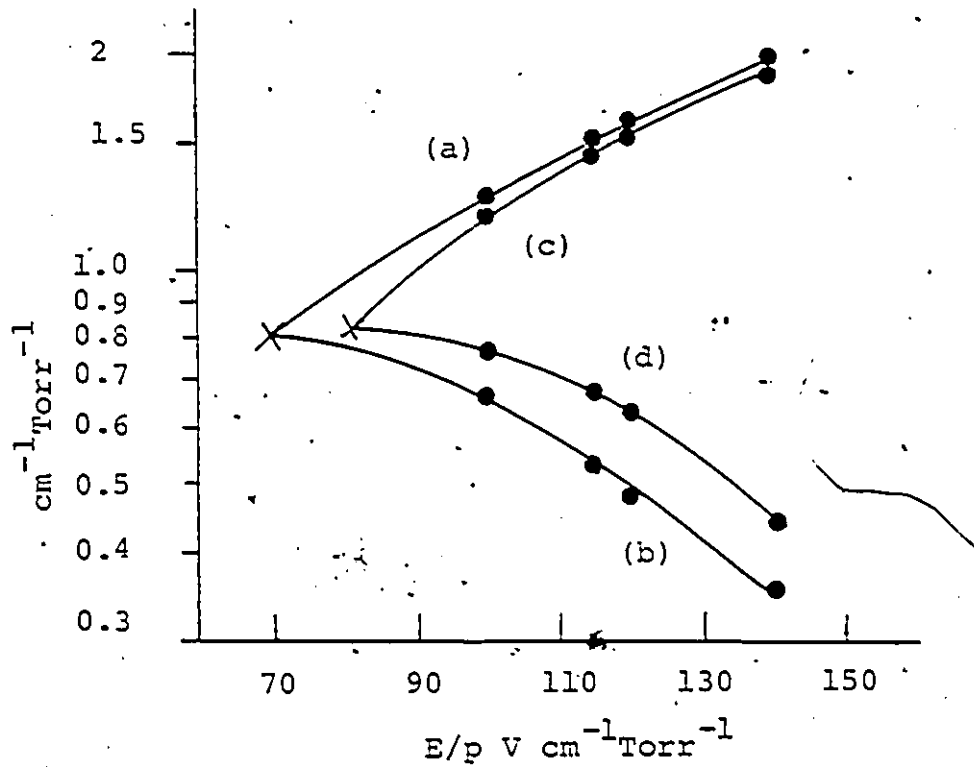


Fig. 4.9. Variation of α/p and n/p in CCl_2F_2 + CO_2 mixtures with 40% and 60% CO_2 . (a) α/p 60% CO_2 ; (b) n/p 60% CO_2 ; (c) α/p 40% CO_2 ; (d) n/p 40% CO_2 .

duction in the attachment coefficient becomes faster with increasing E/p. Also, it can be observed that ionization coefficients in 40% and 60% CO₂ mixtures are higher than those of 20% CO₂ mixture.

CHAPTER V

THEORETICAL CALCULATION OF SWARM PARAMETERS

IN SF₆ UNDER UNIFORM FIELDS

5.1 INTRODUCTION

The current extensive use of SF₆ as an insulating medium has prompted efforts towards correlating the observed discharge phenomena with the basic processes. Though the relevance of macroscopic coefficients, particularly, the first ionization coefficient and the attachment coefficient, to the dielectric strength has long been recognized, dielectric behaviour of a gas is traditionally predicted through empirical and semi-empirical formulas. To provide a basis for prediction of dielectric behaviour in gases or gaseous mixtures, a more general description is necessary [19].

This description is the link between microphysical properties and macroscopic properties (Fig. 5.1). There are two theoretical approaches: solution of the Boltzman transport equation and Monte Carlo simulations of the processes which occur within the electron swarm.

The conventional solution of the Boltzman equation may become inadequate when the sum of the inelastic cross

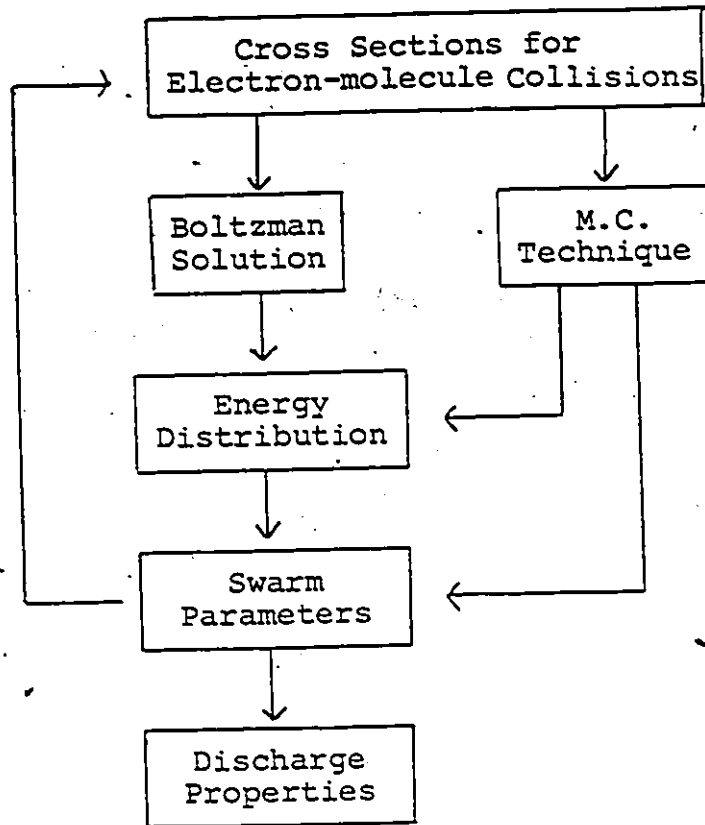


Fig. 5.1. The link between microphysical and macroscopic properties.

sections becomes a significant fraction of the elastic scattering cross section [66]. Though the effects of including higher order terms of the spherical harmonic expansion have been investigated in other gases [67], such an analysis is not available for SF₆.

An alternate approach which is much closer in spirit to the actual experiment is the Monte Carlo Technique. Several authors have used Monte Carlo techniques in a number of gasses, but not in SF₆ [68]. Particularly, at high-reduced electric fields where the two term Boltzman equation analysis is not adequate [69], Monte Carlo simulation is a powerful method for calculation of electron swarm parameters. The method can also be extended to a non-uniform electric field, which is encountered more frequently in engineering applications.

In the presence of an electric field, during the free time of flight between collisions, there is a gain of energy of the electron. This gain can be approximated by

$$\Delta\epsilon = eEL \cos \theta \quad (5.1)$$

where L is the mean free path, -e is the electronic charge, -E is the applied electric field and θ is the angle between electron velocity and negative field direction.

For an isotropic distribution, the r.m.s. average value of $\cos \theta$ is equal to $1/\sqrt{3}$. The mean free path L is related to the momentum transfer cross section Q_m and the number of gas molecules per cm^3 N by $L^{-1} = NQ_m$. The time required for an electron to achieve an average energy of ϵ is given by Chandrasekhar [70] as

$$t = \epsilon^2 / [v(\overline{\Delta\epsilon^2})] \quad (5.2)$$

where v is the frequency of collision between an electron and a gas molecule, and $\overline{\Delta\epsilon}$ is the average electron energy gain during a mean free path.

The average number of collisions in the time t , n_c , can be expressed as

$$n_c = vt = 3(\epsilon N Q_m / eE)^2 \quad (5.3)$$

Let us consider an electron which has attained an energy 10 eV. For SF_6 , taking Q_m as $1.2 \times 10^{-15} \text{ cm}^2$ and using a number density of $3.3 \times 10^{-16} \text{ cm}^3$ corresponding to 1 Torr at 20°C , Eq. 5.3 gives an average number of collisions of the order of 5×10^5 for $E/p = 1 \text{ V cm}^{-1} \text{ Torr}^{-1}$. The average number of collisions for $E/p = 100 \text{ V cm}^{-1} \text{ Torr}^{-1}$ is 50.

The above approximate calculation indicates that, at high values of E/p the gas discharge problem is well within the solution of a straightforward random walk technique. The previous Monte Carlo simulations also

support this behaviour [71,72].

The assumptions of the present simulation are as follows:

1. A background of SF_6 molecules is considered to be at rest with respect to electron motion.
2. The d.c. electric field is oriented antiparallel to the z axis and assumed to be uniform.
3. A point source is assumed to be located at the origin of the coordinate system and the electrons are started initially from the origin with a constant emission energy of 0.1 eV. Since particles emanating from a surface are limited to half of direction space, the polar angle of the initial electron emanating from the point source is simulated due to cosine distribution.
4. Isotropic scattering is assumed in the laboratory system.
5. An electron that reflects back (reaches to $z=0$ position) is assumed to be absorbed by the cathode.

When an electron is emitted from the cathode position ($z=0$), it is assigned the required directions and a mean free flight time is calculated corresponding to

its energy. The mean free flight time which represents the time taken on the average for an electron between collisions with gas molecules is divided into fine steps. In a fine time step the electron is let to drift under the action of the electric field. At the end of each fine time step the new state of the electron is found with its position and energy. Then a test is made for collision. If a collision is assumed to occur, the appropriate energy loss mechanism depending on the type of collision is considered. After finding the new state of the electron, corresponding to its energy a new mean free flight time is decided on and the above procedure is repeated. At the end of a time step, if the test for collision fails, again from the new state of the electron a new mean free flight time is found and after dividing this time interval into fine time steps, the electron is let to drift in the new fine time step.

This process is continued until either the electron has remained in the field for a fixed time or lost due to an attachment process.

More detailed information on the simulation is provided in the coming sections of the present chapter.

5.2 ELECTRON DYNAMICS IN UNIFORM ELECTRIC FIELDS

The gas is acted upon by a D.C. electric field, E , antiparallel to the z axis and spacial homogeneity of the electric field is assumed. A background gas of SF_6 molecules with a number density of $N = 3.294 \times 10^{16} \text{ cm}^{-3}$ which corresponds to a gas pressure of 1 Torr at 20°C is considered. The essential feature of the gas discharge phenomena consists in the motion of charged particles and mutual interaction of the particles. If the charged particle density is very low compared to that of the gas molecules, only two-body collisions between an electron and a neutral molecule become dominant. Hence, coulomb interaction between charged particles are neglected in view of the fact that the gas is weakly ionized.

The time during an encounter of an electron with a neutral is assumed negligible, and the effect of the electric field on the electron motion is accounted for during the free time between collisions.

For the coordinate system selected, the position and energy of an electron in the time step, Δt , undergo the following variations for an initial velocity V_0 , and kinetic energy of $\epsilon = \frac{1}{2} m V_0^2$.

$$\Delta z = V_{0z} \Delta t + \frac{1}{2} a (\Delta t)^2, \text{ where } a = \frac{eE}{m}$$

$$\Delta y = V_{0y} \Delta t$$

$$\Delta x = V_{ox} \Delta t$$

$$\Delta \varepsilon = eE \Delta z$$

(5.4)

In which, $-E$ is the electric field, $-e/m$ the charge to mass ratio of an electron, a the acceleration, Δx and Δy the position components with respect to the axes, Δz the distance traveled along the applied field direction and $\Delta \varepsilon$ is the energy change in the interval Δt .

V_{ox} , V_{oy} and V_{oz} are the components of the initial velocity parallel to the respective axes, and are given by

$$V_{oz} = V_o \cos \theta$$

$$V_{oy} = V_o \sin \theta \sin \phi$$

$$V_{ox} = V_o \sin \theta \cos \phi$$

(5.5)

where, θ and ϕ are, respectively, the polar and azimuthal angles.

If the collision frequency is constant, that is

$$\nu = \nu Q_T N = \text{constant}$$

(5.6)

then the mean free flight time is given accordingly as

$$\tau = \frac{1}{|\nu| Q_T N}$$

(5.7)

where Q_T is the magnitude of the total collision cross

section. Then, the actual time to collision can be determined as

$$t = -\tau \ln R \tag{5.8}$$

with a probability distribution function of [Appendix I]

$$P(t) = 1 - \exp(-N Q_T v t) \tag{5.9}$$

In Eq. 5.8, R is a random number equally probable between 0 and 1.0 [Appendix II].

However, the constant collision time model is not satisfactory for SF₆, particularly in the lower energy range, where the difference in mean collision time before and after a free path traversed becomes large. Hence, it is not possible to assign a time of flight to an electron of given energy or velocity at the beginning of a free path by directly using Eq. 5.8. For this reason the following procedure which was first employed by Itoh and Musha [73] on the free path is used.

Let ε₀ be the electron energy at time t₀ when the electron starts the free path. The corresponding time of flight is τ(ε₀) = v⁻¹(ε₀) which is Eq. 5.7. Depending on the energy change possible in τ(ε₀), the mean free flight time is divided into a given number of parts so that Δt = sτ(ε₀), where s⁻¹ is an integer. If s is sufficiently small, the collision frequency, ν(ε), can be

considered as constant during the time interval Δt . The probability of collision in the time interval Δt is

$$P = 1 - \exp(-\Delta t/\tau) \quad (5.10)$$

The test for collision is carried out by calling a random number R , $0 \leq R \leq 1.0$ and checking if $R \leq P$. If not, the process is repeated. That is, a new mean free flight time is calculated at the end of the time step and a new $\Delta t = s\tau(\epsilon_1)$ is assigned. Equation 5.10 is again tested for a collision with a new random number. A collision is assumed to occur when the condition $R \leq P$ is satisfied.

In the simulation, the number of intervals into which each collision time is divided is determined by dividing the electron energy into two regions. For the energy range $0 \leq \epsilon \leq 3$ eV, the mean collision time is divided into 40 intervals ($s=0.025$) and $\epsilon > 3$ eV 10 intervals ($s=0.1$) are chosen.

In Figs. 5.2 and 5.3 the percentage difference in mean free flight time at the beginning and end of time step, Δt , is shown with respect to electron energy at $180 \text{ V cm}^{-1} \text{ Torr}^{-1}$ for the worst case observed. In Fig. 5.2 curve a and b show an electron which is decelerating. Curve c shows an electron in acceleration mode. This difference reaches -10% for an electron subjected to deceleration in the interval of 10-100 meV. (Fig. 5.2).

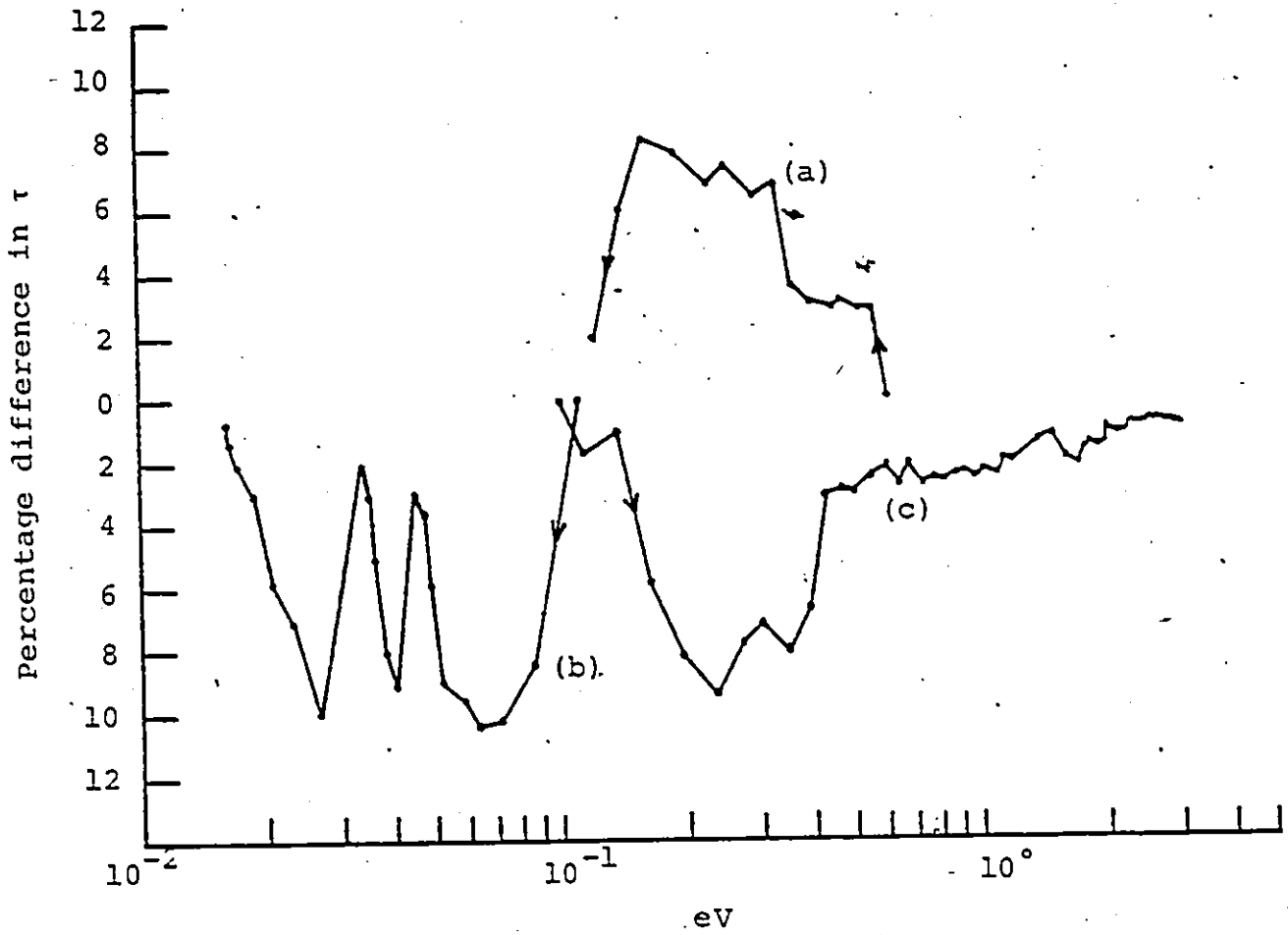


Fig. 5.2. Percentage difference in mean free flight times at the beginning and end of a time step. (a) and (b) deceleration; (c) acceleration.

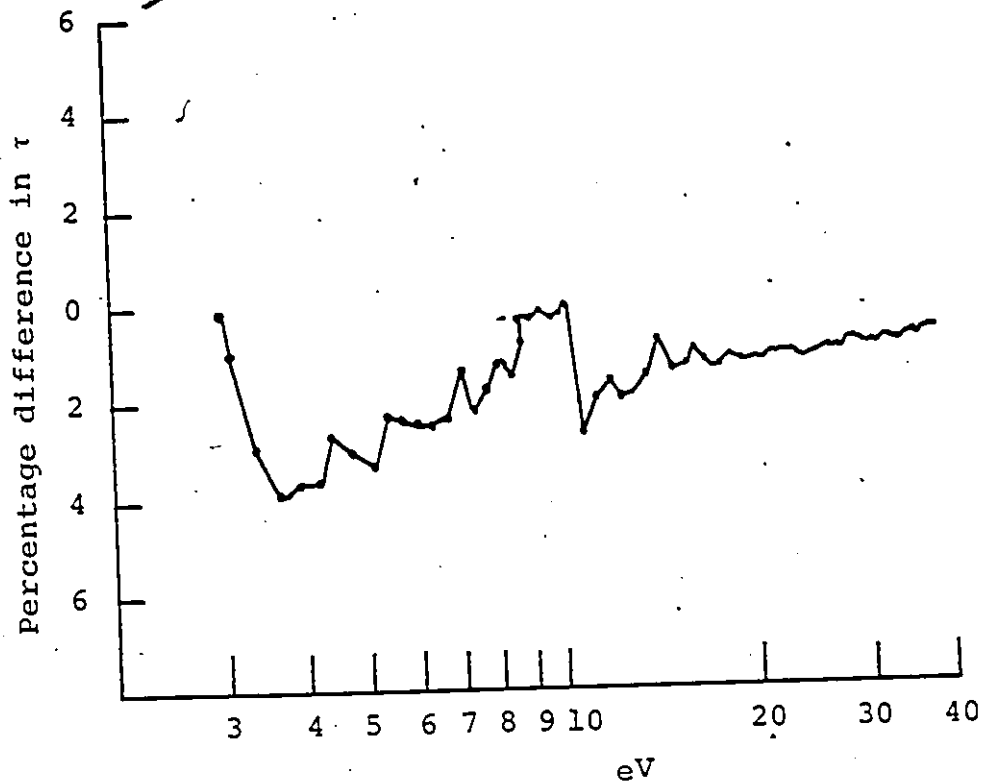


Fig. 5.3. Percentage difference in mean free flight times at the beginning and end of a time step for electron energies over 3 eV.

In the range of 0.1-3 eV the error improves from 9.2% to 1%.

Figure 5.3 gives the percentage difference for electron energies above 3 eV. As the energy increases, the error improves from a maximum value of 4% to 1%.

At the end of each time step, the new position and energy of the electron are calculated using the relations in Eq. 5.4. If a collision has occurred, then the polar angle associated with the electron velocity is estimated from the expression $\cos \theta = 2R-1$ considering isotropic scattering in the laboratory system [Appendix III], where R is a random number varying uniformly from 0 to 1.0.

The azimuthal angle, ϕ , is set equal to a uniformly distributed random number R to be selected at each collision. Since R varies from 0 to 1.0 and ϕ varies from 0 to 2π radians, the constant of proportionality is 2π . Hence,

$$\phi = 2\pi R \quad (5.11)$$

However, if the test for collision fails, then the new state of the electron, $(v', \cos \theta', z', t')$, is related to the previous state, $(v, \cos \theta, z, t)$ by the following relations:

$$v' \sin \theta' = v \sin \theta$$

$$mv' \cos \theta' = mv \cos \theta + eE\Delta t$$

$$1/2 (mv')^2 = 1/2 mv^2 + eE\Delta z \quad (5.12)$$

5.3 COLLISION CROSS SECTIONS

A collision is said to have taken place when any physical change can be detected after the distance between two particles has been first decreased and then increased. Such physical changes include angular deflection, kinetic energy, momentum changes and internal energy change of a particle. If there is an internal energy change, the collision is termed to be inelastic otherwise it is called elastic.

The cross section of a stationary target particle for particles of energy ϵ , relative to a given simple process can be thought as the area presented by target, assumed stationary in the laboratory system to a beam of particles of the same energy.

When a single fast particle moves through a differential distance in gas whose molecular velocities can be neglected in comparison, the probability of making a collision in this distance is proportional to a parameter of the system which is called the collision cross section.

The electron-molecule collision cross sections adopted for SF_6 in the simulation are shown in Fig. 5.4.

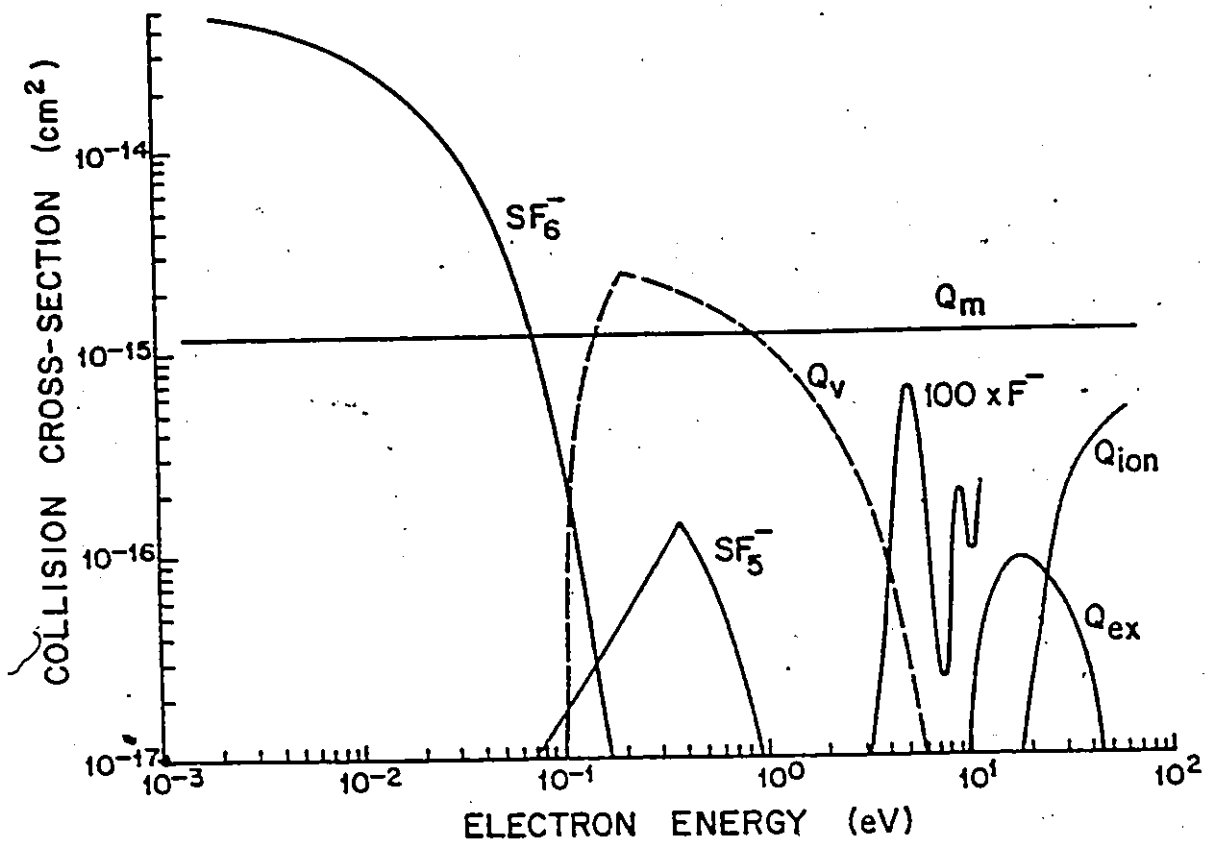


Fig. 5.4. Electron-molecule collision cross sections in SF₆.

5.3.1 Momentum Transfer Cross Section

Srivastava et al [74] have reported the momentum transfer cross section, Q_m , of elastic scattering in the energy range $5 \leq \epsilon \leq 75$ eV. The momentum transfer cross section was calculated by extrapolations of $\sigma(\theta)$ between 0 and 20° and between 135 - 180° , and using the measured $\sigma(\theta)$ (differential elastic scattering cross section at an angle θ) between 20° - 135° . The differential elastic scattering cross section is the cross section for an electron scattered into a small element of solid angle $d\Omega$, making a polar deflection angle θ with the direction of impact and defined in azimuth by an angle ϕ . The estimated error in the momentum transfer cross section, both due to experimental factors and extrapolations add up to $\pm 20\%$. This cross section can be represented to be constant because the variation in magnitude with respect to energy is 9% in the range of $5 \leq \epsilon \leq 60$ eV, with a mean value of $1.2 \times 10^{-15} \text{ cm}^2$.

For the momentum transfer cross section at 0.5 eV, the angular dependence of elastic e-SF₆ scattering data of Rohr [75] between 10° - 120° is considered using the relation

$$Q_m = \int_0^{2\pi} \int_0^\pi \sigma(\theta) (1 - \cos \theta) \sin \theta \, d\theta d\phi \quad (5.13).$$

This approximate calculation resulted in a magnitude

of $1.1 \times 10^{-15} \text{ cm}^2$. Hence, a constant momentum transfer collision cross section with a magnitude of $1.2 \times 10^{-15} \text{ cm}^2$ is adopted at $\epsilon = 0.5 \text{ eV}$.

5.3.2 Electronic Excitation Cross Section

Trajmar and Chutjian [76] have reported threshold energies for electronic excitation of SF_6 of 9.8, 11, 11.6, 12.8 and 13.3 eV. Threshold energy is the energy of the electron at which the onset of excitation of a particular level is observed. The shape and magnitude of this cross section is not given. Yoshizawa et al [77], in their calculation of Boltzman solution adopted an excitation cross section with a threshold of 9.8 eV and the same shape is employed in this simulation, however, with a maximum magnitude of $0.95 \times 10^{-16} \text{ cm}^2$ which occurs at 18 eV. The excitation cross section is given by

$$Q_{\text{ex}} = 0.95 \times 10^{-16} \frac{\epsilon - 9.8}{18 - 9.8} \exp\left[\frac{18 - \epsilon}{18 - 9.8}\right] \text{cm}^2 \quad (5.14)$$

where, ϵ is the electron energy.

5.3.3 Attachment Collision Cross Section

Yoshizawa et al. [77] summarized the attachment cross sections for formation of SF_6^- ions as determined by various authors. Although the shapes of the cross section curves as a function of electron energy are generally in contradiction to each other, the peak

value of the cross section lies very close to the origin of the energy scale except in the case of the earliest work in this gas of Ahearn and Hanney [78] who have reported a maximum cross section at 2 eV of incident electron energy. Yoshizawa et al. [77] employed a cross section similar to that given by Hickam and Fox [79] according to which a part of the cross section curve lies at negative ion accelerating voltages, and shifting the cross section in such a way that a peak value of $1.5 \times 10^{-14} \text{ cm}^2$ occurs at 0.18 eV. The cross section for SF_6^- measured by Kline et al. [80] is probably instrumental in the energy range $10 \leq \epsilon \leq 100 \text{ meV}$. This cross section is measured by Chutjian [81] in the energy interval of 0-200 meV. We have employed the results of Chutjian because the experimental uncertainty at threshold which occurs at 0 eV is 4 meV. Results of the fit for SF_6^- attachment process in Ref. [81] are

$$\begin{aligned}
 Q_{\text{AT}}(\text{SF}_6^-) &= 5.2 \times 10^{-14} \exp \frac{-\epsilon}{0.044} \text{ cm}^2 \quad 0 \leq \epsilon \leq 0.045 \text{ eV} \\
 &= 5.2 \times 10^{-14} \times 0.868 \exp \frac{-\epsilon}{0.0516} \text{ cm}^2 \\
 &\quad 0.045 \leq \epsilon \leq 0.200 \text{ eV}
 \end{aligned} \tag{5.15}$$

where ϵ is in electron volts.

In the present simulation good agreement with the experimental attachment coefficients is achieved by decreasing the width of this cross section that is replacing 0.044

and 0.0516 in Eq. 5.15 by 0.0177 and 0.02, respectively.

In addition to the formation of SF_6^- other predominant ions are SF_5^- and F^- . For SF_5^- collision cross sections we have adopted the results of Christopherou et al. [82] with a peak of $1.425 \times 10^{-16} \text{ cm}^2$ at 0.37 eV. Yoshizawa et al. [77] employed the same cross section with a peak 20 times smaller than it should be [83]. Novak and Fiechette [84], for this cross section, used a peak value normalized to the data of Kline et al. [80], which is $3.4 \times 10^{-16} \text{ cm}^2$ at 0.36 eV. The cross section for the formation of F^- ions is represented according to the measurements of Kline et al. [80] in the range of $3 \leq \epsilon \leq 11.4 \text{ eV}$.

5.3.4 Ionization Collision Cross Section

The ionization cross section of Rapp and Englander-Golden [85] is used in the investigation with an ionization threshold energy of 15.8 eV.

5.3.5 Vibrational Collision Cross Section

Vibrational excitation by electron impact can be measured in a crossed beam experiment from the energy loss spectrum of electrons.

Rohr [86] has measured the vibrational collision cross section in SF_6^- from the threshold energy of 0.0954 eV up to 3 eV for $v=1$. He has also reported

[75] $e\text{-SF}_6$ ($\Delta v=0$) scattering cross sections with $e\text{-SF}_6(v=0)+Q_v$ where Q_v is the total vibrational excitation cross section in the interval $0.25 \leq \epsilon \leq 6$ eV. The cross section used by Kline et al. [80] is negligible compared with Rohr's cross section. However, they did not find any significant influence of this cross section on the calculated parameters even if the magnitude is increased by an order. Although this collision cross section is ignored, the influence of Q_v will be discussed in energy distributions.

5.4 DECIDING ON THE NATURE OF COLLISION

The total collision cross section is defined as the sum of the individual cross sections,

$$Q_T = Q_{el} + Q_{AT} + Q_{ex} + Q_{ion} \quad (5.16)$$

To determine the type of encounter at each collision a random number R is drawn from a set of numbers uniformly distributed over the interval from 0 and 1.0. Then the nature of collision is decided according to Fig. 5.5, where the position of the arrow indicates the nature of collision. Since the ratio of a collision cross section for a particular event to the total cross section gives the probability of this event, each box in the figure corresponds to the probability of a certain event [Appendix III].

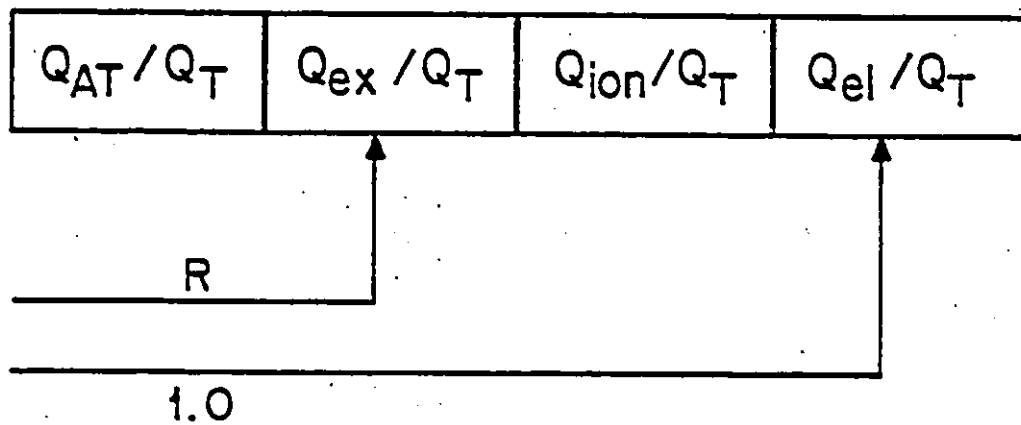


Fig. 5.5. Deciding on the nature of collision.

After the event of a collision, if the probabilities of inelastic collisions fail, the collision is deemed to be elastic and the loss of energy in the collision is $(2m/M)\epsilon$ where m and M are the masses of an electron and an SF_6 molecule, respectively. If the electron is attached it is lost in the swarm and its subsequent fate is ignored. For the other inelastic processes the appropriate threshold energy of the process is subtracted from the electron energy. However, in the case of an ionizing collision, after subtracting the threshold energy, the remaining energy is evenly ascribed to the two electrons. That is, a total average loss of $(\epsilon + \epsilon_{\text{onset}})/2$ energy is assumed for the original electron.

5.5 COMPUTATIONAL METHOD

5.5.1 Introduction

At time $t=0$, initial electrons with a constant energy of 0.1 eV are injected from the origin of the coordinate system assuming a cosine distribution [Appendix II] for the angle of entry with respect to the z axis. All the electrons in the swarm moving forward and backwards including the electrons formed during the ionization process are traced until the termination time or loss due to attachment. The state of the new electrons are stored in stocks with their position, energy and

time of birth until the original electron has been followed to the termination time or it is lost in the swarm. Then a new electron is released at its place of birth with its initial state and traced until termination criteria is reached. Any further new electrons produced are included into the stock. By scan-pointers and shifting the time frame from t_{\max} to t_{\min} where, t_{\min} is the time of appearance of the first electron due to ionization and t_{\max} corresponds to the most recently stored electron, this procedure is repeated until all new electrons have been tracked. It is assumed that the back scattered electrons are completely absorbed by the cathode.

5.5.2 Swarm Parameters

The electron drift velocity is defined as the velocity of the centre of mass of an avalanche which can be written as

$$W = \frac{d\bar{z}(t)}{dt} \quad (5.17)$$

$$\text{or } W = \frac{(1/n_2) \sum_{k=1}^{n_2} z_k(t_2) - (1/n_1) \sum_{k=1}^{n_1} z_k(t_1)}{t_2 - t_1} \quad (5.18)$$

where $z_k(t_j)$ is the position of the k^{th} electron in the swarm at sampling time t_j , and n_j is the number of electrons at t_j , where $j=2$ or 1 .

The longitudinal diffusion coefficient D_L may be found from the relation

$$\langle (z - \langle z \rangle)^2 \rangle = 2D_L t \quad (5.19)$$

or may be obtained from the formula

$$D_L = \frac{(1/n_2) \sum_{k=1}^{n_2} [z_k(t_2) - \bar{z}(t_2)]^2 - (1/n_1) \sum_{k=1}^{n_1} [z_k(t_1) - \bar{z}(t_1)]^2}{2(t_2 - t_1)} \quad (5.20)$$

The ratio of radial diffusion coefficient to mobility is defined as

$$\frac{D_L}{\mu} = \frac{\langle R^2 \rangle E}{4Wt} \quad (5.21)$$

where, D_L is the radial diffusion coefficient, μ is the mobility of the electron and $R = (x^2 + y^2)^{1/2}$ is the radial position of the electron normal to the applied field, E .

The mean square displacement $\langle R^2 \rangle$ at time t , is obtained using the following equation:

$$\langle R^2 \rangle = \frac{1}{n} \sum_{k=1}^n \sum_{i=1}^r [(x_k)_i^2 + (y_k)_i^2] \quad (5.22)$$

where $(x_k)_i$ and $(y_k)_i$ represent the displacement of the k^{th} electron in the directions x and y during its i^{th} flight and r is the total number of displacements at time t .

The first ionization coefficient is defined as

$$\alpha = \frac{\ln\left(\frac{n_+}{n_0} + 1\right)}{\bar{z}} \quad (5.23)$$

where, n_+ is the number of positive ions in the swarm, n_0 is the initial electrons and \bar{z} is the average distance traversed in the field direction.

The attachment coefficient is given according to the following expressions:

$$n = \frac{n_-}{n_0} \times \frac{1}{z} \quad (\text{in the absence of ionization})$$

and

$$n = \left(\frac{n_-}{n_+}\right) \alpha \quad (\text{with ionization}) \quad (5.24)$$

where, n_- is the number of negative ions in the swarm.

The excitation coefficient α_{ex} is defined similarly as

$$\alpha_{\text{ex}} = \frac{n^*}{n_0} \times \frac{1}{z} \quad (\text{no ionization})$$

$$\text{and } \alpha_{\text{ex}} = \left(\frac{n^*}{n_+}\right) \alpha \quad (\text{with ionization}) \quad (5.25)$$

where, n^* is the number of excited states.

5.6 RESULTS AND DISCUSSION

In the E/p range of interest $100 \leq E/p \leq 180 \text{ V cm}^{-1} \text{ Torr}^{-1}$, the number of initial electrons considered range from 140 to 40. Up to 400 electrons are traced

in the swarm with total number of free flight paths ranging from 1.5×10^4 to 2.7×10^4 . To ensure that the calculations are carried out in the equilibrium region the temporal positions of the swarm centroid together with its variation are calculated with 0.5×10^{-8} s or 1.0×10^{-8} s time intervals. The termination time corresponds to an average gap distance of .87 cm at $100 \text{ V cm}^{-1} \text{ Torr}^{-1}$ and -1.4 cm at $180 \text{ V cm}^{-1} \text{ Torr}^{-1}$.

5.6.1 Back Scattering Coefficient

Figure 5.6 shows the variation of back scattering coefficient, which is defined as the ratio of back scattered electrons to total emission as a function of applied electric field. As expected the number of electrons back scattered decreases with increasing E/p.

5.6.2 Drift Velocity, Longitudinal Diffusion Coefficient, and Ratio of Radial Diffusion Coefficient to Mobility

In Figs. 5.7-5.10 the centroid positions along the electric field direction are given together with their variations with respect to sampling times. The lines drawn through the data points are the linear least square lines.

For $100 \text{ V cm}^{-1} \text{ Torr}^{-1}$, the $\langle z \rangle$ line intercepts the time axis at -0.5×10^{-8} seconds resulting in a negative

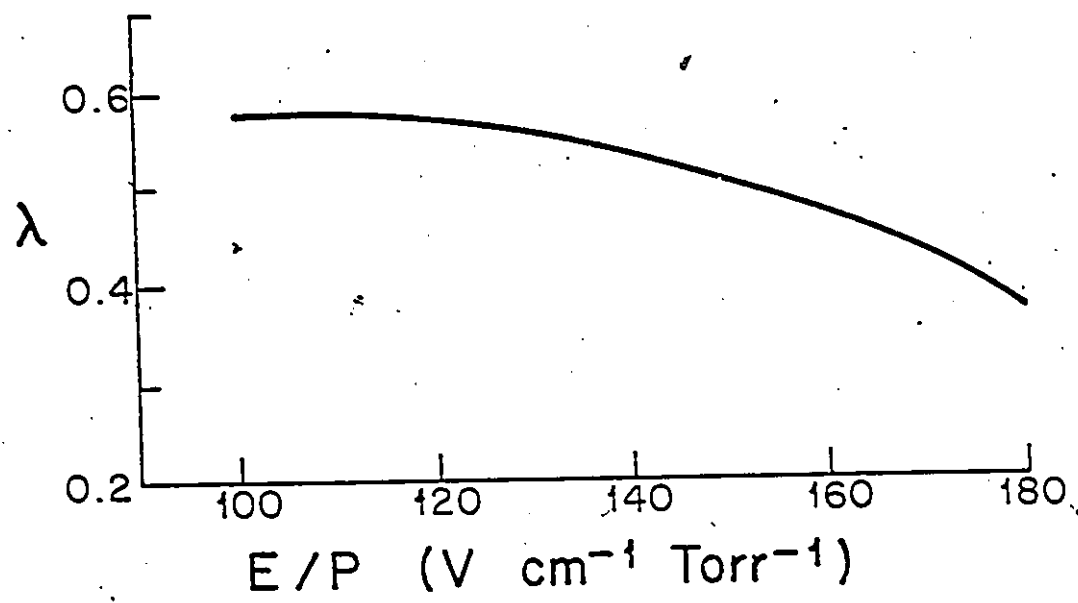


Fig. 5.6. Back scattering coefficient at 0.1 eV emission energy.

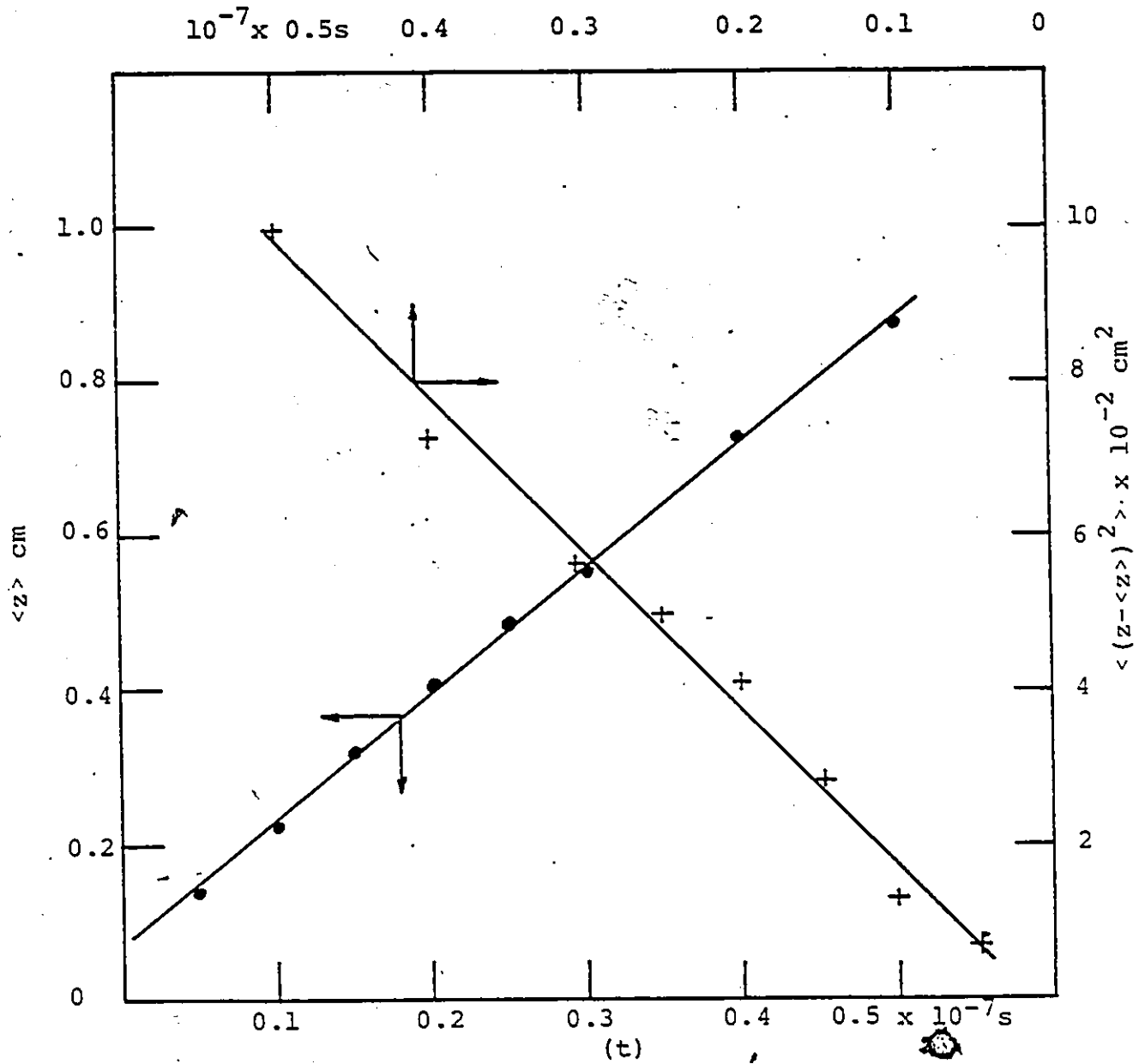


Fig. 5.7. Variation of average distance along the field direction with respect to time at $E/p=100$ V $\text{cm}^{-1}\text{torr}^{-1}$.

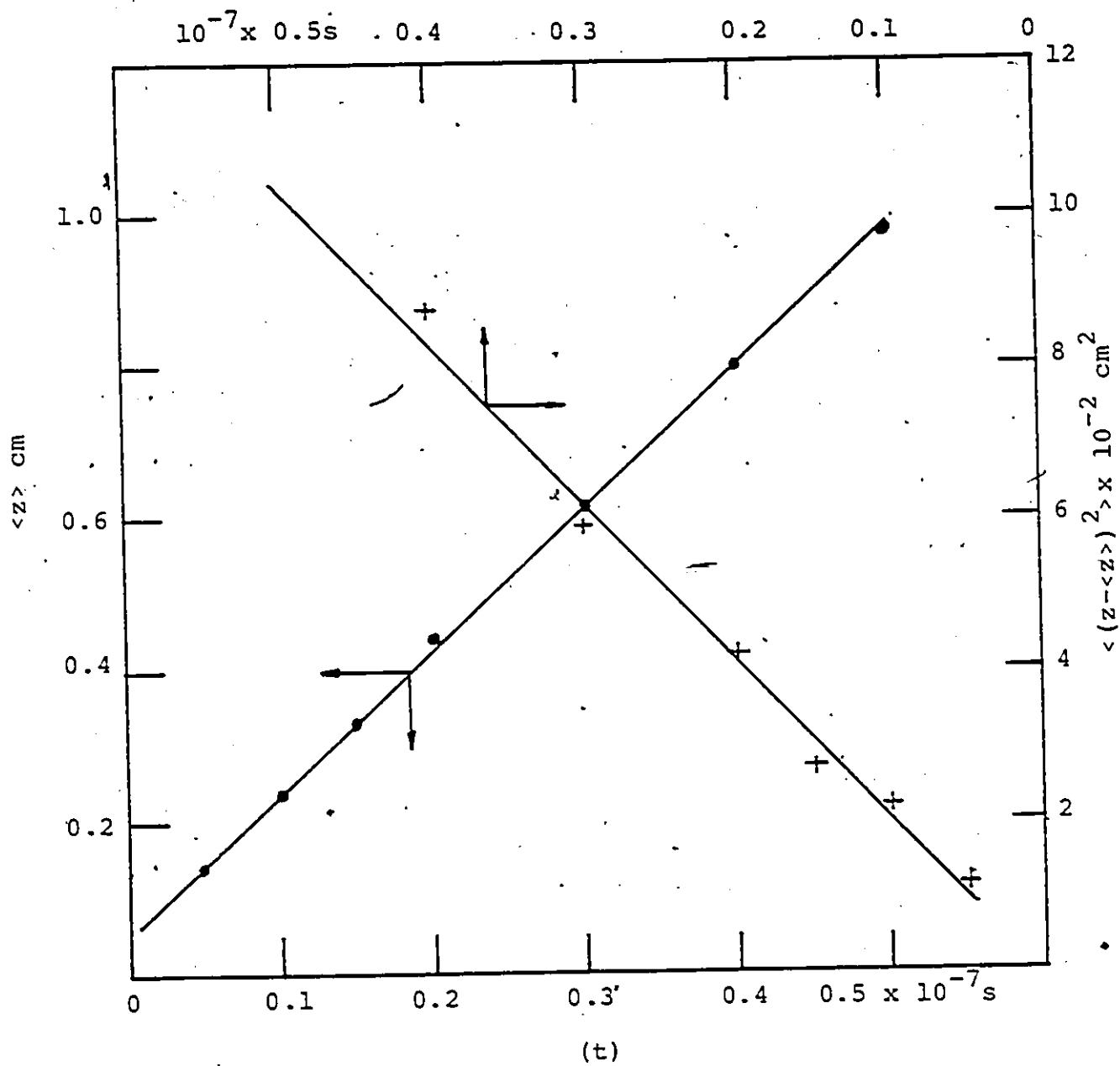


Fig. 5.8. Variation of average distance along the field direction, with respect to time at $E/p=120$ V $\text{cm}^{-1}\text{Torr}^{-1}$.

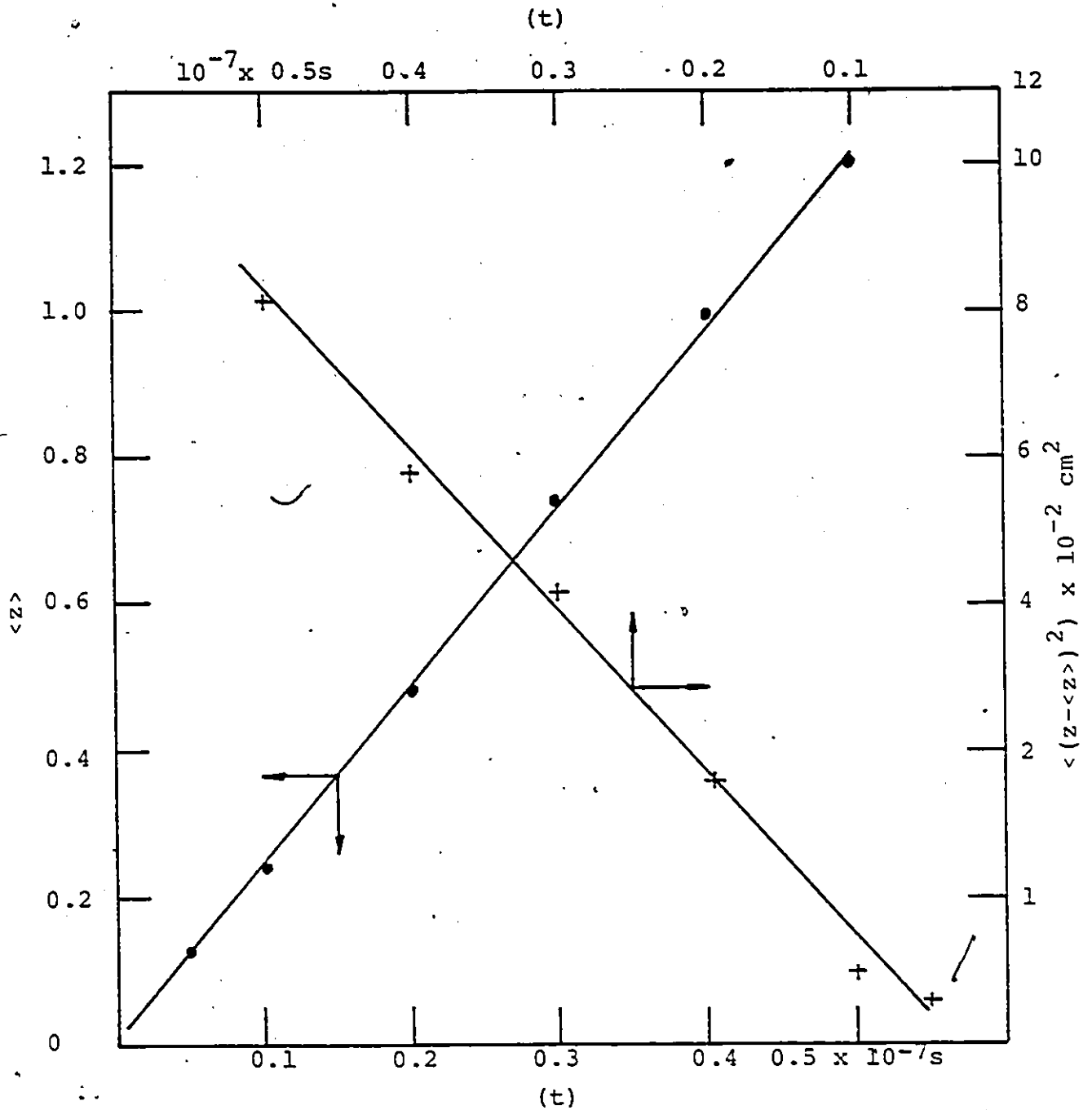


Fig. 5.9. Variation of average distance along the field direction with respect to time at $E/p=150.V \text{ cm}^{-1}\text{Torr}^{-1}$.

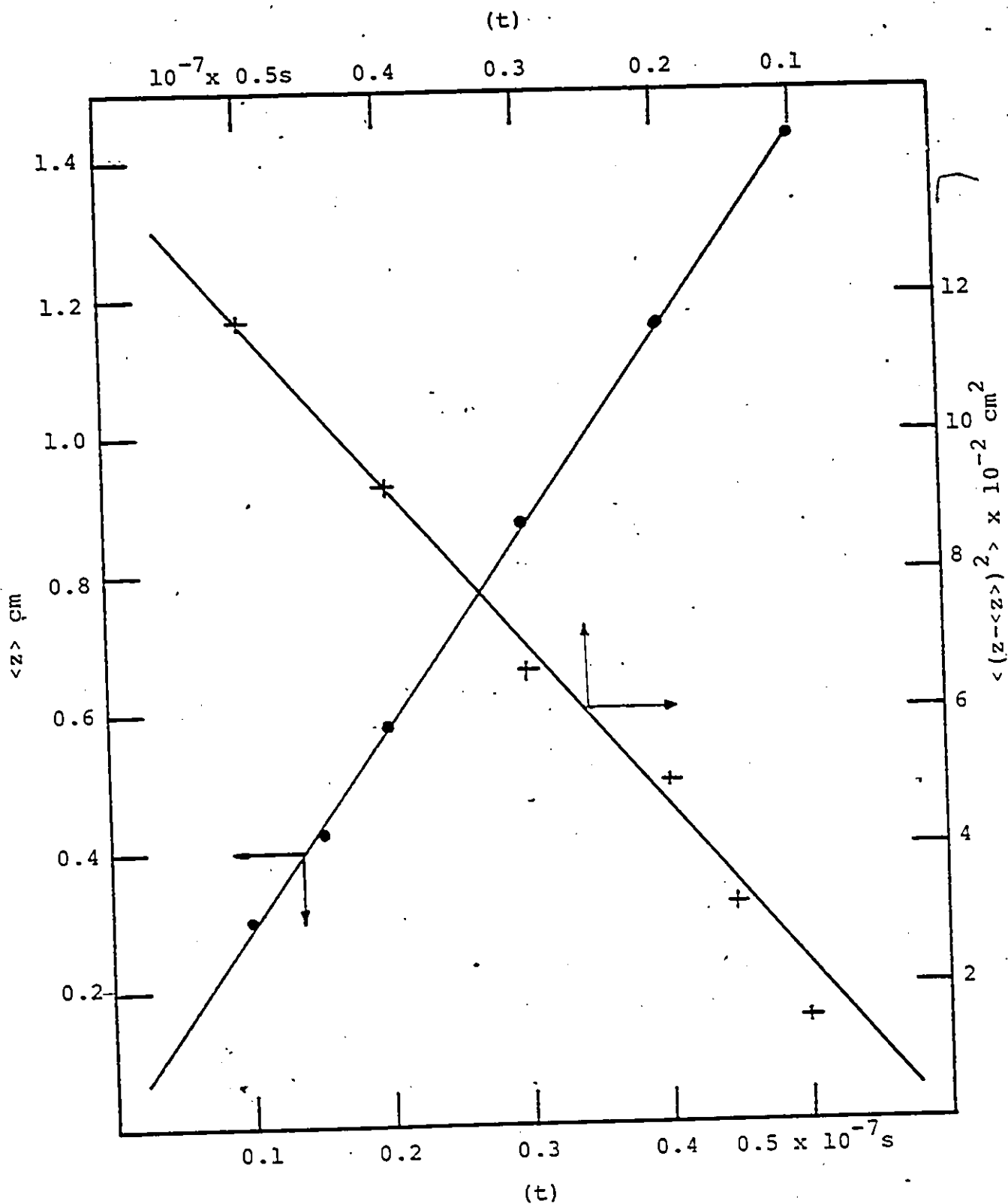


Fig. 5.10. Variation of average distance along the field direction with respect to time at $180 \text{ V cm}^{-1} \text{ Torr}^{-1}$.

time effect. This time interval may be considered as a relaxation time for the swarm to reach equilibrium. The relaxation time is the same as t in Eq. 5.3 and can also be calculated.

At $100 \text{ V cm}^{-1} \text{ Torr}^{-1}$, the average energy of the swarm is 8.6 eV (simulation result, Fig. 5.21). Equation 5.3 gives the relaxation time to exchange 8.6 eV as 5.05×10^{-9} seconds which is in very good agreement with the simulation. At $180 \text{ V cm}^{-1} \text{ Torr}^{-1}$, the time to exchange an average energy of 11 eV is lower. With increasing E/p , therefore, the time required to reach equilibrium is lower for the electron swarm. This behavior of the relaxation time is also observed in previous Monte Carlo calculations [72,87].

Drift velocities are calculated from the slopes of $\langle z \rangle - t$ graphs using the least square technique. The results are given in Fig. 5.11 together with the measured values of Teich and Sangi [88], Naidu and Prasad [89] and calculated values of Novak and Frechette [84]. There is a very good agreement particularly in high E/p values.

The longitudinal diffusion coefficient is obtained using the slopes of $\langle (z - \langle z \rangle)^2 \rangle - t$ square lines. This coefficient is shown in Fig. 5.12.

The ratio of radial diffusion coefficient to electron

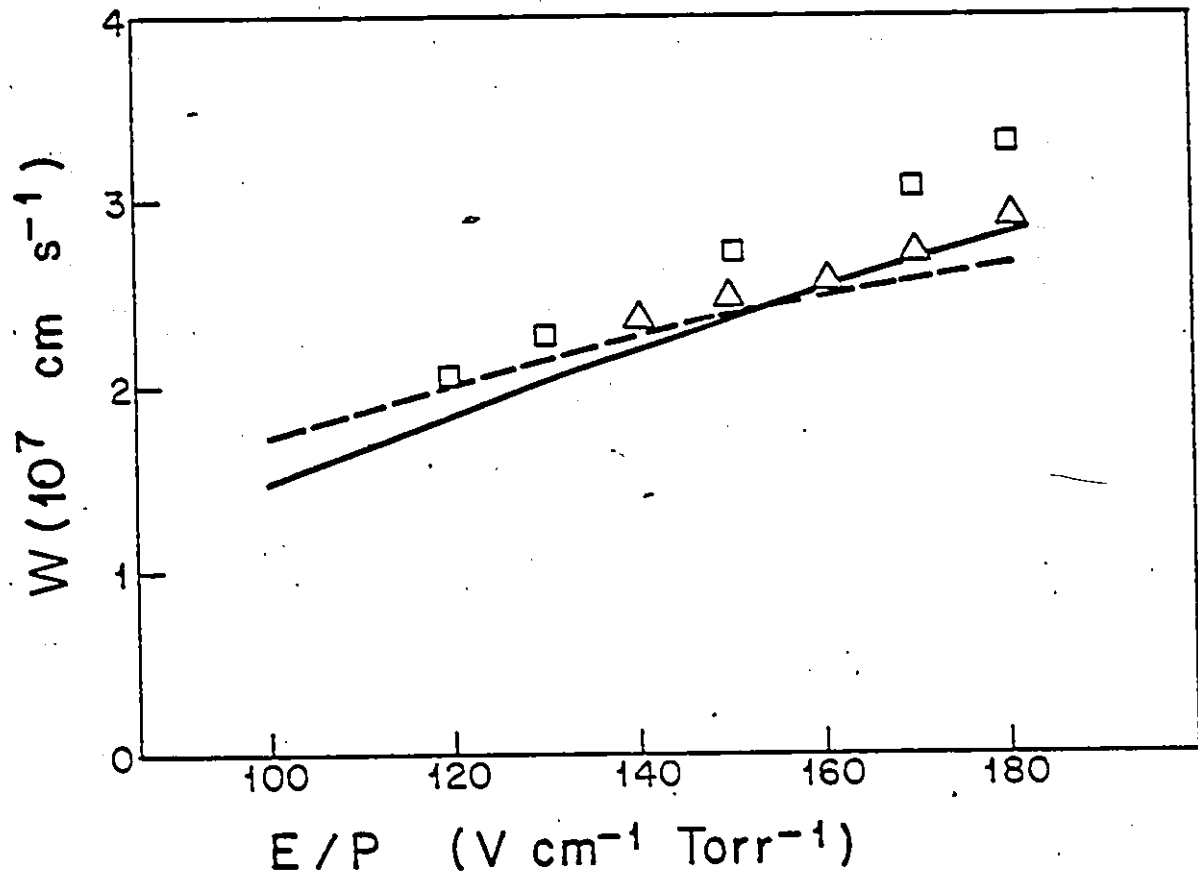


Fig. 5.11. Drift velocities in SF_6 .
— present study; \square Ref. 89; \triangle Ref. 88;
--- Ref. 84.

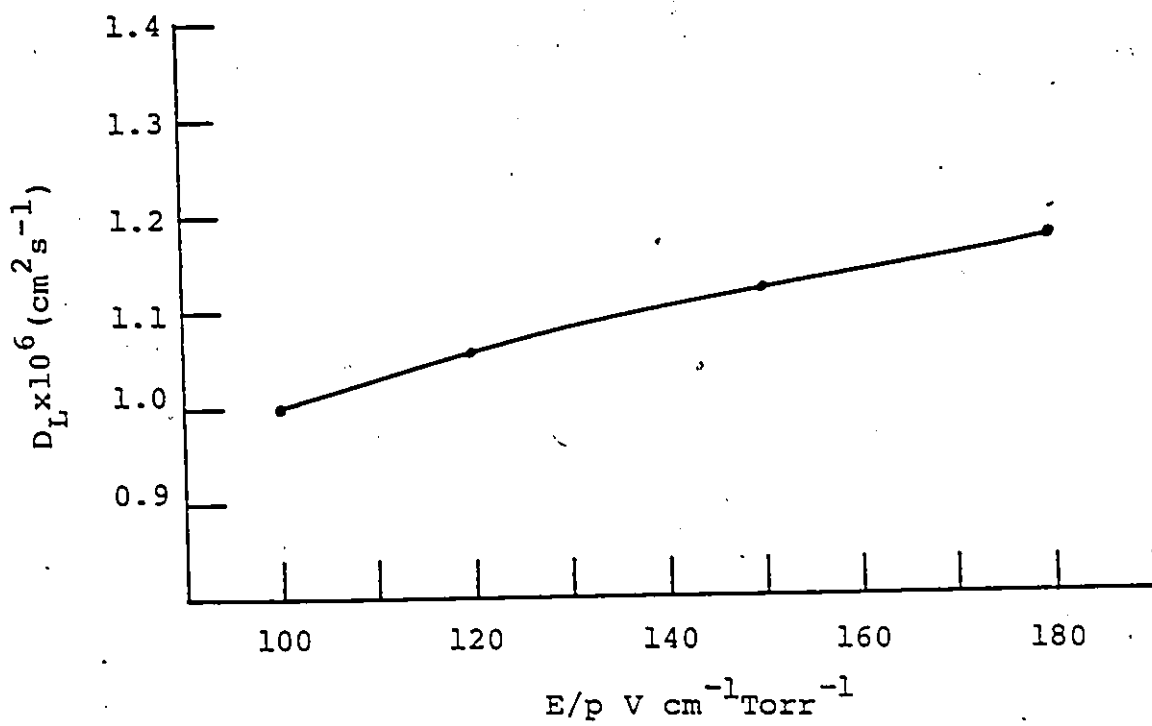


Fig. 5.12. Longitudinal diffusion coefficient.

mobility is shown in Fig. 5.13 and compared with the experimental results of Naidu and Prasad [89].

Since the average values are calculated at time intervals, the group sizes corresponding to sampling times vary from each other. In Figs. 5.7-5.10, the variance of average drift distance is shown on the right hand scale. If a group of 100 electrons is considered, at 100 E/p the drift velocity is measured within $\pm 4\%$. This statistical error is reduced to $\pm 2.4\%$ for 180 $\text{V cm}^{-1}\text{Torr}^{-1}$. Considering the standard error of variances the error in D_L is within $\pm 14\%$.

The statistical errors can be assumed reasonable due to the fact that the experimental measurements of D_L have typically a $\pm 8\%$ to $\pm 15\%$ error associated with them [90]. Typical error for the measurement of electron drift velocity is within $\pm 2\%$ to $\pm 6\%$ [90,91].

5.6.3 Ionization and Electronic Excitation Coefficients

Figure 5.14 shows the Townsend first ionization coefficients calculated together with the experimental data of Bhall and Claggs [44], Boyd and Crichton [45] and the experimental results obtained in our laboratory (see Chapter III).

In Fig. 5.15 the electronic excitation coefficients are given and compared with results of Yoshizawa et al.

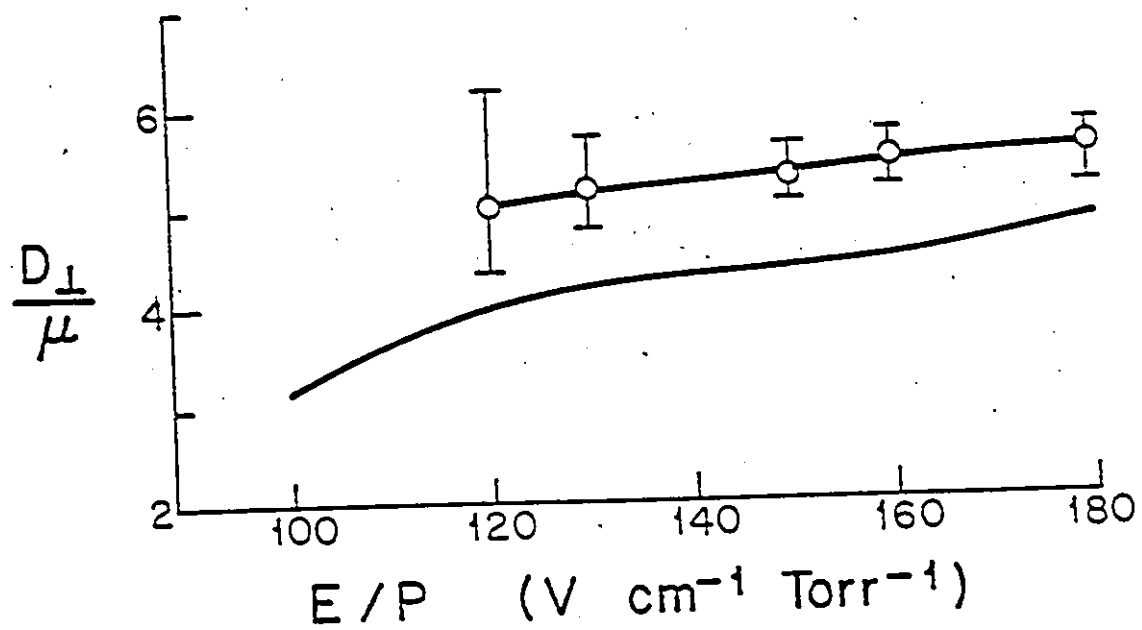


Fig. 5.13. D_{\perp}/μ in SF_6 .

— present study; \circ Ref. 89.

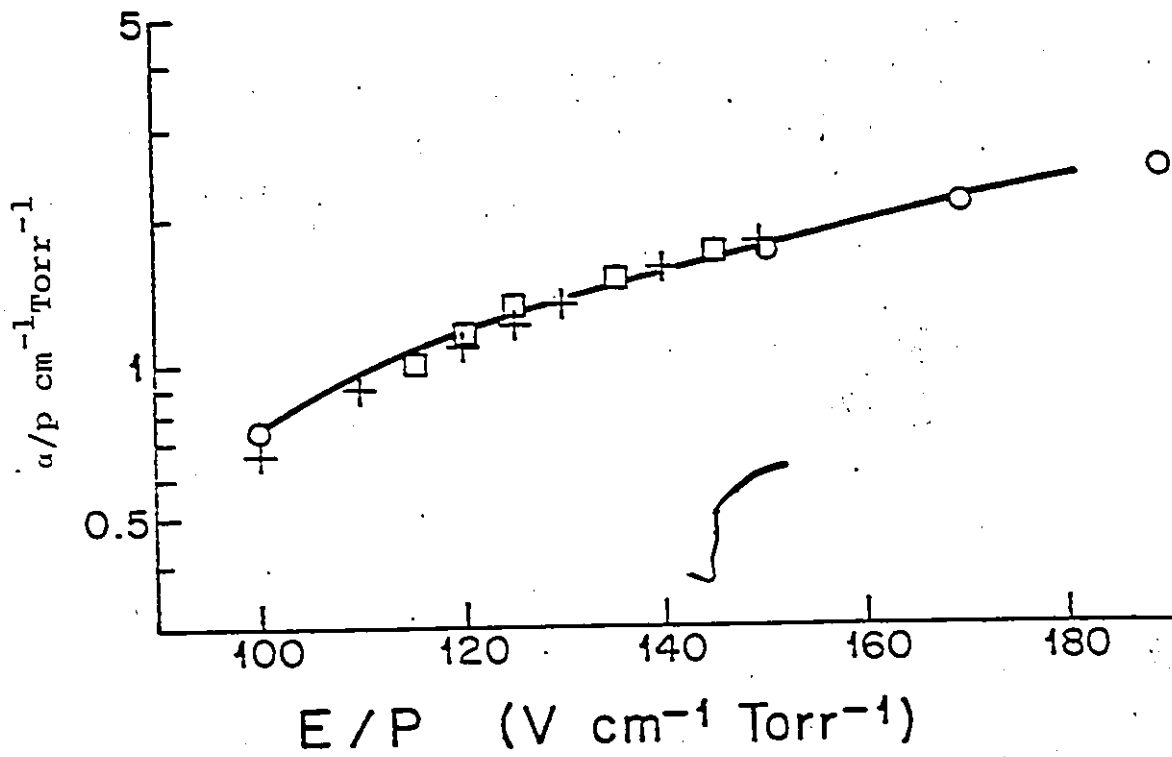


Fig. 5.14. Ionization coefficient in SF_6 .

— present study; o - measurements;
+ - Ref. 44; \square Ref. 45.

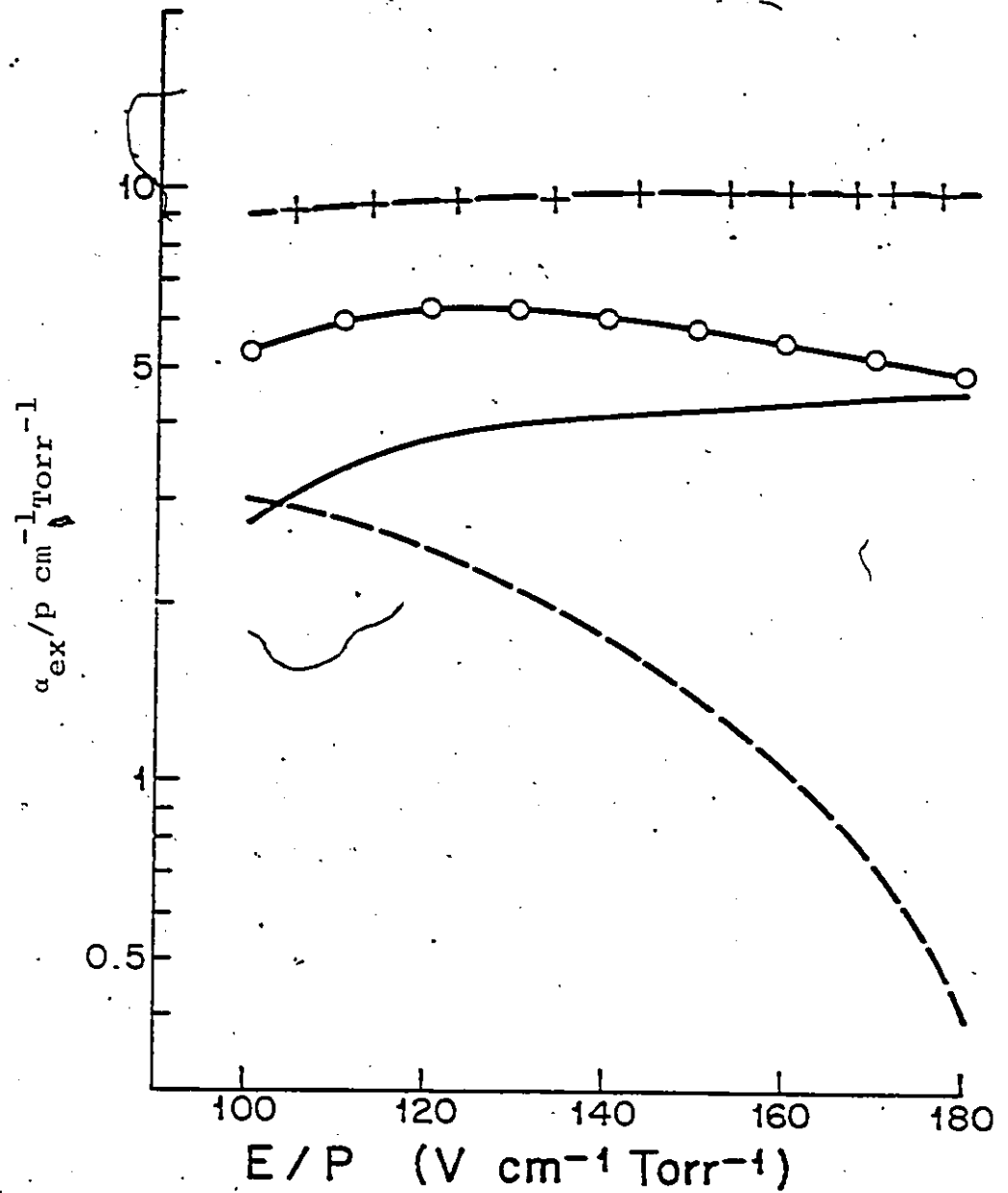


Fig. 5.15. Electronic excitation coefficient.

— α_{ex} (with ionization); - - - α_{ex} (absence of ionization); —○— α_{ex} total;
 -+- Ref. 75.

[77]. The values obtained in this simulation are lower possibly due to the fact that the adopted cross section has a peak of $0.95 \times 10^{-16} \text{ cm}^2$ which is about 40% lower than Yoshizawa et al. The electronic excitation coefficient decreases with increasing E/p for $E/p > 120 \text{ V cm}^{-1} \text{ Torr}^{-1}$ unlike the results of Ref. [77]. However, if the peak value is increased above $0.95 \times 10^{-16} \text{ cm}^2$, it is observed that ionization coefficients do not agree with the measurements.

5.6.4 Attachment Coefficient

Figure 5.16 shows the attachment coefficients obtained and these results are compared with the experimental measurements. Good agreement is obtained.

5.6.5 Energy Distributions and Mean Energy

The energy distributions sampled per collision in 1 eV steps and normalized according to $\int_0^{\infty} f(\epsilon) d\epsilon = 1$ are shown in Figs. 5.17-5.20. The corresponding mean energies obtained are given in Fig. 5.21 together with the results of Yoshizawa et al. [77].

As expected the magnitude of peak of the distribution decreases with increasing E/p and shifts towards high energy scale. The full lines show the Maxwellian distribution at mean energies corresponding to those in Fig. 5.21.

The influence of the vibrational excitation cross section on the energy distribution is investigated by introducing this cross section in the simulation and

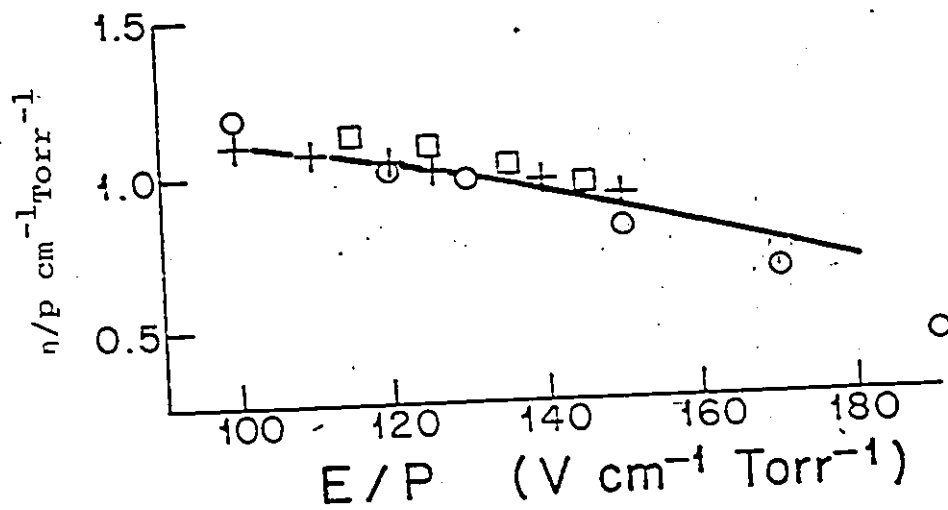


Fig. 5.16. Attachment coefficient.

— present study; o - present study (measurements); + - Ref. 44; □ Ref. 45.

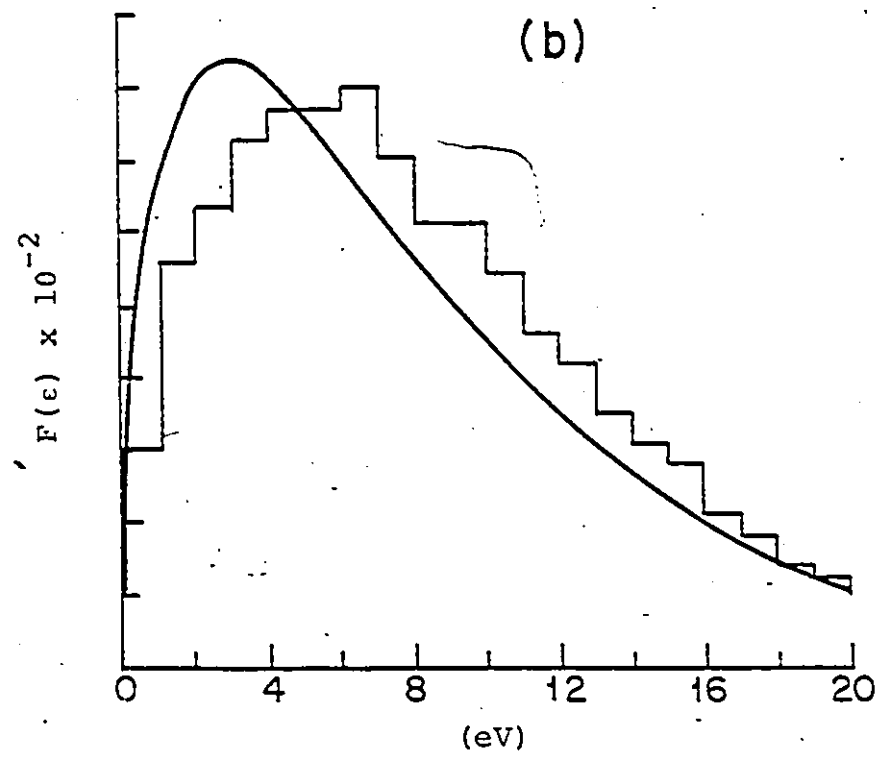
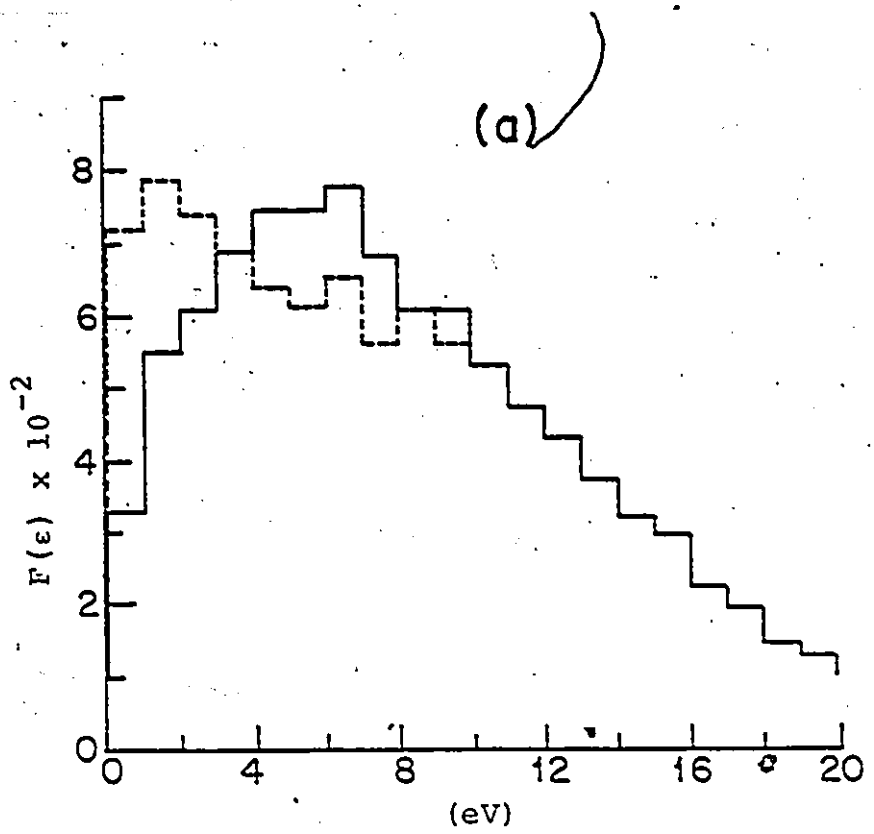


Fig. 5.17. Energy distribution sampled per mean free flight time at 100 E/p $V \text{ cm}^{-1} \text{ Torr}^{-1}$. (a) sampled at collision; (b) sampled after collision; broken lines - effect of vibrational excitation; full curve - Maxwellian at the same mean energy.

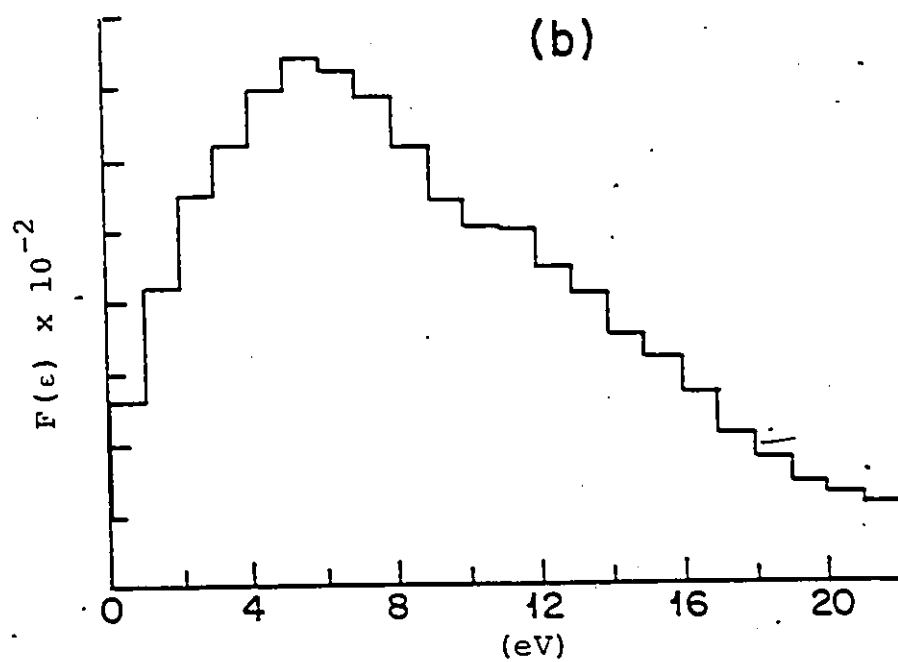
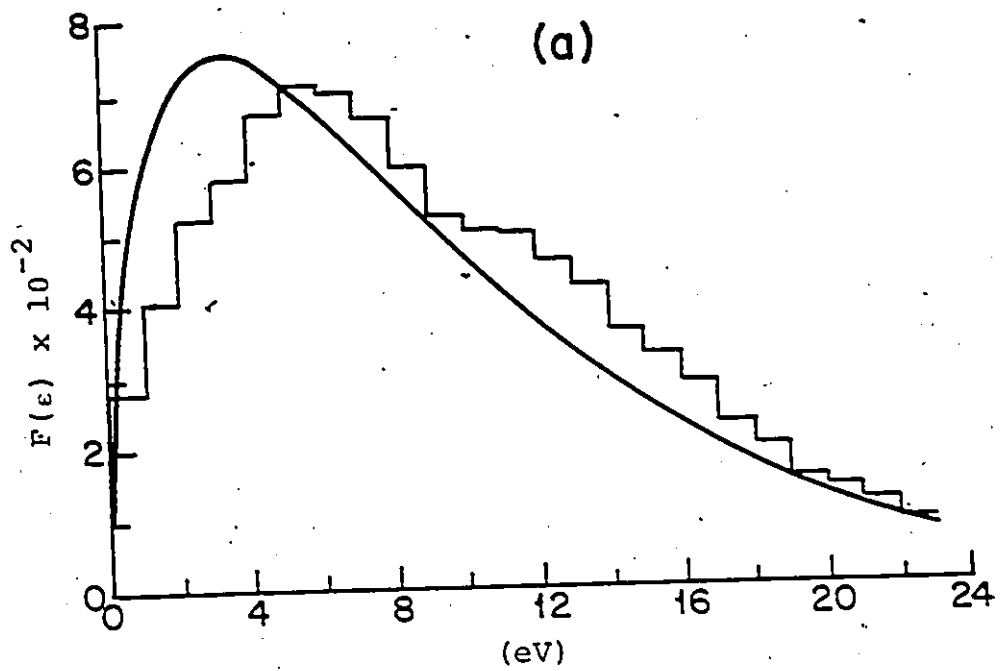


Fig. 5.18. Energy distributions sampled per mean flight time at $E/p=120$ V $\text{cm}^{-1}\text{Torr}^{-1}$.

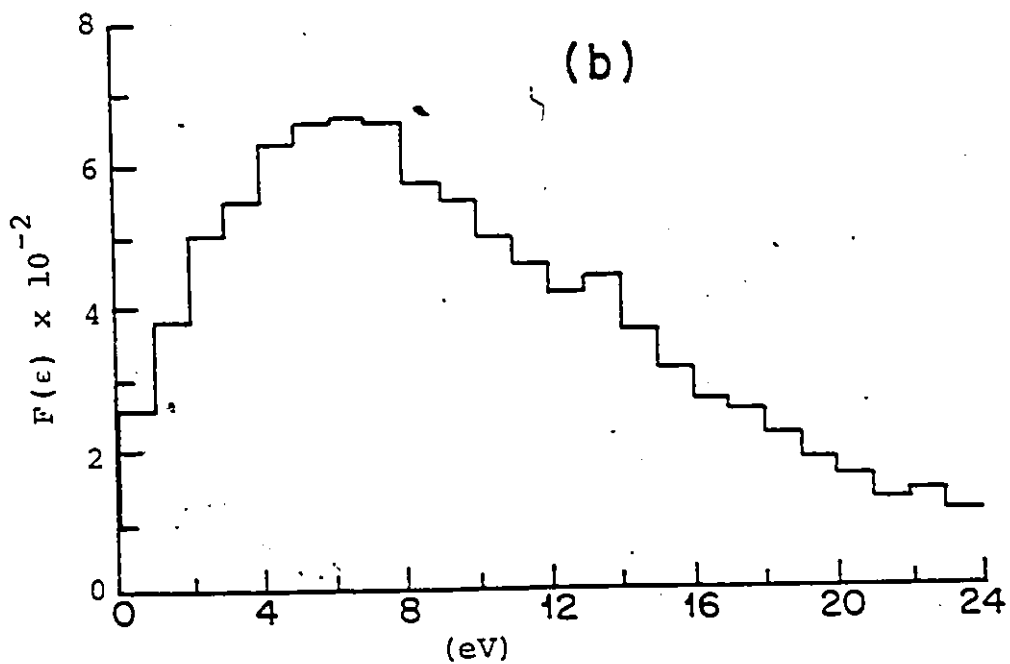
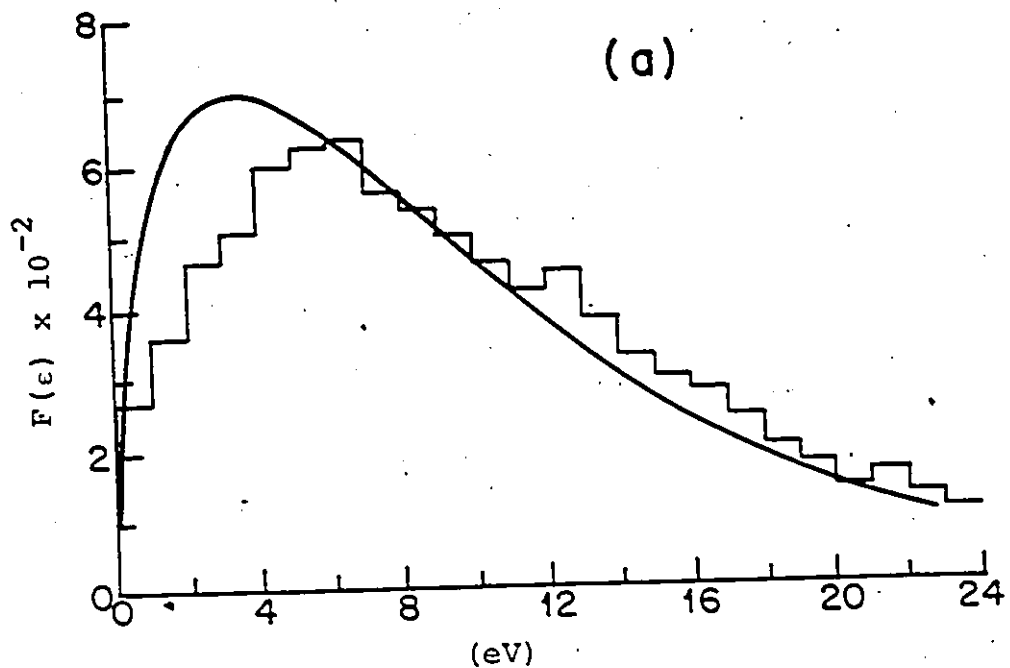


Fig. 5.19. Energy distributions sampled per mean free flight time at $E/p=150 \text{ V cm}^{-1}\text{Torr}^{-1}$.

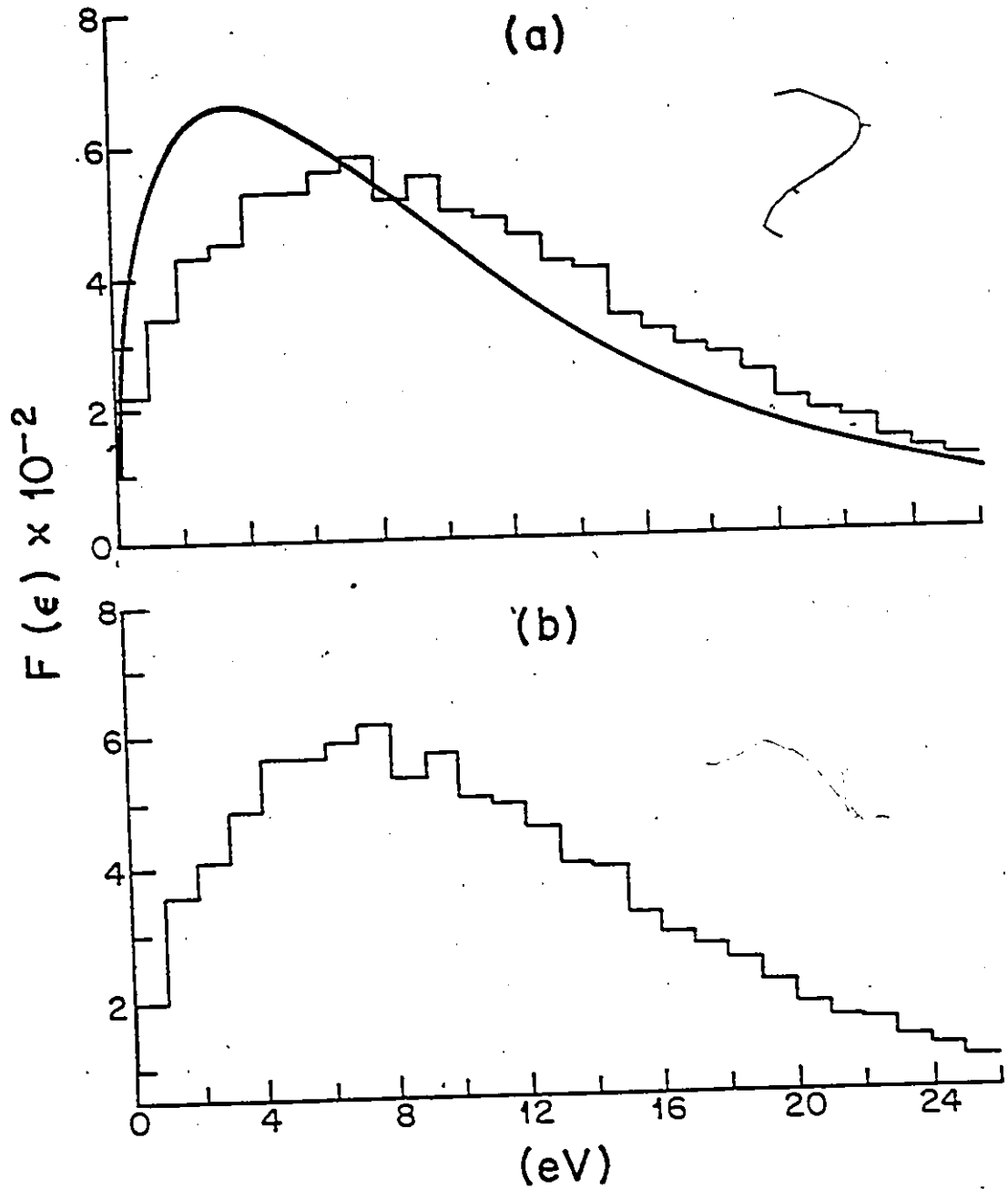


Fig. 5.20. Energy distributions sampled per mean free flight time at $E/p=180 \text{ V cm}^{-1}\text{Torr}^{-1}$.

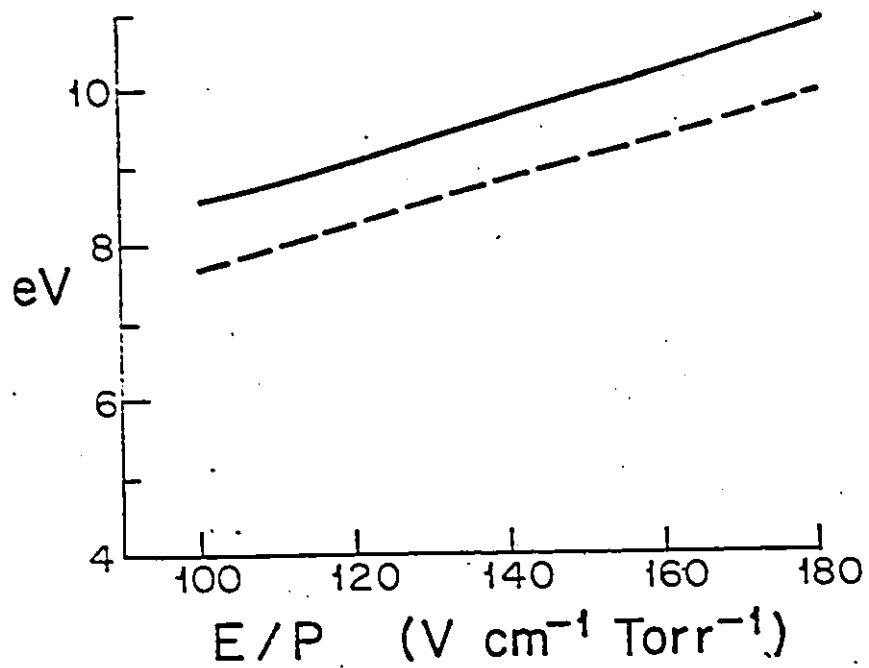


Fig. 5.21. Mean energy in SF₆.

— present study; - - - Ref. 77.

retaining the other cross sections as before. The total vibrational excitation cross section is defined as:

$$Q_v = 2.4 \times 10^{-14} (\epsilon - \epsilon_i) \text{ cm}^2 \text{ for } 0.1 < \epsilon < 0.2 \text{ eV}$$

where ϵ_i is the threshold energy, and

$$\text{and } Q_v = 2.4 \times 10^{-15} \exp \frac{0.2 - \epsilon}{1.1} \text{ cm}^2$$

for $0.2 \leq \epsilon \leq 6 \text{ eV}$

(5.26)

This cross section has a maximum magnitude of $2.4 \times 10^{-15} \text{ cm}^2$ at 0.2 eV.

As shown in Fig. 5.17 the introduction of this cross section introduced depressions in the energy distribution at lower energy scales. For E/p $120 \text{ V cm}^{-1} \text{ Torr}^{-1}$, n/p increased by 9%. Although the threshold energy for the vibrational excitation is about 0.1 eV, the depressions observed indicate that there is an increase in the number of low energy electrons in the swarm and, therefore, the coefficient n/p increases. Yoshizawa et al. [77] employed an SF_6^- cross section with a peak at 0.18 eV which is very close to the peak in the vibrational cross section adopted by them. They have observed that a reduction of Q_v by an order of magnitude reduces n/p by 6% at $120 \text{ V cm}^{-1} \text{ Torr}^{-1}$. Novak and Flechette [84] observed relatively minor influence of Q_v on the coefficients. Kline et al [80], did not observe any change on the calculated coefficients

even if their vibrational cross section is increased by an order of magnitude. However, it may be argued that depending on the location of the peak of attachment and vibrational cross sections, there is an interrelationship between the two that effects n particularly at lower values of E/p .

5.7 CONCLUSIONS

Because of the lack of uniqueness resulting from the multiplicity of cross sections, the usual aim of high E/p transport coefficient analysis is not to derive individual cross sections but to obtain a consistent cross section set. The collision cross section set adopted in the simulation results is in a good agreement with the experimental values over the range of E/p investigated. These cross sections can be used with confidence for the study of electrical discharges in SF_6 in non-uniform electrical fields as well.

CHAPTER VI

BEHAVIOUR OF SWARM PARAMETERS IN EXB UNIFORM FIELDS

6.1 INTRODUCTION

In recent years considerable work has been carried out to investigate the influence of a magnetic field applied perpendicularly to the electric field on the ionization and the breakdown mechanism in gasses. For uniform EXB fields the change in the ionization coefficients and the breakdown voltage has been interpreted in terms of the equivalent pressure concept first proposed by Blevin and Haydon [92] and examined in considerable detail by Govinda Raju and coworkers [93,94,95]. From energy balance considerations in the presence and absence of a crossed magnetic field Allis [96], and independently Heylen [97] have developed the equivalent reduced electric field (EREF) concept. This approach defines an equivalent reduced electric field which is the value of E/p required in the absence of a magnetic field to keep the average electron energy the same as that engendered by the applied E/p in the presence of a magnetic field. The progress in the study of EXB discharges has been reviewed by Heylen [98] and it is noteworthy that there is no published data, either experi-

mental or theoretical, on the behaviour of discharges in EXB fields in SF_6 . In this chapter, the simulation used in Chapter V is extended to EXB uniform fields.

6.2 MODEL AND THEORY

Neglecting three body collisions and coulomb interactions on the assumption that the gas is weakly ionized an electron with velocity v situated in EXB fields is subjected to Lorentz force given by

$$F = e(E + v \times B) \quad (6.1)$$

where E is the applied electric field, B is the uniform magnetic field and e is the electronic charge.

If the Lorentz force is the only force acting on a charged particle then

$$m \frac{dv}{dt} = e(E + v \times B) \quad (6.2)$$

in which m is the mass of the electron. The equation of motion shows that in EXB fields the motion is the sum of the circular Larmor gyration plus a drift of the guiding center due to the applied electric field.

If the electric field is along negative z direction and the magnetic field in the negative x direction, then

$$\begin{aligned} \dot{v}_x &= 0 \\ \dot{v}_y &= \frac{e}{m} B v_z \end{aligned}$$

$$\dot{v}_z = \frac{eE}{m} - \frac{eB}{m} v_y \quad (6.3)$$

where \dot{v}_x , \dot{v}_y and \dot{v}_z are the accelerations respectively in x, y and z directions.

In this case, since the acceleration along the magnetic field is zero, if the initial velocity component along x is also zero, the electron trajectory will be on the plane perpendicular to the magnetic field that is the zy plane. On the basis of this analysis it is clear that an initial velocity component along B would be undisturbed. Considering such a case there will be displacement along x in addition to y and z direction.

The model used is basically the same as described in Chapter V. A flowchart is given in Fig. 6.1. Since there is not any acceleration along the magnetic field, the energy gain for an electron is only along the applied field direction. If a collision is not observed at the end of the time step the angle θ is adjusted according to the expression

$$\tan \theta = \frac{v_p}{v_z} \quad (6.4)$$

where v_p is the perpendicular velocity normal to the applied electric field, that is, $v_p = (v_x^2 + v_y^2)^{1/2}$ and v_z is the velocity along applied electric field direction.

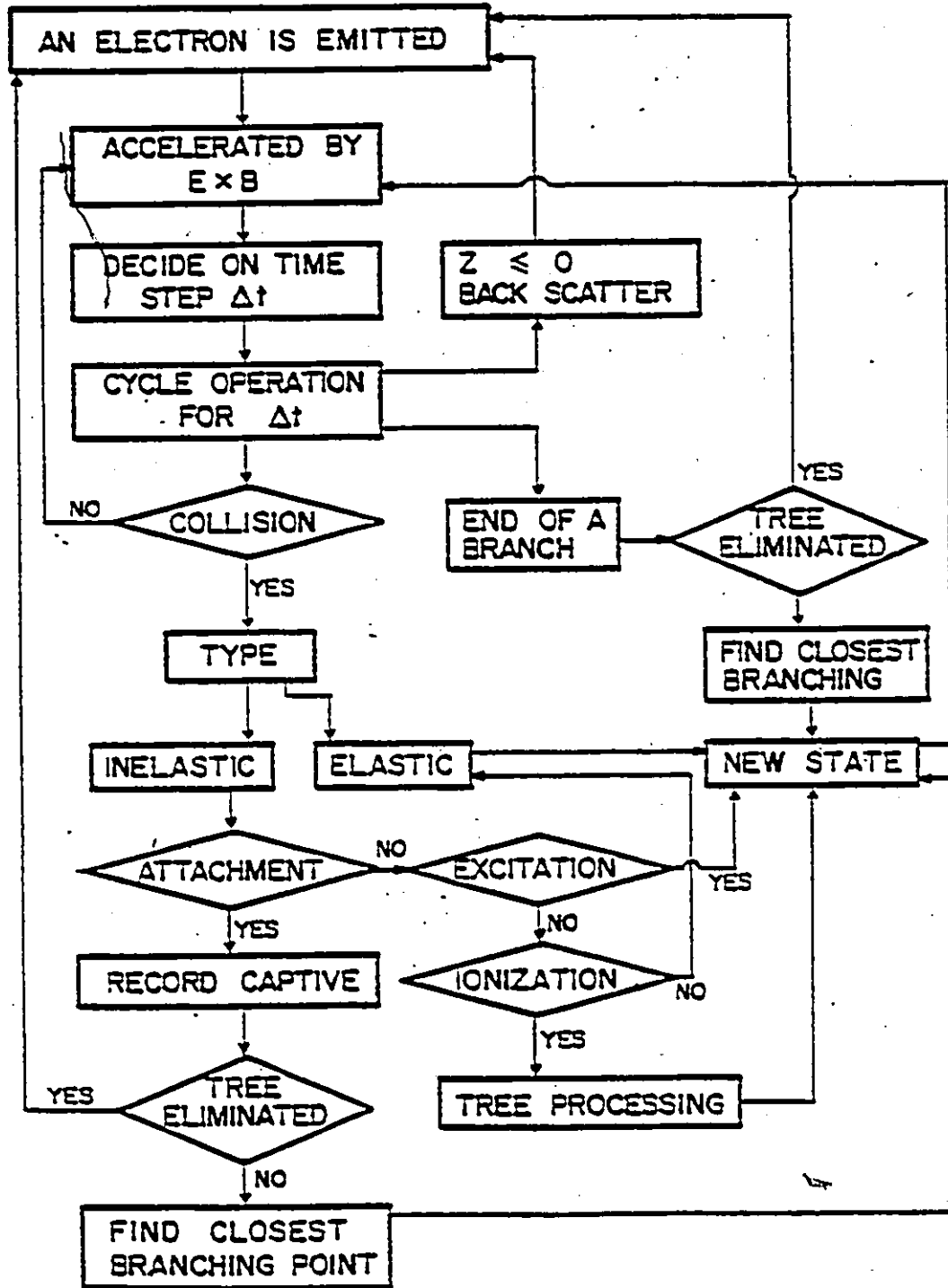


Fig. 6.1. A basic flowchart for the simulation.

The computer simulation is carried out for reduced electric fields of $180 \times 10^2 \leq E/p \leq 300 \times 10^2 \text{ V m}^{-1} \text{ Torr}^{-1}$ and the range of reduced magnetic field applied perpendicularly to the electric field is $1.0 \leq B/p \leq 6 \times 10^{-2} \text{ Tesla Torr}^{-1}$. At time $t=0$, the total number of initial electrons injected varies up to 170. The total number of collisions observed ranges from 2.0×10^4 to 10×10^4 .

6.3 RESULTS AND DISCUSSION

Although a comprehensive analysis is not carried out for back scattering, at a constant reduced electric field the number of back scattered electrons increases with increasing reduced magnetic fields. For $300 \times 10^2 \text{ V m}^{-1} \text{ Torr}^{-1}$ the ratios of back scattered electrons to the total number of initial electrons are 0.35, 0.63 and 0.68 corresponding respectively to the reduced magnetic fields 4×10^{-2} , 5×10^{-2} and $6 \times 10^{-2} \text{ T Torr}^{-1}$. For $210 \times 10^2 \text{ V m}^{-1} \text{ Torr}^{-1}$ these values are found as 0.48, 0.58, 0.70 and 0.73 corresponding respectively to the magnetic fields of 2×10^{-2} , 3×10^{-2} , 3.5×10^{-2} and $4 \times 10^{-2} \text{ T Torr}^{-1}$.

6.3.1 Transverse, Perpendicular Drift Velocities and the Magnetic Deflection Angle

The transverse drift velocities are obtained from the slopes of $\langle z \rangle$ versus t curves. Such curves are given

in Figs. 6.2 and 6.3. As can be seen from these figures, at a constant reduced electric field the slope of the curves decreases with increasing reduced magnetic fields and also, with increasing applied magnetic field, the non-equilibrium region increases. In Fig. 6.4 calculated transverse drift velocities are given for constant reduced electric fields as a function of applied reduced magnetic fields. In this chapter, for all figures and tables, E/p values are given as $V \text{ cm}^{-1} \text{ Torr}^{-1}$. It can be seen from Fig. 6.4 that the variation of transverse drift velocity with respect to increasing reduced magnetic field is nonlinear.

The variation in perpendicular drift velocity is also nonlinear and it is a function of both reduced fields. At a constant reduced electric field perpendicular drift velocity V_p increases with increasing reduced magnetic field and reaches a maximum of a specific value of the field. Further increase in the magnetic field results in reduction for V_p at a constant applied electric field.

The ratio of perpendicular drift velocity to transverse drift velocity are given in Table 6.1 together with corresponding magnetic deflection angle, θ_M .

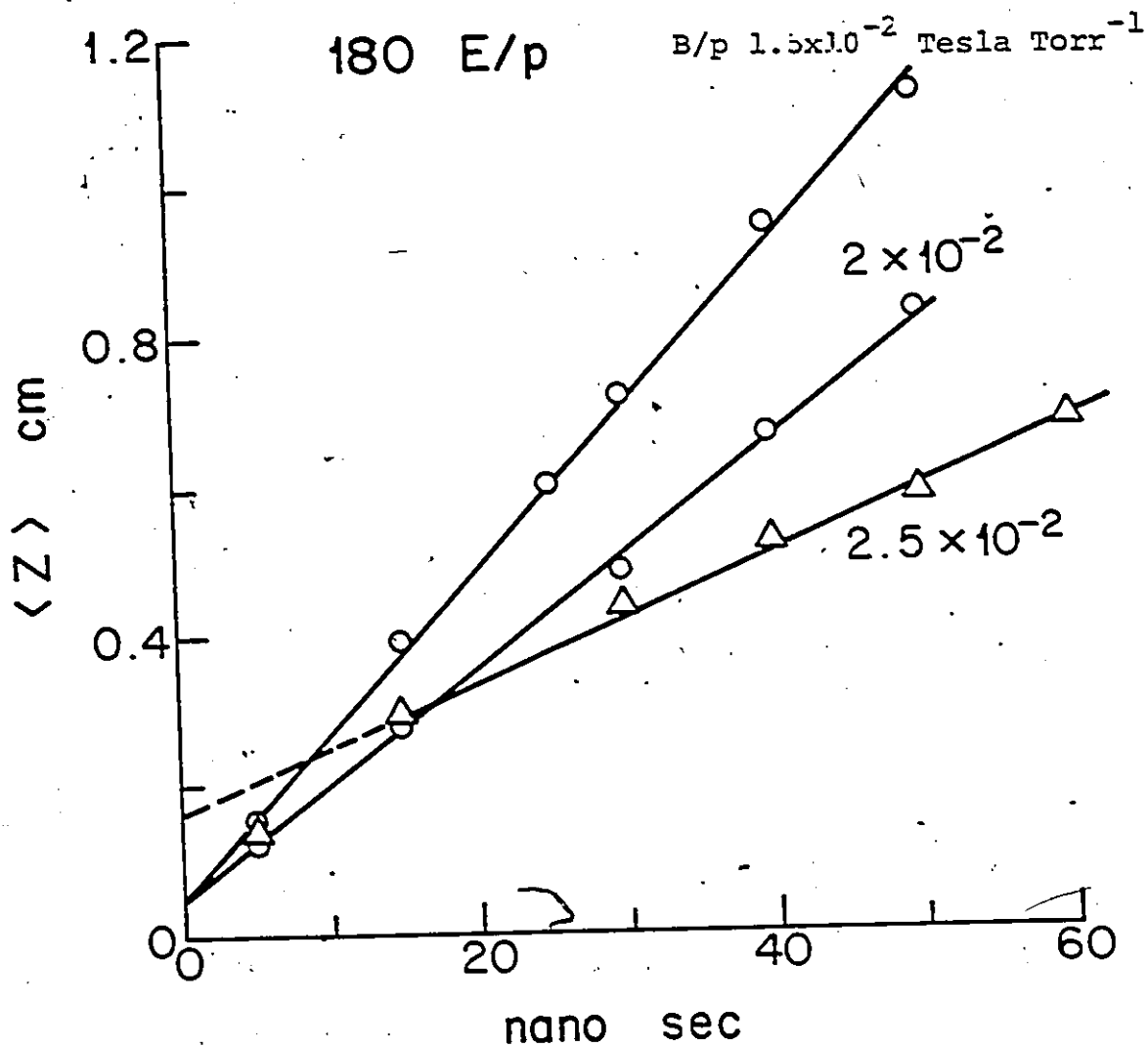


Fig. 6.2. Average drift distances along the electric field direction with respect to time at $180 \text{ V cm}^{-1} \text{ Torr}^{-1}$ for various magnetic fields.

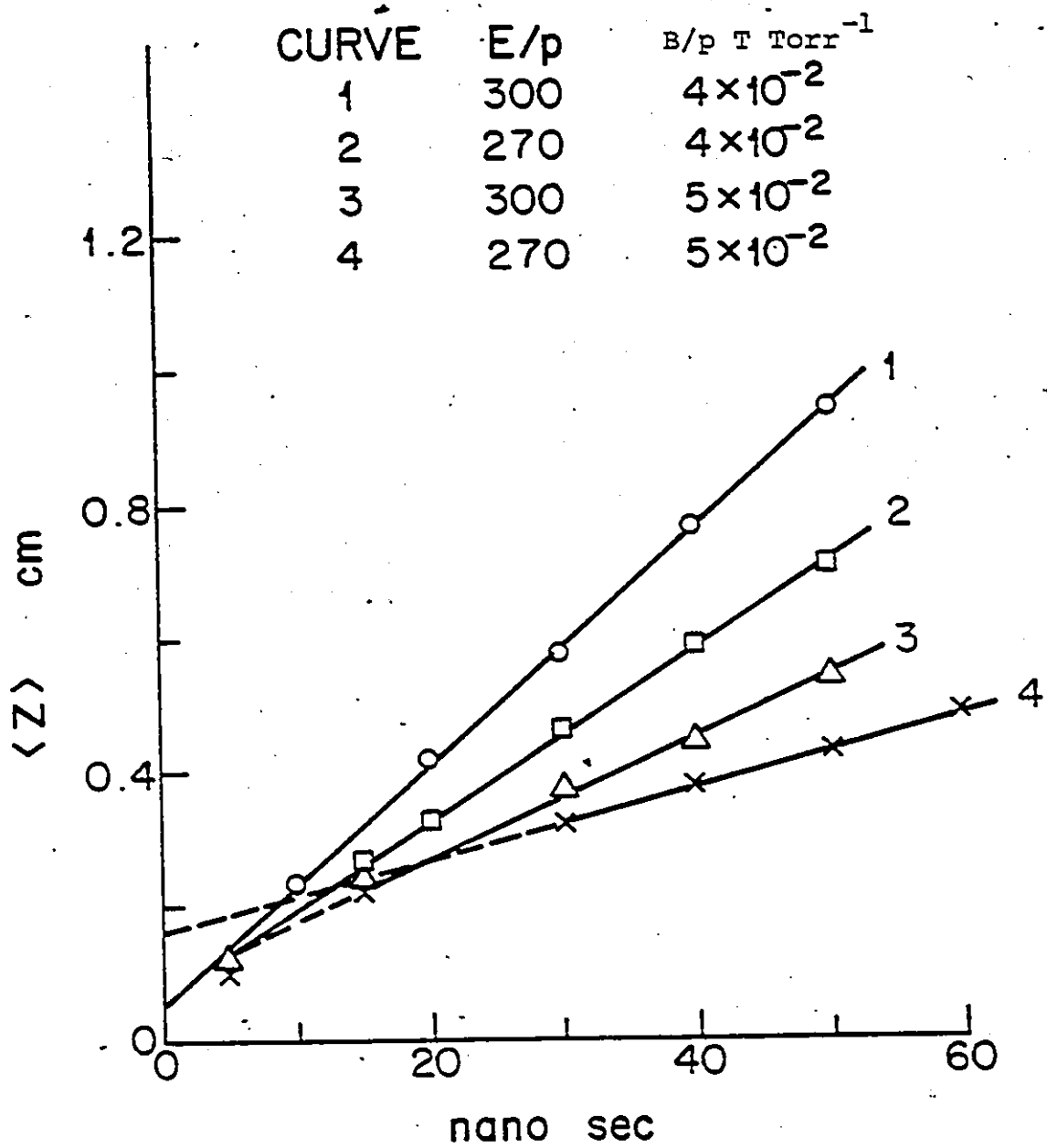


Fig. 6.3. Average drift distances with respect to time along the electric field direction for various applied electric and magnetic fields. E/p in V cm⁻¹ Torr⁻¹

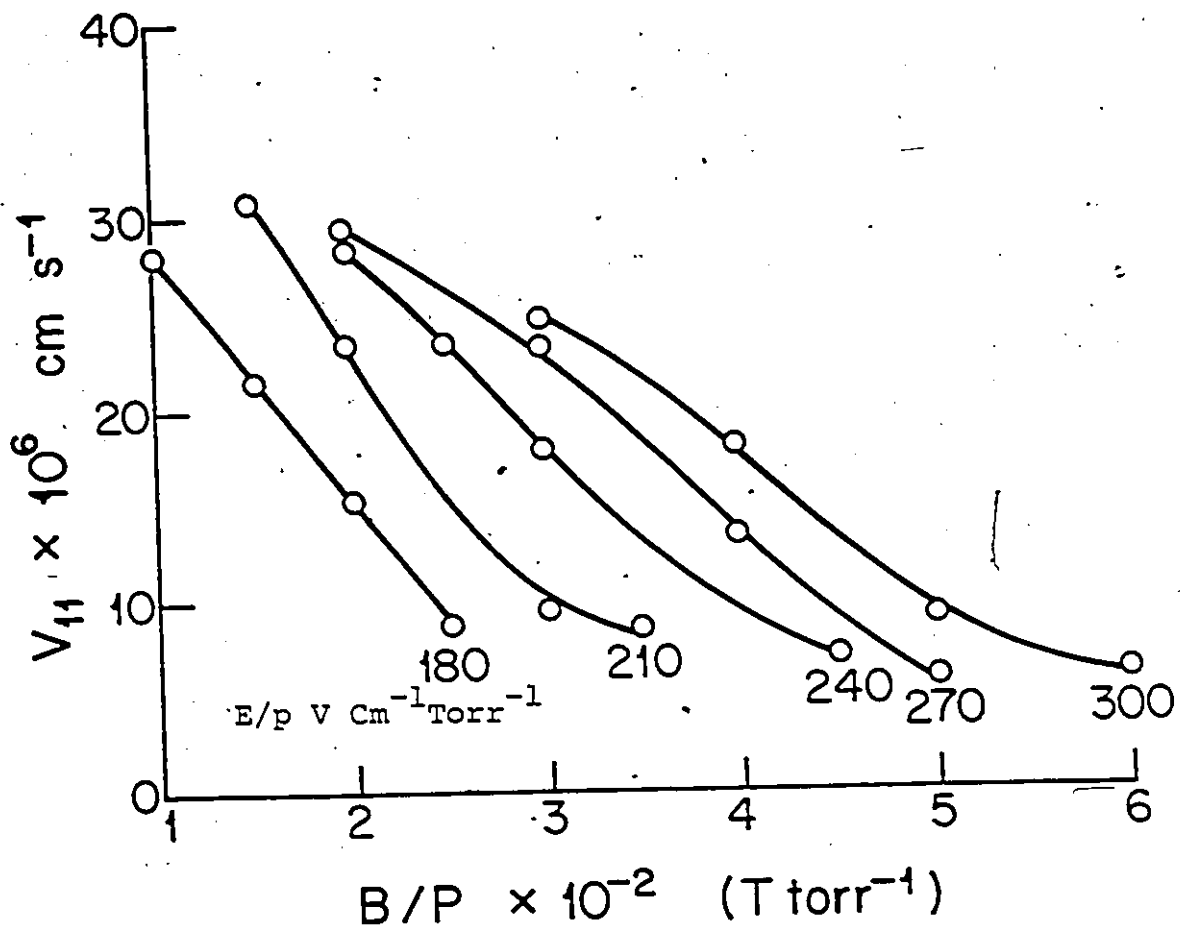


Fig. 6.4. Variation of transverse drift velocity with respect to increasing magnetic fields at constant applied electric fields.

Table 6.1
 Ratio of Perpendicular Drift Velocity to Transverse Drift Velocity
 and the Magnetic Deflection Angle

E/p	B/p x 10 ⁻² T Torr ⁻¹										
	1.25	1.5	2.0	2.5	3.0	3.5	4.0	4.5	5.0	6.0	
180	0.207 11.750*	0.418 22.700	0.485 25.870	0.65 33.03							
210		0.256 14.39	0.330 18.400		0.668 33.760	0.704 35.160					
240		0.192 10.88		0.383 20.950	0.585 30.320			0.90 41.67			
270			0.314 17.440		0.396 21.630		0.772 37.650		1.204 50.300		
300					0.341 18.850		0.694 34.770		1.075 47.050	1.386 54.18	

* θ_M in degrees.

6.3.2 Energy Distributions and Average Energy

The energy distributions sampled per mean free flight time are shown in Figs. 6.5, 6.6 and 6.7 for various applied reduced electric and magnetic fields. At a constant reduced electric field the peak value of the distribution increases with increasing magnetic fields while shifting towards lower energy scale. This behaviour shows that with increasing B/p a larger number of electrons are driven into the lower range. Qualitatively similar behaviour is observed by Govinda Raju and Gurumurthy [95] in N_2 in which the Boltzmann equation was employed to investigate the influence of crossed magnetic field.

Hence, with increasing B/p the average energy in the swarm decreases for a constant E/p . Figure 6.8 gives the variation in average energy with respect to increasing B/p for constant E/p fields.

6.3.3 Ionization and Attachment Coefficients

The Townsend's ionization coefficients and attachment coefficients are calculated from the same expressions given in Chapter V. The amplification in the swarm is determined from the region where $\langle z \rangle$ varies linearly with respect to time.

Figures 6.9 and 6.10 show the influence of a crossed

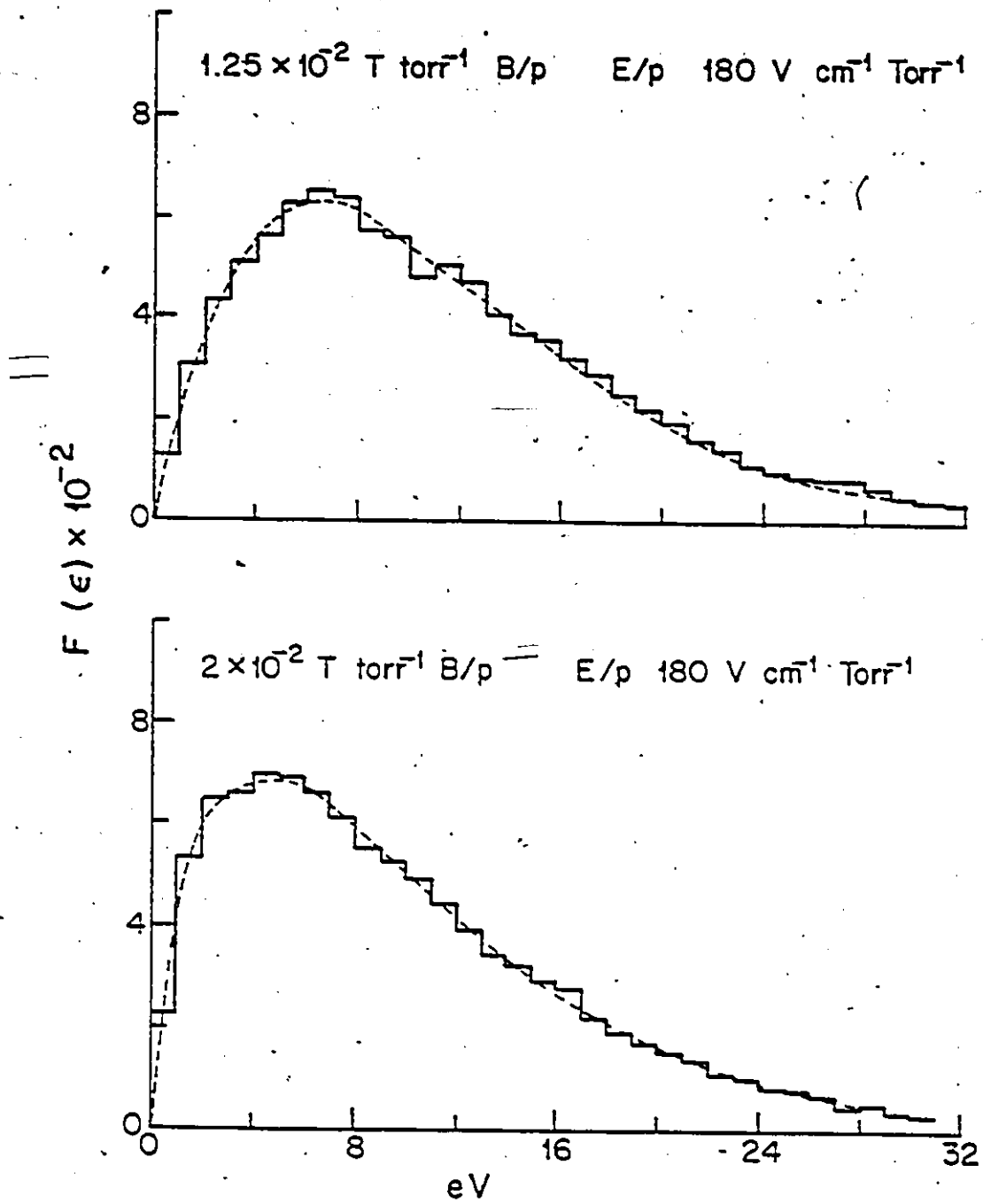


Fig. 6.5. Energy distributions in EXB fields at $\text{E/p} = 180 \text{ V cm}^{-1} \text{ Torr}^{-1}$.

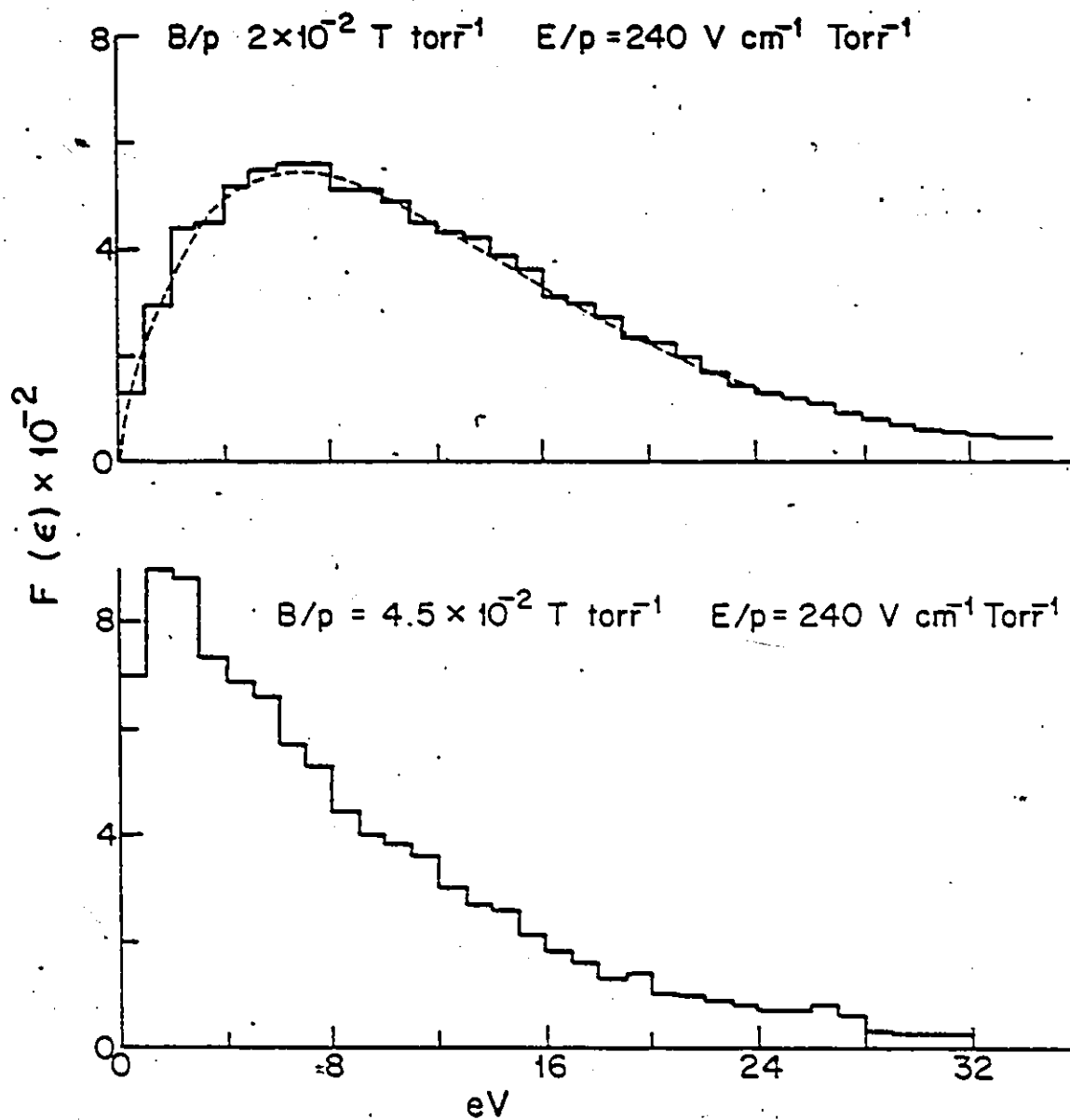


Fig. 6.6. Energy distribution in EXB fields at $E/p = 240 \text{ V cm}^{-1} \text{ Torr}^{-1}$.

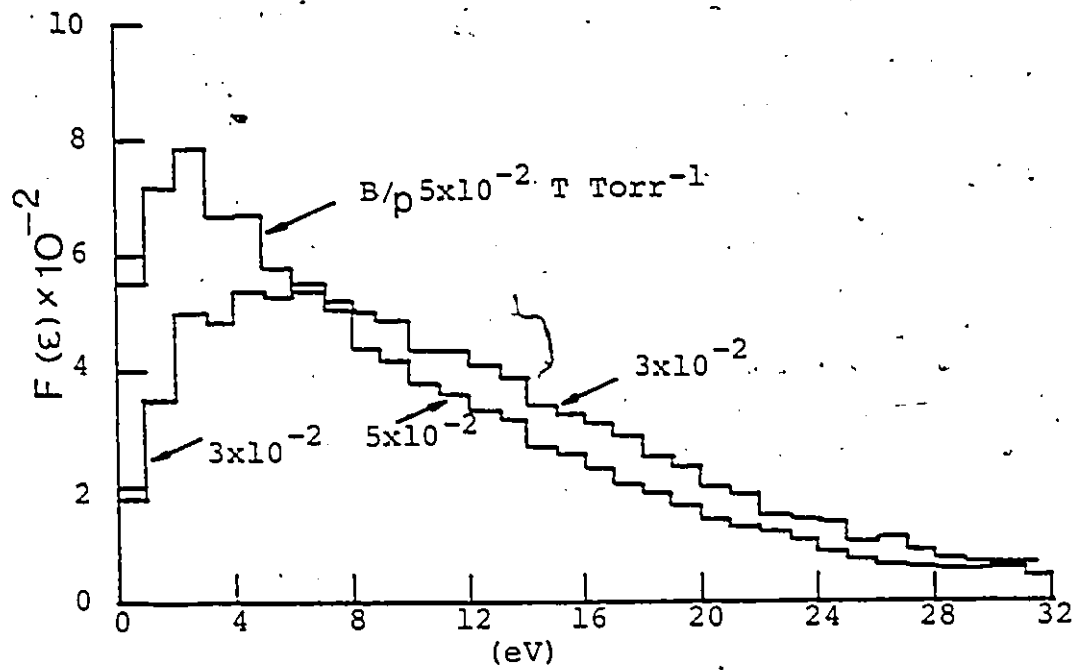


Fig. 6.7. Energy distributions in EXB fields at $E/p=300 \text{ V cm}^{-1} \text{ Torr}^{-1}$.

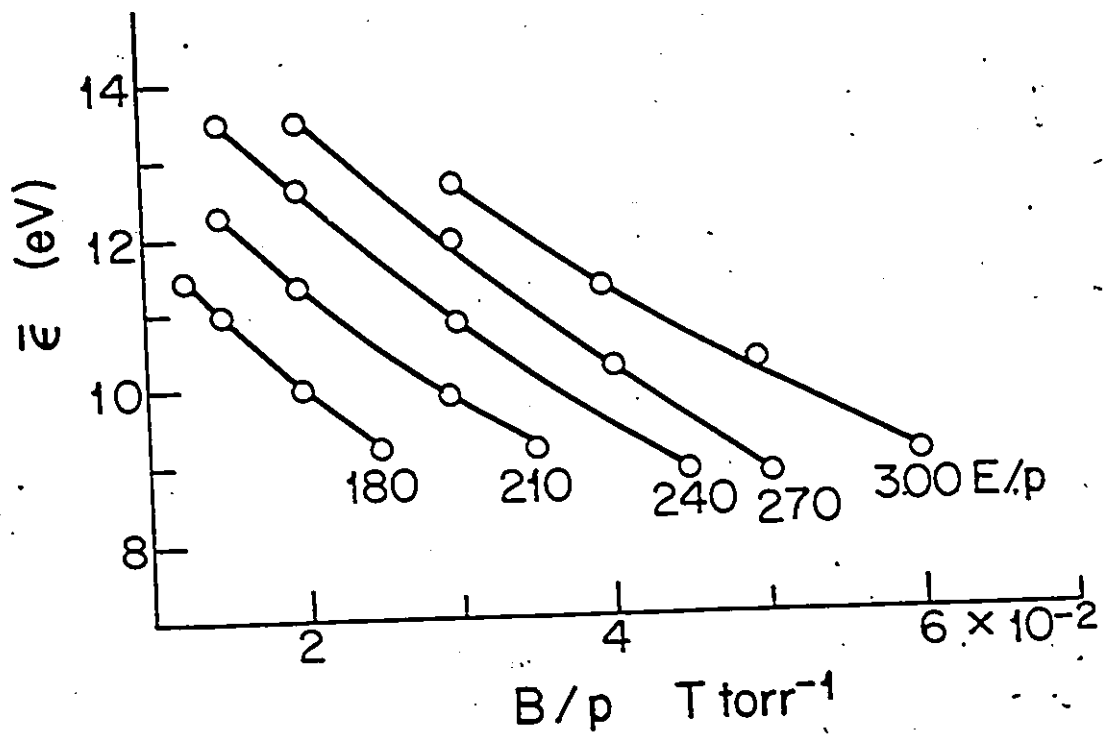


Fig. 6.8: Variation of average energy with increasing magnetic fields at constant electric fields. E/p in $V\text{ cm}^{-1}\text{ Torr}^{-1}$.

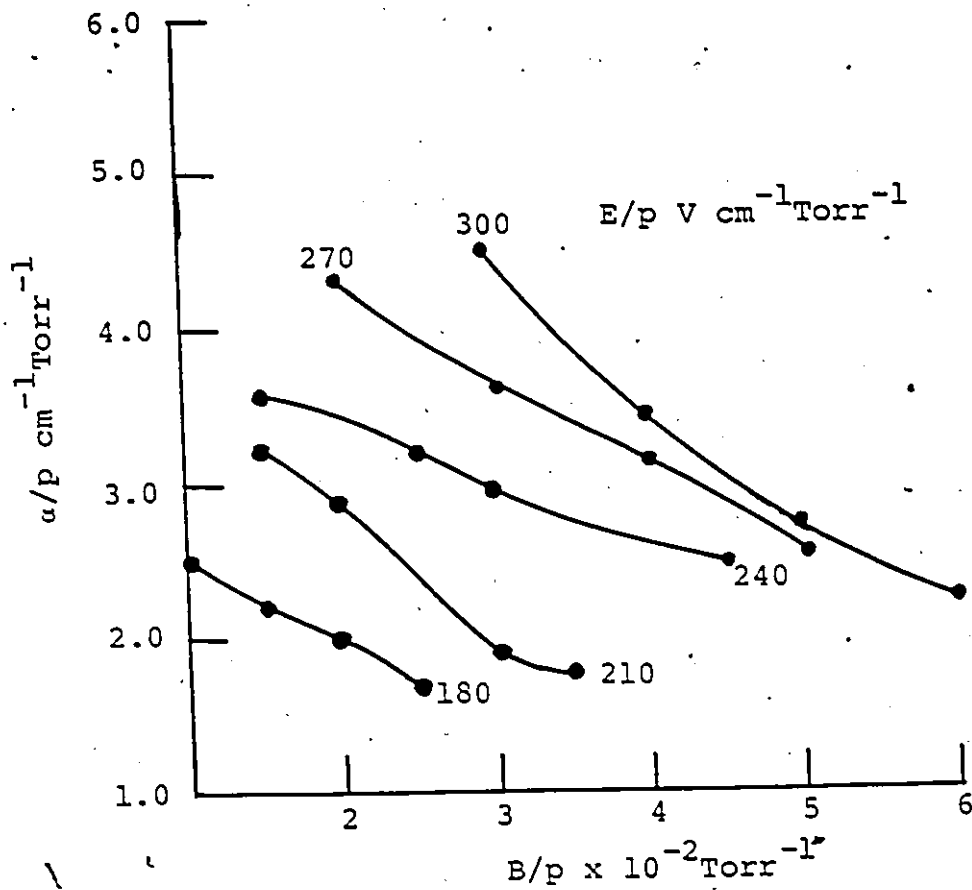


Fig. 6.9. Ionization coefficients in EXB fields.

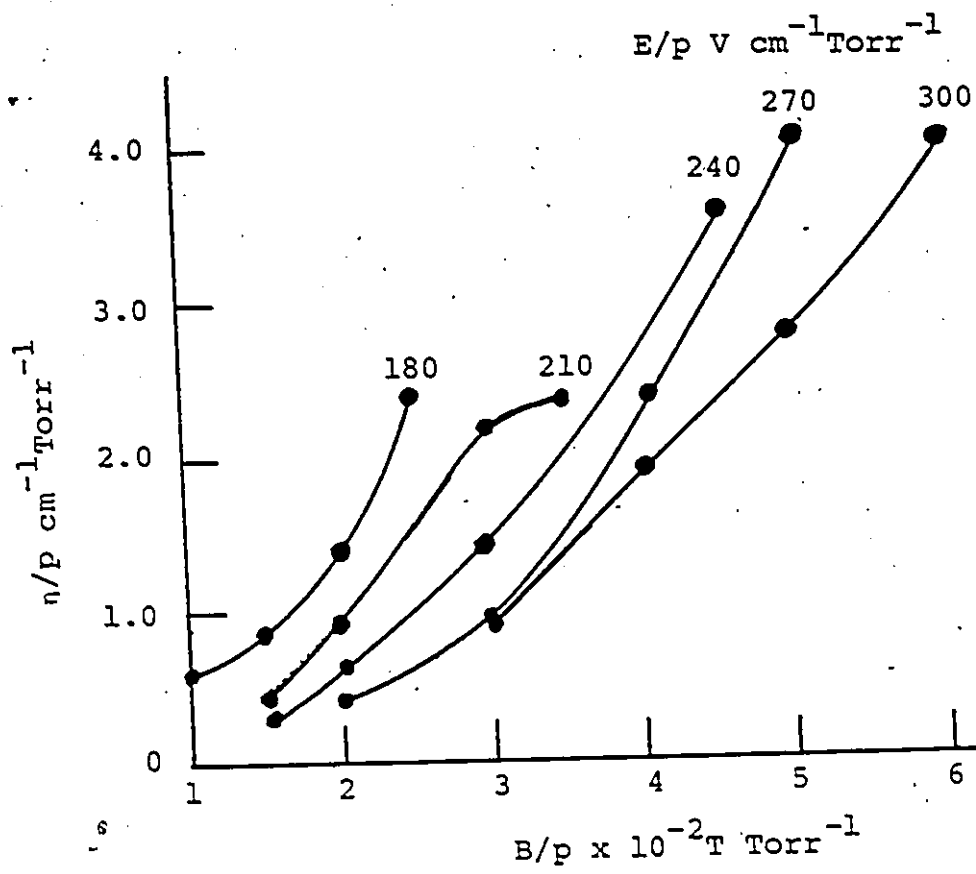


Fig. 6.10. Attachment coefficients in EXB fields.

magnetic field on the Townsend's first ionization coefficient α/p and attachment coefficient η/p . At a constant value of E/p the ionization coefficient decreases with increasing B/p while the attachment coefficient increases and both these results are consistent with the change in the electron energy distribution.

Since application of a magnetic field has been shown to increase η/p and decrease α/p it is possible to discern from Figs. 6.9 and 6.10 a critical value of B/p at which the condition $\alpha/p = \eta/p$ is satisfied. This critical value could be of considerable engineering importance. Table 6.2 gives (B/p) critical corresponding to reduced electric fields.

Table 6.2
Critical B/p Limits in SF_6

E/p	B/p	$\alpha/p = \eta/p$
$V \text{ cm}^{-1} \text{ Torr}^{-1}$	Tesla Torr^{-1}	$\text{cm}^{-1} \text{ Torr}^{-1}$
180	2.35×10^{-2}	1.8
210	3.0×10^{-2}	2.0
240	4.0×10^{-2}	2.6
270	4.4×10^{-2}	2.8
300	5.0×10^{-2}	2.8

The general behaviour of the swarm parameters in the present study indicates that the dielectric strength

of SF₆ can be considerably improved by applying magnetic fields perpendicular to the applied electric field.

CHAPTER VII

CONCLUSIONS AND RECOMMENDATIONS

7.1 CONCLUSIONS

1. The quantitative data provided experimentally on the effective ionization, ionization and attachment coefficients together with E/p limits reveals the importance of SF₆+N₂ gas mixtures as an insulant in power and high voltage engineering applications. This data can be used to set up theoretical models to estimate discharge inception voltage levels for different degrees of non-uniformity depending on the design configuration of an actual high voltage device.
2. The variation of $(\alpha-n)/p$ in SF₆+N₂ mixtures is found to be nonlinear with the percentage mixture ratio. Hence, linear addition of some property of the individual gasses in proportion to their concentration in the mixtures for predicting the dielectric strength of gas mixtures would lead to incorrect results, particularly in divergent fields.
3. Effective ionization, ionization and attachment

coefficients are also measured in $\text{CCl}_2\text{F}_2 + \text{CO}_2$ gas mixtures. Similar to $\text{SF}_6 + \text{N}_2$ mixtures the variation of $(\alpha - \eta)/p$ with respect to percentage ratio is non-linear. Furthermore, with 20% CCl_2F_2 concentration, the effective ionization coefficients measured is higher than that of either component of the mixture in the E/p range $100 \leq E/p \leq 180 \text{ V cm}^{-1} \text{ Torr}^{-1}$.

4. For $\text{SF}_6 + \text{N}_2$ at a given E/p the effective ionization coefficient decreases with increasing SF_6 component in the mixture. The reduction in the effective ionization coefficient becomes relatively higher as E/p decreases. However, once a certain SF_6 concentration in the mixture is reached, further addition of SF_6 responds with relatively little effect on the reduction of this coefficient. In the E/p interval $100 \leq E/p \leq 190 \text{ V cm}^{-1} \text{ Torr}^{-1}$, beneficial gain is negligible if SF_6 concentration is increased above 60%.
5. The saturation behaviour in effective ionization coefficients is also confirmed in sparkover voltage measurements. For constant pd (Torr-cm) values, variation of V_s with SF_6 concentration in the mixture shows down curving with increasing SF_6 concentration. The saturation tendency becomes more sig-

nificant for decreasing pd levels.

6. The apparent secondary ionization coefficients have been deduced in $SF_6 + N_2$ mixtures. The reduction in this coefficient with increasing partial pressure of SF_6 is attributed to the increased photon absorption coefficient of the mixture.
7. The quantitative data on swarm-parameters of SF_6 is provided by using a Monte-Carlo simulation technique. The simulation results are compared with available experimental data in literature and good agreement is found. As a prerequisite to this technique, it is necessary to have a set of measured (or estimated) collision cross sections. However, if sufficient data is available for individual gasses, this technique can be used to obtain swarm data for gas mixtures avoiding the effort consumed for experimental measurements. Furthermore, information on average energy and energy distributions can also be gathered which would be very difficult to measure.
8. Swarm behaviour of SF_6 in EXB uniform fields, is very interesting. Application of a magnetic field results in a change in the energy distribution, reduces the average energy and first ionization coefficient and increases the attachment coefficient at

a constant value of E/p .

With increasing magnetic field at a constant E/p , the magnetic deflection angle increases while there is a reduction in the transverse drift velocity. Hence, the variation observed in swarm parameters with respect to increasing perpendicularly applied magnetic field are consistent with each other. This information indicates that the dielectric strength of SF_6 can be upgraded in the presence of EXB fields. All the results are obtained for a background of SF_6 molecules with a number density corresponding to 1 Torr. Since the "bending" effect of the magnetic field is significant during free flight of the electron in between collisions, at high pressures, there may not be a substantial deflection for the electron swarm. However, EXB field applications could be very suitable for high voltage devices which operate at lower gas pressures.

7.2 RECOMMENDATIONS FOR FURTHER STUDIES

This study has been confined experimentally as well as theoretically for swarm parameters in uniform fields in order to get a better insight into the dielectric behaviour and discharge phenomena in strongly electronegative gasses and gas mixtures.

Key basic data on polyatomic molecules are necessary

to optimize gas mixtures. In the area of cross sections there is a lack of data on basic electron scattering cross sections. For polyatomic molecules low energy electron scattering cross sections are almost non-existing. To set a reliable theoretical model, the key data for cross sections should be measured.

Exposure and health risk assessment of SF_6 has shown that SF_6 is non-toxic. However, when a spark occurs in a gas insulated system the gas molecules in the volume of spark will be dissociated due to high local temperatures. For SF_6 , the atomic species formed will react quickly to form sulfur fluoride ions and neutrals which in turn can react with impurities to form by-products. In the presence of an aluminium conductor AlF_3 may form which is a toxic solid product.

Hence, another essential feature which has to be seriously considered is the discharge by-products and their evolution since they exhibit an essence both from the viewpoint of environmental aspects and the long term behaviour of high voltage devices used in energy systems.

In practice, due to the design configuration of the high voltage equipment and surface imperfections, it is so often that the gaseous insulant is subjected to non-uniform fields. However, there are only simple semi-empirical models available to estimate discharge incep-

tion voltages for divergent fields. There is a great need for more accurate models to investigate gaseous breakdown in divergent fields. Particularly, a rigorous research related to SF_6+N_2 mixtures on this subject is still not available.

APPENDICES

APPENDIX I

Distribution of Free Time Between Collisions

Let $n(t)$ be the number of particles that have survived a collision at time, t , out of an original number $n_0 = n(0)$. Hence, the fraction of free times in a differential time element dt is

$$f(t)dt = [n(t) - n(t+dt)]/n_0 \quad (\text{A.1})$$

where,

$$n(t+dt) = n(t) + \frac{dn}{dt} dt$$

therefore, A.1 can be written as

$$f(t)dt = - \frac{1}{n_0} \frac{dn}{dt} dt \quad (\text{A.2})$$

In a differential time element dt , the number of collisions, dn , an electron suffers is $nQ_T v$ where, N is the density of gas molecules, Q_T is the total collision cross section and v is the velocity of the electron. Thus,

$$\frac{dn}{dt} = -nNQ_T v \quad (\text{A.3})$$

gives the rate at which free paths are terminated. Substituting A.3 into A.2 results in the distribution of free times as

$$f(t)dt = \frac{n}{n_0} NQ_T v dt \quad (\text{A.4})$$

If A.3 is integrated,

$$\frac{n}{n_0} = \exp(-NQ_T vt) \quad (\text{A.5})$$

substituting A.5 into A.4 gives

$$f(t)dt = \exp(-NQ_T vt) NQ_T v dt$$

hence, the probability distribution function for a collision is

$$\begin{aligned} P(t) &= \int_0^t \exp(-NQ_T vt) NQ_T v dt \\ &= 1 - \exp(-NQ_T vt) \end{aligned} \quad (\text{A.6})$$

The mean collision time, τ , is the first moment of the function $f(t)$,

$$\tau = \int_0^{\infty} t f(t) dt = [NQ_T v]^{-1}$$

Therefore,

$$P(t) = 1 - \exp(-t/\tau) \quad (\text{A.7})$$

APPENDIX II

Isotropic Scattering

A. Scattering Isotropic in the Laboratory System

The problem involved is tantamount to that of choosing a point (u, v, w) uniformly distributed on the unit sphere $u^2+v^2+w^2 = 1$ (Fig. A.1). In spherical coordinates θ, ϕ , the element of area for the unit sphere is

$$\sin \theta d\theta d\phi = -dw dv$$

where, θ is the polar angle, ϕ is the longitude and $w = \cos \theta$.

The probability density function is, therefore, given by

$$p(w) dw = -2\pi \cdot \sin \theta d\theta / 4\pi$$

Hence, $p(w) dw = 1/2 dw$. Therefore, we can determine w as

$$R = \int_{-1}^w 1/2 dw = 1/2(w+1)$$

The routine to find the direction cosines is shown in Fig. A.2.

B. Cosine Distribution

Particles emanating from a surface are naturally limited to half of direction space. If we consider a

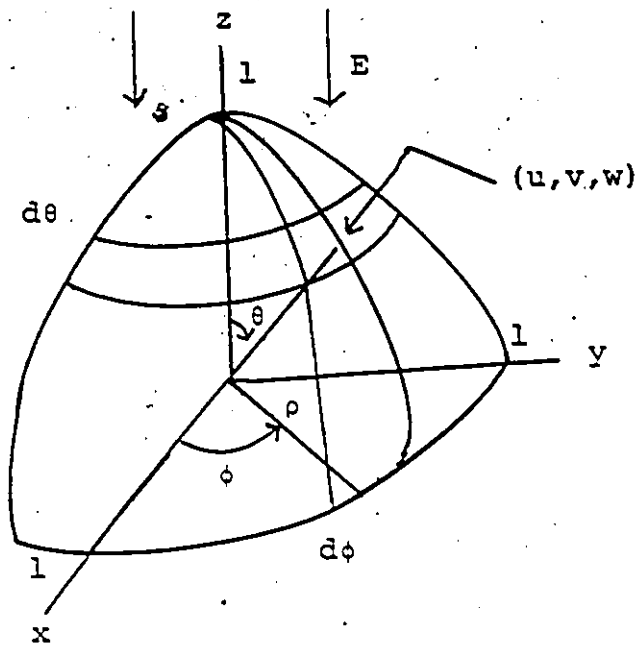


Fig. A.1. A point uniformly distributed on unit sphere.

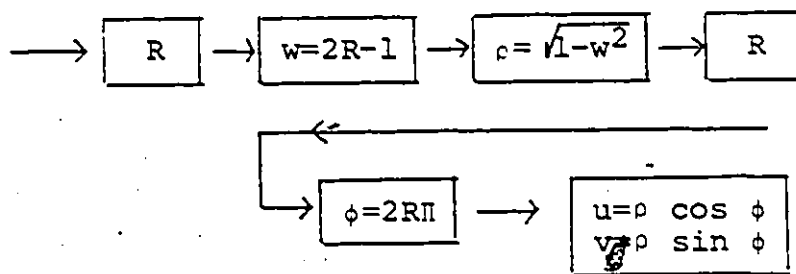


Fig. A.2. Routine to find direction cosines.

point source emanating from a surface, the outer normal to the surface at the point has the direction $u=0$, $v=0$, $w=1$, then the cosine distribution has by definition the probability density function $p(w)=2w$ with $w \geq 0$.

Thus,

$$R = \int_0^w 2wdw \Rightarrow w = \sqrt{R}$$

Hence, the flow diagram in Fig. A. 2 can be used with w replaced by \sqrt{R} .

C. Random Number Generator

The random number generator used computes uniformly distributed random real numbers between 0 and 1.0 and random integers between zero and 2^{31} .

Four different random number strings are used in the simulation to decide on collision, type of collision and to estimate the polar and azimuthal angles.

The strings have 2^{29} terms before repeating.

cf. IBM Manual C20-8011.

APPENDIX III

Deciding on the Nature of Collision

If G_1, \dots, G_n are n independent, mutually exclusive events with probabilities

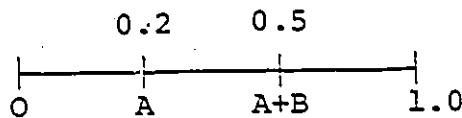
P_1, \dots, P_n respectively, and

$P_1 + \dots + P_n = 1$, then

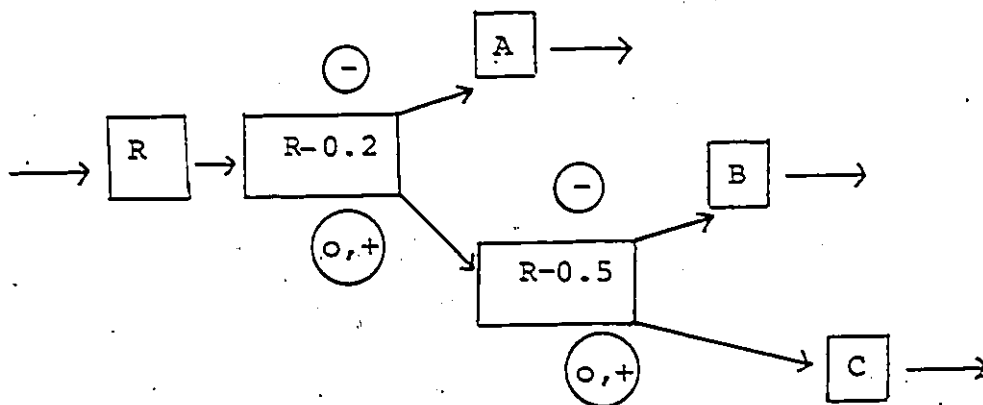
$P_1 + \dots + P_{i-1} \leq R_Q < P_1 + \dots + P_i$

determines the event G_i .

For example, at a certain electron energy level, if the probability of a collision type A is 0.2, type B is 0.3 and type C is the remaining 0.5, then the lengths of the intervals are accordingly as follows:



Hence, the corresponding flow diagram decides on the collision type.



REFERENCES

1. P. R. Howard, "Insulation Properties of Compressed Electro-negative Gases." Proc. IEE, Vol. 104, Part A, No. 13, 1957, pp. 123-138.
2. A. H. Cookson, "Electrical Breakdown for Uniform Fields in Compressed Gases." Proc. IEE, Vol. 117, No. 1, 1970, pp. 269-279.
3. I. A. Wieland, "Gasdurchschlags mechanismen in electronegativen gasen (SF_6) und in gasgemischen." ETZ-A, Bd-94, H-7, 1973, pp. 370-373.
4. R. G. Baumgartner, "Dielectric Characteristics of Mixtures of Sulphur-Hexafluoride (SF_6) and Nitrogen (N_2)." Proc. 3rd International Conf. on Gas Discharges, IEE Conf. Publ. No. 118, 1974, pp. 366-369.
5. M. Ermel, "Das N_2 - SF_6 -Gasgemisch als Isoliermittel der Hochspannungs technik." ETZ-A, Bd-96, H-5, 1975, pp. 231-235.
6. M. O. Pace, L. G. Christophorou, D. R. James, P. Y. Pai, R. A. Mathis, and D. W. Bouldin, "Improved Unitary and Multi-component Gaseous Insulators." IEEE. Trans. Electr. Insul., Vol. EI-13, No. 1, 1978, pp. 31-36.
7. R. E. Wooton, S. J. Dale, and N. J. Zimmerman, in L. B. Christophorou (Ed.), Gaseous Dielectrics II. Pergamon Press, New York, 1980, pp. 137-148.
8. D. W. Bouldin, D. R. James, M. O. Pace, and L. G. Christophorou, in L. G. Christophorou (Ed.) "Working Proceedings of Fourth International Symposium of Gaseous Dielectric," Knoxville, Tennessee, 1984.
9. A. Pedersen, "The Effect of Surface Roughness on Breakdown in SF_6 ." IEEE Trans. on PAS, Vol. PAS-94, 1975, pp. 1749-1753.
10. O. Farish, O. E. Ibrahim, and B. H. Crichton, "Effect of Electrode Surface Roughness on Breakdown in Nitrogen- SF_6 Mixtures." Proc. IEE, Vol. 123, No. 10, 1975, pp. 1047-1050.

11. C. Korosli, I. C. Somerville, and O. Farish, "Electrode-Area and Surface Roughness Effects on Breakdown of SF₆/N₂ Mixtures." In L. G. Christophorou (Ed.) Gaseous Dielectrics II. Pergamon Press, New York, 1980, pp. 218-223.
12. A. H. Cookson and R. E. Wooton, "Particle-Initiated A.C. and D.C. Breakdown in Compressed Nitrogen, SF₆ and N₂-SF₆ Mixtures." Conf. on Elect. Insulation and Dielectric Phenomena, Montreal, October 1973.
13. A. H. Cookson and R. E. Wooton, "Movement of Filamentary Conducting Particles under A.C. Voltages in High Pressure Gases." Proc. Intern. Symp. on High Voltage Technology, Zurich; 1975, pp. 416-420.
14. R. D. Garzon, "The Effect of SF₆-N₂ Mixtures upon the Recovery Voltage Capability of a Synchronous Interruptor." IEEE Trans. on PAS, Vol. PAS-95, No. 1, 1976, pp. 140-144.
15. D. M. Grant, J. F. Perkins, L. C. Campbell, O. E. Ibrahim and O. Farish, "Comparative Interruption Studies of Gas-Blasted arc, in SF₆-N₂ and SF₆-He Mixtures." Proc. 4th Intern. Conf. on Gas Discharges, IEEE Conf. Publ. No. 143, 1976, pp. 48-51.
16. K. B. Miners, M. J. Mastroianni, P. N. Sheldon and D. P. Wilson, "Dew Points of SF₆/N₂ Gas Mixtures," In L. G. Christophorou (Ed.) Gaseous Dielectrics III. Pergamon Press, New York, 1982.
17. T. Takuma, T. Watanabe and K. Kita, "Breakdown Characteristics of Compressed-Gas Mixtures in Nearly Uniform Fields." Proc. IEE, Vol. 119, No. 7, 1972, pp. 927-928.
18. R. E. Wooton and P. J. Chantry, "A Critique of Methods for Calculating the Dielectric Strength of Gas Mixtures and a Proposed Test for η-synchgism." In L. G. Christophorou (Ed.), Gaseous Dielectrics II. Pergamon Press, New York, 1980, pp. 32-42.
19. G. R. Govinda Raju and R. Hackam, "Breakdown Field Strength of SF₆, N₂O, SF₆+N₂, and SF₆+N₂O," J. Apply Phys. Vol. 52(6), 1981, pp. 3912-3920.

20. W. Zaengl, "Forum I: Future Research Directions in Gaseous Dielectrics," (Transcribed by R. Y. Pai), Gaseous Dielectrics II. Pergamon Press, New York, 1980, pp. 471.
21. Th. Aschwanden, Proc. 3rd Int. Sym. High Voltage Engineering, Milan, Vol. 1, 1979, Paper 31-12.
22. H. Itoh, M. Shimosuma, H. Tagashira and S. Sakamoto, "Ionization and Breakdown in SF₆ and N₂ Mixtures." J. Phys. D., Vol. 12, 1979, pp. 2167-2172.
23. G. R. Govinda Raju and M. S. Dincer, "Measurement of Ionization and Attachment Coefficients in SF₆ and SF₆+N₂", J. Appl. Phys. 53(12), December 1982, pp. 8562-8567.
24. M. S. Dincer and G. R. Govinda Raju, "Ionization and Attachment Coefficients in SF₆+N₂ Mixtures." IEEE Trans. Electrical Insulation, Vol. EI-19, No. 1, 1983, pp. 40-44.
25. M. S. Dincer and G. R. Govinda Raju, "Monte Carlo Simulation of the Motion of Electrons in SF₆ in Uniform Electric Fields." J. Appl. Phys. 54(11), 1983, pp. 6311-6316.
26. M. S. Dincer and G. R. Govinda Raju, "Monte Carlo Simulation of Ionization and Attachment of Electrons in SF₆". Fourth International Symposium on Gaseous Dielectrics, Knoxville, Tennessee.
27. M. S. Dincer and G. R. Govinda Raju, "Ionization and Attachment Coefficients in F₁₂, SF₆ and CO₂ Gas Mixtures." Accepted for publication in IEEE Trans. Elect. Insulation in 1985.
28. G. R. Govinda Raju and M. S. Dincer, "Monte Carlo Calculation of the Ionization and Attachment Coefficients in SF₆ in EXB Fields." Accepted for publication in Proceeding of IEEE 1985.
29. E. Kuffel and M. Abdullah, High Voltage Engineering. Pergamon Press, New York, 1966.

30. J. D. Cobine, Gaseous Conductors. New York-London: McGraw-Hill, 1941, pp. 177-181.
31. J. A. Harrison, "A Computer Study of Uniform-field Electrodes." Brit. J. Appl. Phys., Vol. 8, 1967, pp. 1617-1627.
32. J. S. Pearson and J. A. Harrison, "The Effect of an Anode Hole on Measurements of Townsend's α ." Brit. J. Appl. Phys., Vol. 2, 1969, pp. 1583-1588.
33. In L. G. Christophorou (Ed.), Electron and Ion Swarms. Pergamon Press, New York, 1981, pp. 241-250.
34. B. C. O'Neill and J. D. Craggs, "Collisional Detachment of Electrons in Sulphur Hexafluoride." J. Phys. B., Vol. 6, 1973, pp. 2634-2640.
35. T. H. Teich, "Electrons and Ions in Sulphur Hexafluoride." Proceedings of the Second International Swarm Seminar, July 22-23, 1981. (Also given in Ref. 33).
36. V. H. DiBeler and F. L. Mohler, "Dissociation of SF₆, CH₄ and SiF₄ by Electron Impact." J. Res. U.S. National Bureau of Standards, Washington, D.C., Vol. 40, January 1948.
37. R. Gabelle and M. A. Harrison, "Negative Ion Formation in Oxygen." Phys. Rev., Vol. 85, 1952, pp. 372-373.
38. R. Gabelle and M. L. Reeves, "A Condition on Uniform Field Breakdown in Electron-Attaching Gases." Phys. Rev., Vol. 92, 1953, pp. 867-868.
39. D. J. Debitetto and L. H. Fisher, "Second Townsend Coefficient in O₂ at High Pressures." Phys. Rev., Vol. III, 1958, pp. 390-394.
40. SAS User's Guide (1979), pp. 317-329.
41. H. O. Hartley, "The Modified Gauss-Newton Method for the Fitting of Non-Linear Regression Functions by Least Squares." Technometrics, Vol. 3, 1961, pp. 269-280.

42. G. R. Govinda Raju, "Calculation of Ionization and Attachment Coefficients from Pre-breakdown Current Measurements." J. Phys. D., Vol. 16, 1965, pp. 279-280.
43. D. K. Davies, "Analysis of Current Growth Measurements in Attaching Gases." J. Appl. Phys., Vol. 47, 1976, pp. 1916-1919.
44. M. S. Bhalla and J. D. Craggs, "Measurement of Ionization and Attachment Coefficients in Sulphur Hexafluoride in Uniform Fields." Proc. Phys. Soc., Vol. 80, 1962, pp. 151-160.
45. H. A. Boyd and G. C. Crichton, "Measurement of Ionization and Attachment Coefficients in SF₆." Proc. IEEE, Vol. 118, 1971, pp. 1782-1877.
46. V. N. Maller and M. J. Naidu, "Sparking Potentials and Ionization Coefficients in SF₆." Proc. IEEE, Vol. 123, 1976, pp. 107-108.
47. J. Urguijo-Carmona, "Determination of Discharge Parameters in Sulphur Hexafluoride and Oxygen by Observation of Laser Light Initiated Electron Swarms." Ph.D. Thesis, University of Manchester, 1980.
48. B. Sangi, "Basic Discharge Parameters in Electronegative Gases." Ph.D. Thesis, University of Manchester, 1971.
49. H. Itoh, M. Shimosuma and H. Tagashira, "Boltzman Equation Analysis of the Electron Swarm Development in SF₆ and Nitrogen Mixtures." J. Phys. D. Vol. 13, 1980, pp. 1201-1209.
50. H. Tagashita and J. Lucas, "Measurements of Ionization Coefficients in N₂ and H₂." J. Phys. D., Vol. 2, 1969, pp. 867-880.
51. S. C. Haydon and O. M. Williams, "Ionization Growth in Nitrogen." J. Phys. D., Vol. 9, 1976, pp. 523-536.
52. M. A. Folkard and S. C. Haydon, "Experimental Investigations of Ionization Growth in Nitrogen." J. Phys. B., Vol. 6, 1978, pp. 214-226.

53. D. Q. Posin, "The Townsend Coefficients and Spark Discharge." Phys. Rev., Vol. 50, 1936, 650-658.
54. W. Legler, "Anregung von UV-Strahlung in Stickstoff und Wasserstoff durch einen Electronenschwarm," Z. Phys., Vol. 173, 1963, pp. 169-183.
55. D.T.A. Blair, N. M. Macleod and J. S. Orr, "Radiation in the Vacuum Ultra-violet from Discharges in Gas Mixtures." Proc. Int. Conf. Gas Discharges, IEEE London, 1976, pp. 401-403.
56. M. A. Harrison and R. Geballe, "Simultaneous Measurement of Ionization and Attachment Coefficients," Phys. Rev., Vol. 91, 1953, pp. 1-7.
57. M. S. Bhalla and J. D. Craggs, "Measurements of Ionization and Attachment Coefficients in Carbon Dioxide in Uniform Fields." Proc. Phys. Soc., Vol. 76, 1980, pp. 369-377.
58. C. S. Lakshminarasimha, J. Lucas and N. Kontoleon, "Diffusion and Ionization Studies for Electron Swarms in Carbon Monoxide and Carbon Dioxide." J. Phys. D: Appl. Phys., Vol. 7, 1974, pp. 2545-2553.
59. H. N. Kucukorpaci and J. Lucas, "Simulation of Electron Swarm Parameters in Carbon Dioxide and Nitrogen for High E/N." J. Phys. D: Appl. Phys., Vol. 12, 1979, pp. 2123-2138.
60. J. L. Moruzzi, "Ionization and Attachment in Difluorodichloromethane." Brit. J. Appl. Phys., Vol. 14, 1963, pp. 938.
61. V. N. Maller and M. S. Naidu, "Ionization and Breakdown in SF₆-Air and Freon-Nitrogen Mixtures." IEEE Trans. on Plasma Science, Vol. PS-3, 1975, pp. 49-51.
62. Raja Rao and G. R. Govinda Raju, "Sparking Potentials and Swarm Coefficients in Freon and Mixtures of Freon and Air." Brit. J. Electronics, Vol. 35, 1973, pp. 49-54.
63. J. L. Moruzzi, "Estimation of Initial Cathode Current in Townsend Attachment Experiments." Brit. J. Appl. Phys. 14, pp. 929-930, 1963.

64. L. G. Christophorou, D. R. James, R. Y. Pai, M.O. Pace, R. A. Mathis, and D. W. Bouldin, "High Voltage Research (Breakdown Strengths of Gaseous and Liquid Insulators." Fourth Quarterly Report, ORNL/TM-5917, 1977.
65. M. C. Siddagangoppa, C. S. Lakshminarasimha and M. S. Naidu, " Ionization and Attachment in Binary Mixtures of SF_6-N_2 and $CCl_2F_2-N_2$." J. Phys. D. Appl. Phys., Vol. 16, 1983, pp. 763-772.
66. In L. G. Christophorou (Ed.), Electron and Ion Swarms. Pergamon Press, New York, 1981, pp. 11-19.
67. L. C. Pitchford, S. V. O'Neil and J. R. Rumble, "Extended Boltzman Analysis of Electron Swarm Experiments," Phys. Rev., A23, 1981, 294-304.
68. E. Marode and J. P. Boeuf, as quoted by T. H. Teich in L. G. Christophorou (Ed.), Electron and Ion Swarms. Pergamon Press, New York, 1981.
69. In L. G. Christophorou (Ed.), Electron and Ion Swarms." Pergamon Press, New York, 1981, pp. 45-53.
70. S. Chandrasekhar, Astrophys. J., Vol. 97, 1943, pp. 255.
71. J. Lucas, "A Theoretical Calculation of Electron Swarm Properties in Helium." Int. J. Electronics, Vol. 32, 1972, pp. 393-410.
72. S. R. Hunter, "Monte Carlo Simulations of Electrons in H_2 ," Aust. J. Phys., Vol. 30, 1977, pp. 83-103.
73. T. Itoh and T. Musha, "Monte Carlo Calculations of Motion of Electrons in Helium." J. Phys. Soc. Japan, Vol. 15, 1960, pp. 1675-1680.
74. S. K. Srivastava, S. Trajmar, A. Chutjian and W. Williams, "Absolute Eleactic Differential Electron Scattering Cross Sections in the Intermediate Energy Region, SF_6 and UF_6 ." J. Chem. Phys. Vol. 64, 1976, pp. 2767-2771.
75. K. Rohr, "Absolute Differential Cross Sections for $e-SF_6$ Scattering in the a_{1g} and t_{1u} Resonance Region." J. Phys. B., Vol. 12, L185, 1979.

76. S. Trajmar and C. Chutjian, "Electron Impact Excitation of SF₆," J. Phys. B., Vol. 10, 2943, 1977.
77. T. Yoshizawa, Y. Sakai, H. Tagashira and S. Sakamoto, "Boltzman Equation Analysis of the Electron Swarm Development in SF₆." J. Phys. D., Vol. 12, 1979, pp. 1839-1852.
78. A. J. Ahearn and N. B. Hanney, "The Formation of Negative Ions of Sulfur Hexafluoride." J. Chem. Phys., Vol. 21, 1953, pp. 119-124.
79. W. M. Hickam and R. E. Fox, "Electron Attachment in Sulfur Hexafluoride." J. Chem. Phys., Vol. 25, 1956, pp. 642-647.
80. L. E. Kline, D. K. Davies, C. L. Chen and P. J. Chantry, "Dielectric Properties of SF₆ and SF₆ Mixtures Predicted from Basic Data." J. Appl. Phys., Vol. 50, 1979, pp. 6789-6796.
81. A. Chutjian, "Experimental SF₆⁻/SF₆ and Cl⁻/CFCl₃ Electron-Attachment Cross Sections in the Energy Range 0-200 meV." Phys. Rev. Lett., Vol. 46, 1981, pp. 1511-1514.
82. L. G. Christophorou, D. L. McCorkle and J. G. Carter, "Cross Sections for Electron Attachment Resonances Peaking at Subthermal Energies." J. Chem. Phys. Vol. 54, 1971, pp. 253-260.
83. L. G. Christophorou, D. L. McCorkle and J. G. Carter, "Cross Sections for Electron Attachment Resonances Peaking at Subthermal Energies." J. Chem. Phys., Vol. 57, 1972, p. 2228.
84. J. P. Novak and M. Frechette, "Calculation of SF₆ Coefficients from Revised Data." J. Phys. D15, L105, 1982.
85. D. Rapp and P. Englander Golden, "Total Cross Sections for Ionization and Attachment in Gases by Electron Impact." J. Chem. Phys., Vol. 43, 1965, pp. 1464-1479.
86. K. Rohr, "Vibrational Excitation of SF₆ by Low-energy Electron Impact." J. Phys., B, Vol. 10, 1977, pp. 1175-1177.
87. H. A. Blevin, J. Fletcher and S. R. Hunter, "A Monte Carlo Simulation of the Behaviour of Electron

- Swarms in Hydrogen." Aust. J. Phys., Vol. 31, 1978, pp. 299-312.
88. T. H. Teich and B. Sangi. Proceedings of the International Symposium on High Voltage Technology, Munich, 391, 1972.
 89. M. S. Naidu and A. N. Prasad, "Diffusion and Drift of Electrons in SF₆." J. Phys. D., Vol. 5, 1972, pp. 1090-1095.
 90. L.G.H. Huxley and R. W. Crompton, The Diffusion and Drift of Electrons in Gases. John Wiley and Sons, New York-London, 1974.
 91. In L. G. Christophorou (Ed.), Electron and Ion Swarms. Pergamon Press, New York, 1981.
 92. H. A. Blevin and S. C. Haydon, "The Townsend's Ionization Coefficients in Crossed Electric and Magnetic Fields." Aust. J. Phys., Vol. 11, 1958, pp. 18-34.
 93. G. R. Govinda Raju and S. Rajapandian, "Townsend's First Ionization Coefficient in Crossed Electric and Magnetic Fields in Nitrogen." Int. J. Electronics, Vol. 40, 1976, pp. 65-79.
 94. G. R. Gurumurthy and G. R. Govinda Raju, "Townsend's First Ionization Coefficients and Sparking Potentials in Crossed Electric and Magnetic Fields." IEEE Trans. on Plasma Science, Vol. PS-3, 1975, pp. 131-143.
 95. G. R. Govinda Raju and G. R. Gurumurthy "Electron Energy Distributions and Transport Coefficients in N₂ in EXB Fields." Int. J. Electronics, Vol. 44, 1978, pp. 355-365.
 96. W. P. Allis, "Motion of Ions and Electrons." Handbuch der Physik, Springer Verlag, 1956.
 97. A.E.D. Heylen, "The Influence of a Crossed Magnetic Field on a Gaseous Townsend Discharge." Brit. J. Appl. Phys., Vol. 16, 1965, pp. 1151-1159.
 98. A.E.D. Heylen, "Electrical Ionization and Breakdown of Gases in a Crossed Magnetic Field." Proc. IEEE, Vol. 127, 1980, pp. 221-224.

VITA AUCTORIS

Born in Ankara, Turkey, on June 19, 1952.

After graduating from the State Engineering and Architectural Academy of Ankara, with a B.Sc. degree in Electrical Engineering in 1975, attended the Middle East Technical University, Ankara, Turkey, and received M.Sc. degree in Electrical Engineering in 1979.

From 1976 to 1977, worked as a research engineer at the Turkish Electricity Authority, Ankara, Turkey. From 1978 to 1980, instructed High Voltage Engineering and Power System protection courses at the University of Hacettepe and the State Engineering and Architectural Academy of Ankara.

In September 1980, joined the high voltage research group of Electrical Engineering Department at the University of Windsor.

Candidate for Ph.D. degree in January 1985.